GEOLOGY AND ORIGIN OF SAND RIDGES IN A BACK-BARRIER ESTUARY, PAMLICO SOUND, NORTH CAROLINA

By

Brian K. Querry

May, 2018

Directors of Thesis: Dr. David Mallinson and Dr. Stephen Culver

Major Department: Geological Sciences

ABSTRACT

The Outer Banks of North Carolina have undergone significant geomorphic change, exhibiting varying degrees of barrier island continuity during the late Holocene. These changes affect the environmental conditions (salinity, tidal and wave energy, currents, etc.) in Pamlico Sound, the estuarine system behind the Outer Banks. The modern estuarine system is characterized by minimal tidal energy (tidal range of approximately 10 cm) and limited exchange with the marine environment through three inlets, resulting in the accumulation of organic-rich muds in the Pamlico Sound basin, containing mid- to high- salinity estuarine foraminifera. However, a sand ridge field occurs at approximately 2 to 7 m below sea level in the eastern Pamlico Sound basin, suggesting different hydrodynamic conditions at some time during the Holocene. The sand ridge field extends up to 10 km into the basin, and is oriented perpendicular to the barrier islands. Previous paleoenvironmental work suggests the sand ridges were deposited under high salinity conditions. Defining the mechanism of formation of this sand ridge field will assist in understanding the geological evolution of the region.

To understand the geologic history and origin of this sand ridge field six vibracores and 60 km of chirp sub-bottom profiler data were acquired and analyzed. Cored sediments were analyzed for sedimentology, foraminiferal assemblages, bulk magnetic susceptibility, and geochronology. Chirp seismic data were examined to understand the dimensions and stratigraphy of the sand ridges. Surface samples were collected to understand the modern sedimentology. Vibracores reveal that the sand ridge sediments generally lack mud and have a greater average grain–size farther into Pamlico Sound (i.e., distal to the barrier islands) suggesting that the barrier islands are not the source of the sand. Two foraminiferal biofacies were identified, High Brackish biofacies A (more diverse) and High Brackish biofacies B (less diverse), which provide information on the continuity of the barrier islands. Chirp seismic data delineate a Pleistocene interfluve underlying the sand ridges. Geochronology indicates that sand ridge formation began at approximately 2500 cal yr. BP. There are two intervals at 1000 cal yr. BP and 500 cal yr. BP where an increase in wave and current activity is suggested by seismic horizons. Seismically, the top of the Pleistocene interfluve exhibits two topographic highs that demonstrate the sand ridges are juvenile Class I sand ridges. The sand ridges are interpreted as resulting from the reworking of Pleistocene interfluves during intervals of increased tidal influence and possibly storm activity where winds speeds are 20 mph or greater.

GEOLOGY AND ORIGIN OF SAND RIDGES IN A BACK-BARRIER ESTUARY, PAMLICO SOUND, NORTH CAROLINA

A Thesis presented to

The Faculty of the Department of Geological Sciences

East Carolina University

In Partial Fulfillment of the Requirements of the Degree

Master of Science in Geology

By

Brian K. Querry

May, 2018

GEOLOGY AND ORIGIN OF SAND RIDGES IN A BACK-BARRIER ESTUARY, PAMLICO SOUND, NORTH CAROLINA

By

Brian K. Querry

APPROVED BY:

CO-DIRECTOR OF THESIS _____
Dr. David J. Mallinson

CO-DIRECTOR OF THESIS _____
Dr. Stephen J. Culver

COMMITTEE MEMBER _____
Dr. Eduardo Leorri

EXTERNAL COMMITTEE MEMBER _____
Dr. Ryan Mulligan

CHAIR OF THE DEPARTMENT OF GEOLOGICAL SCIENCES _____
Dr. Stephen J. Culver

DEAN OF THE GRADUATE SCHOOL _____
Dr. Paul J. Gemperline

ACKNOWLEDGEMENTS

I would like to thank all those who supported me, give me encouragement, and assisted in making this possible. I would also like to thank Tiffany who pushed me to achieve more than I ever believed I could. Thank you, of course, to my advisors Dr. David Mallinson and Dr. Stephen Culver, for their patience, insights, and guidance with my thesis and in life. Thank you to John Woods and Jim Watson for their tireless assistance with the R/V Riggs and technical help. Thank you to the NSF grant OCE-1130843 and the East Carolina University Geological Department for financial support and making this possible. Thank you to Kyle Prock for assisting with the laboratory work. Finally, thank you to all my fellow graduate students for their friendship and comradery.

TABLE OF CONTENTS

LIST OF TABLES

LIST OF FIGURES

1. Introduction

1.1 Purpose of Study

Coastal systems are affected by a variety of factors including: antecedent geology, relative sea-level change, sediment flux, and storm frequency and intensity (Riggs et al., 1995; Cronin et al., 2000; Burkholder et al., 2004; Culver et al., 2007; Mallinson et al., 2008; Mann et al., 2009; Kemp et al., 2011; Mallinson et al., 2017). These factors influence each other and greatly impact modern geomorphology and processes. Shoals, subaqueous sand ridges, and sandbars are common features in coastal environments and are significant in their role as sources or sinks of sediment (Dalrymple and Hoogendoorn, 1997; Snedden and Dalrymple, 1998, 1999; Snedden and Bergman, 1999; Goff, 2014). Shoals are a general term associated with shallow marine sand bodies in the nearshore environment when currents and tides move sediments to form such sand bodies. Sandbars are small bodies of sand that are built up by offshore waves and longshore currents. Sand ridges are some of the largest sand bodies that can extend tens of km in length, up to 10 km in width, and can be up to 30 m in relief located from the shoreface to the outer shelf (Berné et al., 2002). Sand ridges may store sand temporarily or permanently, greatly affecting the coastal sediment budget, and are potentially useful for beach nourishment along coastlines (Thieler et al., 2014).

Subaqueous sand ridges (elongate sand bodies occurring below mean low tide) occur in a variety of environments and are influenced by hydrodynamic forcing and sediment flux (Dalrymple and Hoogendoorn, 1997; Snedden and Dalrymple, 1999; Snedden and Bergman, 1999). Coastal shoreface attached sand ridges are oriented obliquely to shorelines along the U.S. Atlantic inner shelf (Duane et al., 1972). These types of sand ridges can have relief up to 10 m

with very shallow slopes and can be kilometers long (Duane et al., 1972, McBride and Moslow, 1991, Harrison et al., 2003).

The Albemarle-Pamlico Estuarine System (APES) in North Carolina (Figure 1) is a large and shallow estuarine system with oblique sand ridges on the bed. This system evolved in response to sea-level change, sediment flux, storm activity, through prograding and retrograding of shorelines, the degree of barrier island segmentation via inlets, and from changes in the climate (Culver et al., 2007; Mallinson et al., 2011; Zaremba et al., 2016). The Outer Banks barrier islands, which form the eastern shoreline of Pamlico Sound, separate the Pamlico Sound and the Atlantic Ocean and extend more than 270 km from Virginia to Cape Lookout, North Carolina (Riggs et al., 1995; Mallinson et al., 2011). Changes that have occurred to the Outer Banks on historical and geological time scales include the creation and closure of inlets, formation and destruction of islands, barrier island transgression and regression, and formation of various coastal features including sand ridges on the ocean side and lagoon side of barrier islands (Fisher, 1962; Riggs and Ames, 2003; Culver et al., 2006; Mallinson et al., 2008). Recent investigations have concentrated on the geologic evolution of the Pamlico Sound estuarine system to understand the history, geological processes, and hydrodynamics (Riggs et al., 1995; Culver et al., 2006; Foley, 2007; Kemp et al., 2009; Metger, 2009; Smith et al., 2009; Mallinson et al., 2010; Grand Pre et al., 2011; Peek et al., 2013; Zaremba, et al., 2016).

In the present study, sand ridge features located to the northwest of Hatteras Inlet in Pamlico Sound are investigated in detail, and are herein referred to as the East Pamlico Sand Ridges (EPSR). It is hypothesized that these sand ridges are out of equilibrium with the modern estuarine system (Figure 1), which is dominated by the deposition of mud. The ridges were suggested to be the result of greater marine influence occurring ca 1000 cal yr. BP (Zaremba et

al., 2016), but the age and depositional setting have not been previously determined. The objective of this investigation is to determine the characteristics (geophysical, sedimentology, etc.) and geochronology of the EPSR, and relate the findings to previous investigations on sand ridges, storm activity, and barrier island continuity in order to understand their origin and significance with respect to the Holocene evolution of this estuarine system (Riggs et al., 1995; Riggs et al., 2003; Burdette et al., 2008; Culver et al., 2006; Mallinson, 2008; Mallinson et al., 2010). In this study, multiple hypotheses on the origin of the EPSR are tested. Possible origins of the sand ridges include formation from tsunami events, possibly associated with the Cape Fear slide (Hornbach et al., 2007); increased storm activity driving sand transport from the barrier islands into the estuary basin; tidal deposition during a phase of greater tidal influence; reworking of relict flood-tide delta deposits; or reworking of Pleistocene sediments exposed on interfluves. Foraminiferal assemblages, sedimentology, geophysical data, and geochronology are used to establish the plausible origin of the sand ridges.

1.2 Study Area

APES is the second largest estuarine system in the continental United States, and Pamlico Sound is the largest basin within the estuarine system at approximately 5340 km^2 in area (Figure 1) (Burkholder et al., 2004). The sound is bordered by barrier islands (the Outer Banks) to the east and the mainland to the west. Pamlico Sound is the product of the confluences of several drowned river estuaries and the basin ranges from 7.3 m in depth to the north and 4.8 m in the south with an average depth of 3 m. The sound is dominated by organic-rich mud due to limited exchange with the marine environment (Wells and Kim, 1989; Riggs et al., 2003; Mallinson et al., 2011). Areas of sand in Pamlico Sound are generally constrained to a) the eastern portions

sourced from the barrier islands via inlets, overwash, and eolian activity, b) to the perimeter of the Sound, where sand is sourced from small eroding coastal cliffs, or c) to shoals within the Sound with sand sourced from erosion of the underlying Pleistocene strata (Zaremba et al., 2016).

There are currently three active inlets along the Outer Banks that interact with Pamlico Sound; Oregon Inlet, Hatteras Inlet, and Ocracoke Inlet. Two river systems feed freshwater into Pamlico Sound from the west; the Tar-Pamlico and Neuse Rivers. The EPSR extend northwest of Hatteras Inlet and are nearly perpendicular to the barrier islands. The sand ridges are approximately 6.5 km in length, lie 3–5 m below sea-level, and are 0.5–2.5 m in relief (Figure 1).

On average, 150 m^3s^{-1} of freshwater enters the Pamlico Sound through each of the Tar-Pamlico River and the Neuse River, and 500 m^3s^{-1} enters through the connection to Albemarle Sound (Giese et al., 1979; Wells and Kim, 1989). The interior of Pamlico Sound has an astronomical tidal range of approximately 10 cm (Wells and Kim, 1989; Luettich et al. 2002; Mallinson et al., 2011). Water levels are also affected by strong winds, which may produce a wind setup of 10–100 cm (Luettich et al., 2002; Riggs and Ames, 2003; Abbene et al., 2006).

1.3 Objectives

The primary objective of this study is to understand the geological and geophysical characteristics of the sand ridges northwest of Hatteras Inlet, and to determine their relationship to the Holocene evolution of the Outer Banks and Pamlico Sound. Three specific objectives will be addressed in order to complete the primary objective.

1. **Characterize deposits using geophysical, sedimentological, and microfossil data**

Deposits are characterized using data from cored sediments including grain-size statistics, percent mud, percent bioclasts, and microfossils. These data are then placed in a stratigraphic framework by correlation to geophysical data.

2. **Establish the age of deposition**

Geochronology from radiocarbon analysis is used for constraining the age of depositional units observed in cores and geophysical data.

3. **Relate to other studies of the evolution of Pamlico Sound and determine origin of the ridges**

Relating this study to previous studies will assist in the understanding of the evolution of the local environment in the context of the history of Pamlico Sound.

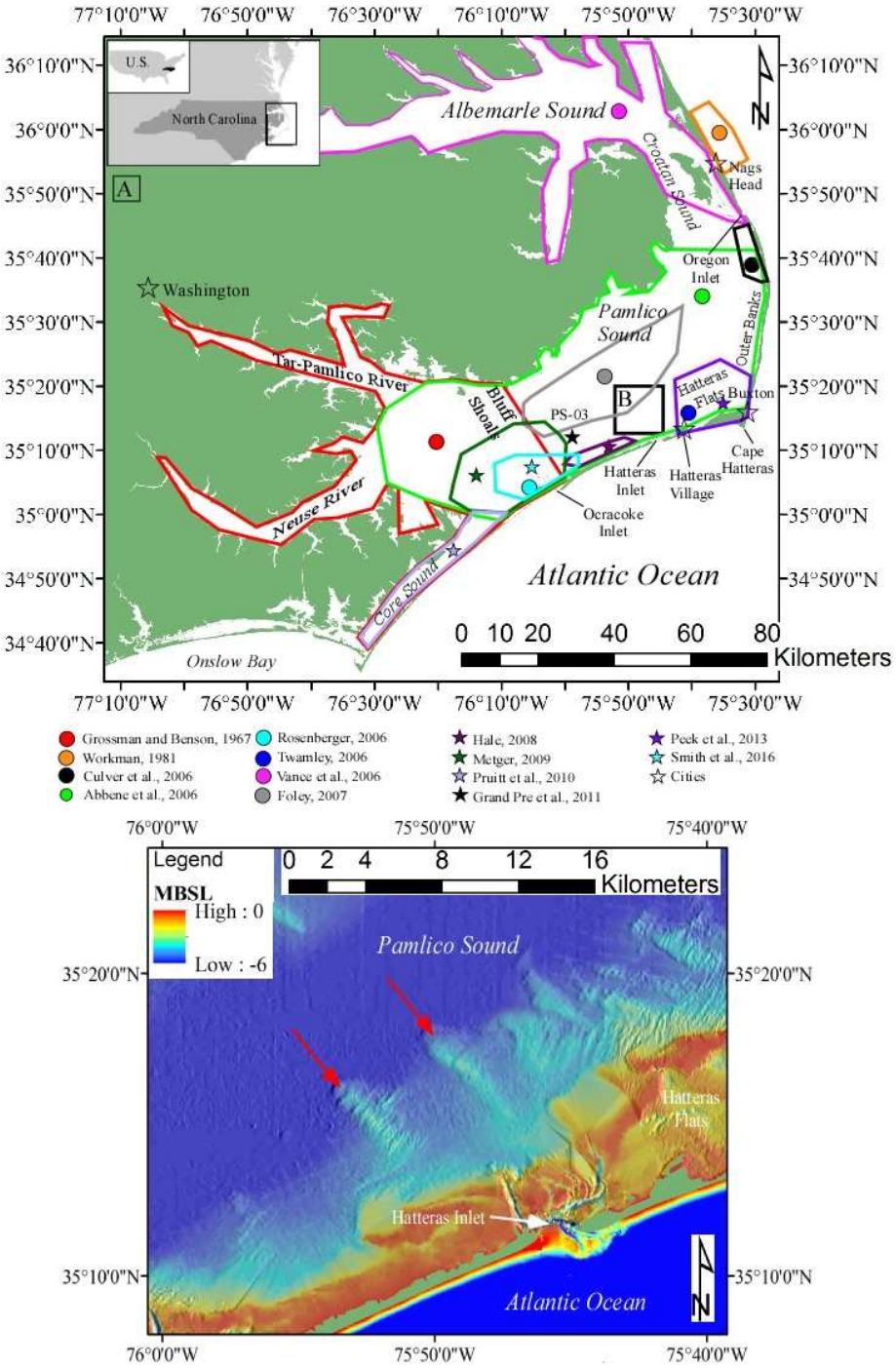

Figure 1: Pamlico Sound in eastern North Carolina. Image A indicates the location of past studies in Pamlico Sound. The location of the study area is indicated by a box in image A. Image B shows the East Pamlico Sand Ridges (EPSR), northwest of Hatteras Inlet. Arrows indicate the two sand ridges that are subject of this study.

2. Previous Work

Pamlico Sound, Croatan Sound, and Albemarle Sound have been studied extensively over the last several decades (e.g., Riggs et al., 2003; Abbene et al., 2006; Culver et al., 2006; Culver et al., 2007; Foley, 2007; Metger, 2009; Smith et al., 2009; Mallinson et al., 2010; Riggs et al., 2011; Zaremba et al., 2016). Some studies focus on climate changes that influence the condition of oceans resulting in variable storm activity and intensity (Mann et al., 2010; Donnelly et al., 2015) which affect the creation and destruction of barrier island and inlets (Culver et al., 2006; Mallinson et al., 2010; Grand Pre et al., 2011; Peek et al., 2013). Foraminifera play a key role in the recognition of past environmental conditions (such as greater or fewer inlets) as they are an indicator of salinity (Abbene et al., 2006; Culver et al., 2006; Grand Pre et al., 2011). Changes in environmental conditions, such as salinity and sediment flux, of Pamlico Sound can be attributed to the combined influence of relative sea-level rise and climate variations during the Holocene (Culver et al., 2007; Foley, 2007; Kemp et al., 2009; Grand Pre et al., 2011; Mallinson et al., 2011; Zaremba et al., 2016).

2.1 Hydrodynamics

The APES is a complex system where hydrodynamic conditions are controlled by wind forcing (Luettich et al., 2002) and the number and width of tidal inlets which influence the salinity, circulation, and bathymetry (Giese et al., 1979; Wells and Kim, 1989; Clunies et al., 2017; Mallinson et al., 2017). Relative sea-level rise of 3–4 mm yr^{-1} also plays an influencing role on the conditions in the APES (Kemp et al., 2009; Kemp et al., 2011). Mulligan et al. (2015) used the Delft3D model to investigate the APES during periods of hurricane forcing and showed that wave heights are higher in the western part of Pamlico Sound during the approach of

the hurricane Irene, and higher in the eastern part of Pamlico Sound after the passage of the storm (Figure 2). Using this model, the maximum shear stress from Hurricane Irene and Hurricane Ophelia (2005) occurred just before the maximum water levels on the west side of Pamlico Sound over Bluff shoals, EPSR, and near the inlets (Figure 3) (Mulligan et al, 2011; Mulligan et al., 2015).

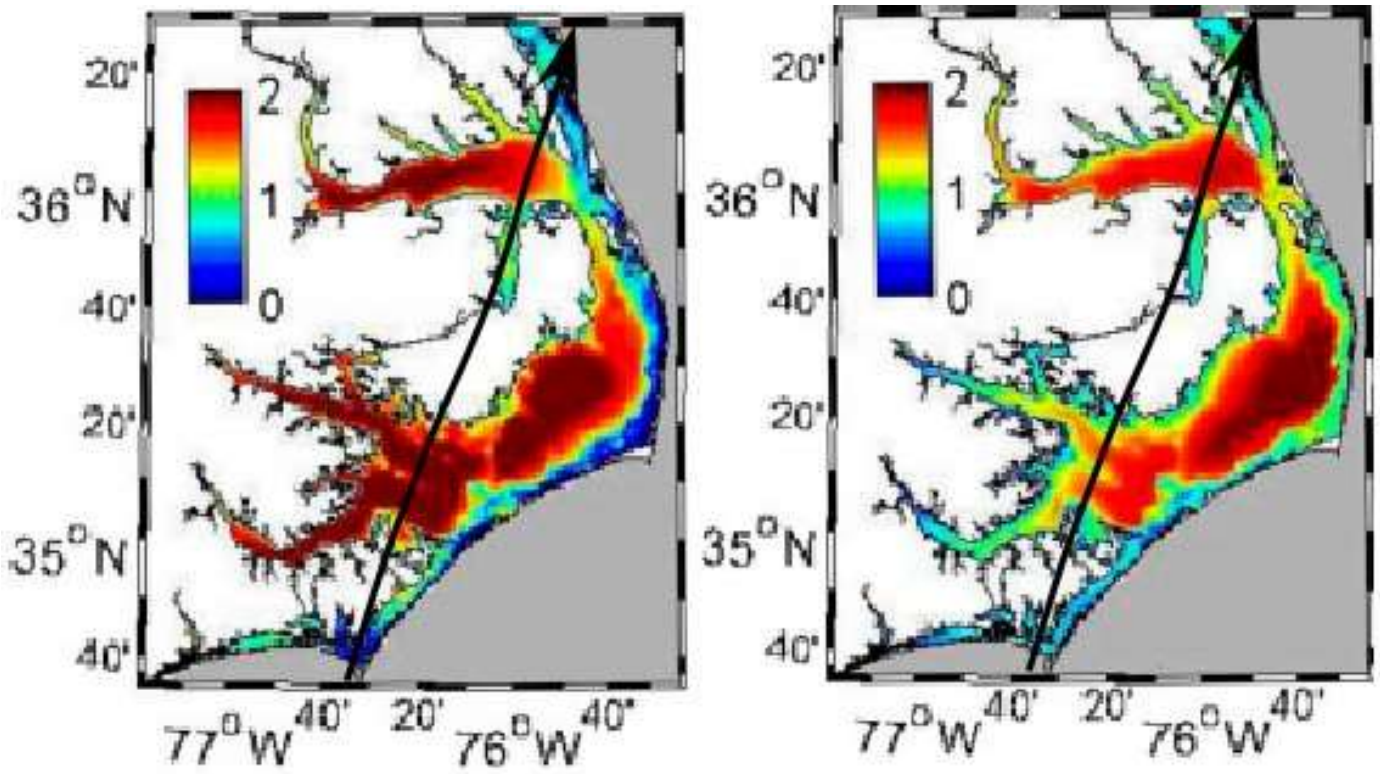

Figure 2: Significant wave height (H_s) during Hurricane Irene. The left panel illustrates H_s at the time of maximum water levels on the west side of the APES (August 27, 2011 at 12:00 UTC), and right panel shows H_s at the time of maximum water levels on the east side of the APES (August 28. 2011 at 0:00 UTC); units in meters (modified from Mulligan et al., 2015). Arrows indicate track of Hurricane Irene.

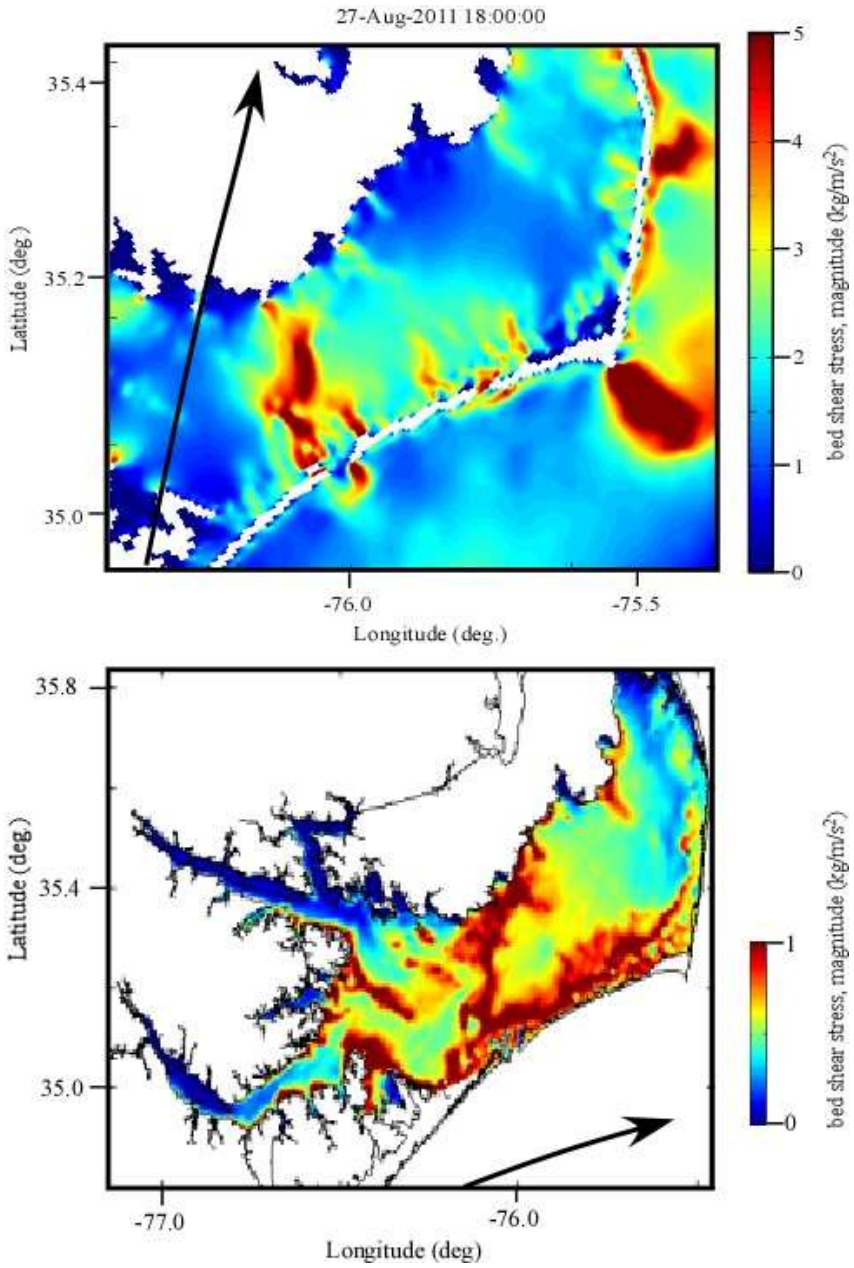

Figure 3: Simulated bottom shear stress during the passage of two hurricanes. The top panel shows bottom shear stress from Hurricane Irene (2011, track is west of the Barrier Islands and through Pamlico Sound) and bottom panel shows bottom shear stress from Hurricane Ophelia (2005, track is along the NC Shelf and east of the Barrier Islands) (modified from Mulligan et al., 2011; Mulligan et al., 2015). (Arrows indicate hurricane tracks). Note different scales.

Clunies (2014) and Clunies et al. (2017) studied the wind and tidally driven hydrodynamics of the APES and used data from two moderate storm events in September 2008. During the two storm events, the maximum wind velocities were approximately 18 ms^{-1}. In the APES there is significant water level set-up during storm events from wind stress on the water surface causing greater bed shear stress.

2.2 Subaqueous Sand Ridges

Large subaqueous sand ridges are variable in size (Table 1) (Duane et al., 1972; Swift and Field, 1981; Dalrymple and Hoogendoorn, 1997; Snedden and Dalrymple, 1999; Harrison et al., 2003; Goff, 2014; Gibbons, 2017). Sand ridges occurring on wave-dominated coasts are typically oriented oblique to the shoreline and form on storm-dominated shorefaces with an abundant sediment supply (Swift and Field, 1981; Hoogendoorn and Dalrymple, 1986; Goff, 2014). Tidally influenced sand ridges, such as those identified by Berné et al., (2002), are sediment supply-dominated and are repeatedly reworked by tides resulting in a lack of bedforms imposed on the surface of the sand ridges. However, most studies of open shelf sand ridges suggest they are accommodation-dominated (i.e., controlled by water depth) and are influenced by waves (Berné et al., 2002). Open shelf sand ridges along the Atlantic Ocean shoreline of the United States (Duane et al., 1972; Swift and Field, 1981; Harrison et al., 2003; McNinch, 2004; Goff, 2014; Thieler et al., 2014; Gibbons, 2017) and Canada (Hoogendoorn and Dalrymple, 1986; Dalrymple et al., 1990) have been studied extensively. McBride and Moslow (1991) discussed the origin of sand ridges and separated them into two categories; relict, such as drowned barrier islands, and active, those that form from sediment transport.

Table 1: Length, width, and thickness of sand ridges from previous studies. * indicates sand bar.

Location	Length	Width	Relief	Author
Sarasota, FL	3–10+ km	1–4 km	1–4 m	Twichell et al., 2003
Off Indian Rocks Headland, FL	2–10 km	0.2–1.5 km	0–4 m	Harrison et al., 2003
Korea Strait	25–63 km	2–9 km	10–22 m	Park et al., 2003
Sable Island, Canada	7.2–25 km	1.5–6.4 km	5.1–12 m	Hoogendoorn and Dalrymple, 1986
Assateague Island, MD	3.7–18.5 km	0.9–2.8 km	3.0–12.1 m	Swift and Field, 1981
East China Sea	20+ km	4–12 km	26 m	Berné et al., 2002
Wimble Shoals, NC	10–13 km	0.5 km	<7 m	Gibbons, 2017
Duck, NC*	100 m	25 m	1–2 m	McNinch, 2004

Swift and Field (1981) described first and second order sand ridges, where first order ridges have greater relief, are longer, and wider than second order ridges, yet second order ridges have steeper slopes. They found that sand ridges on the Atlantic shelf of the U.S. have a relief of 3.0–12.1 m, a length of 3.7–18 km, and width of 0.9–2.8 km. However, Hoogendoorn and Dalrymple (1986) found that near Sable Island Bank, Nova Scotia, Canada, first order ridges are larger and second order ridges are smaller than those found in the U.S. While the ridges in these studies differ in scale, they are similar in distribution pattern and grain size (Hoogendoorn and Dalrymple, 1986). Swift and Field (1981) also suggest that continued sea-level rise and shoreface transgression leads to detachment of sand ridges from the shoreface and offshore migration of the sand ridge transfers sand from the shoreface to the shelf.

Goff et al. (2014) studied sand ridges that overlie the shoreface ravinement surface off Panama City, Florida. These sand ridges are up to 4 m in height and are interpreted as Holocene sands. The shoreface ravinement process impacts the stratigraphy and sand ridges in two ways, by eroding barrier/estuarine/Pleistocene sediments, and extracting sands from eroded material to

form the overlying sand ridge. The ravinement surface underlying the sand ridges is the basal reflector and lower boundary of the sand ridge system in the geophysical data.

Harrison et al. (2003) studied sand ridges on a mixed siliciclastic and carbonate inner shelf off of west-central Florida. The sand ridges were suggested to be mostly relict because of the low sediment supply to this shelf region. These sand ridges are smaller in relief than sand ridges from the Atlantic margin of the U.S. and are covered by a series of small to large two-dimensional subaqueous dunes. These sand ridges are not shoreface-connected and are not moving significantly in comparison to shoreface-connected ridges such as those from Assateague Island (Swift and Field, 1981), Nova Scotia (50 myr^{-1}; Dalrymple and Hoogendoorn 1997), and Chincoteague Shoals (Duane et al., 1972).

Off Sarasota, Florida, Twichell et al. (2003) studied a series of low relief inner continental shelf sand ridges. They observed that the exposed Pleistocene surface (eroded by transgressive ravinement) was coated with a discontinuous surface of shell fragments and that the sand ridges contained the bulk of the Holocene sediments. This indicates an abrupt facies boundary between carbonate and siliciclastic sediments, as opposed to a gradual transition (typical of shoreface sand ridges). Grab samples from the sand ridges show coarser material in the troughs and on the lower part of the updrift flank. They noted that the dominant currents capable of causing sediment transport run parallel to the coast, perpendicular to the sand ridges.

McNinch (2004) examined shore-oblique sandbars along the Outer Banks of North Carolina located near Duck, Kitty Hawk and Nags Head. Bathymetry shows sandbars near Duck measure approximately 100 m in length, 25 m wide, and a 1–2 m relief. McNinch noted that after Hurricane Dennis impacted the region near Duck in 1999, the sandbars were reworked by

significant wave energy and the oblique bars were no longer present after the hurricane, but returned later. However, larger sandbars located near Kitty Hawk appeared to be more stable than the smaller sandbars near Duck and Hags Head. Kitty Hawk sandbars differed from the others as the Kitty Hawk sandbars have greater variability in seafloor gradient. The study concluded that the shore-oblique sandbars near Duck, return through multiple storm-fair weather events.

Saha et al. (2016) compared tidal ridges and sand bars in the Gulf of Khambhat in western India to distinguish the outer Gulf of Khambhat and the inner Gulf of Khambhat. The spatial dimensions differ, as ridges generally are wider and longer than tidal bars but tidal bars can be as wide as a ridge. The sand ridges are found in the outer Gulf of Khambhat, aligned obliquely to the paleo-shoreline, are underlain by an erosional contact and composed of fine to coarse sands. The sand ridges on the Gulf of Khambhat are continuously reworked. Subaqueous dunes were also present on the sand ridges as a result of strong currents in the gulf. The tidal bars are located in the inner shelf and composed of medium to coarse sands. The tidal sand bars in the inner Gulf of Khambhat generally have low relief due to high tidal velocities, despite high sedimentation rates.

2.3 Foraminifera

Utilizing foraminifera to reconstruct down-core environmental changes can supplement sedimentological and geophysical data. Foraminifera are often used to assist in interpretations involving storm activity, sea-level change, climate changes, and paleo-environmental reconstructions (Grossman and Bensen, 1967; Woo et al., 1997; Culver et al., 2006; Kemp et al., 2009; Mallinson et al., 2010). Benthic foraminifera, particularly, can live in a variety of

environments from estuarine, shallow marine, and open marine environments, and have been documented in numerous studies in the Pamlico Sound region (Figure 1) (Grossman and Benson, 1967; Schnitker, 1971; Workman, 1981; Culver et al., 2006; Abbene et al., 2006; Rosenberger, 2006; Twamley, 2006; Vance et al., 2006; Foley, 2007; Hale, 2008; Metger, 2009; Pruitt et al., 2010; Grand Pre et al., 2011; Peek et al., 2013; Smith, 2016). Many of these studies use Fisher's Alpha, which relates species richness and species abundance, to help define biofacies.

Schnitker (1971), studied foraminifera of the North Carolina shelf and recognized three assemblages (Table 3): inner shelf, central shelf, and outer shelf. *Elphidium clavatum* (*Elphidium excavatum* in this study) characterized the inner shelf. The central shelf was characterized by *Hanzawaia concentrica (Hanzawaia strattoni* in this study*), Reophax atlantica, Peneroplis proteus, Quinqueloculina seminula*, and *Asterigerina carinata*. *Lenticulina orbicularis, Cibicides pseudoungerianus*, and *Amphistegina carinata* were dominant in the outer shelf assemblage. Schnitker (1971) also noted that there is an increase in diversity south of Cape Hatteras. Moreover, although the inner and central shelf were both characterized by *Elphidium excavatum*, secondary species were more abundant but less diverse than the outer shelf.

Workman (1981) studied the inner shelf off North Carolina, near Nags Head and off Wilmington in Onslow Bay (Table 3). At Nags Head, the inner shelf is characterized by low diversity foraminiferal assemblages consisting of *Elphidium excavatum* and secondary species *Elphidium gunteri*, *Eggerella advena*, *Quinqueloculina seminula*, *Ammonia tepida*, and *Rosalina floridina.* In Onslow Bay, the inner shelf has higher diversity foraminiferal assemblages than north of Cape Hatteras and is characterized by numerous *Quinqueloculina* species and secondary species *Elphidium excavatum*, *Elphidium gunteri, Elphidium limatulum,* and *Ammonia beccarii* (*Ammonia parkinsoniana* in this study).

Grossman and Benson (1967) determined that foraminifera in saltwater lagoons such as Core Sound in North Carolina are dominated by *Elphidium* species and low salinity waters such as those near the Neuse River, are dominated by *Ammotium salsum* and *Ammobaculites* species (Table 3). Tidal delta biofacies are similar to that of the salt water lagoon biofacies except for the addition of *Hanzawaia strattoni* in the former.

In the back-barrier and nearshore estuarine sands of Pamlico Sound near Pea Island, *Ammobaculites dilatatus* dominates the low diversity assemblages and the modern marsh deposits are characterized by *Trochamma inflata, Miliammina fusca, Trihotrocha comprimata, Jadammina macrescens, Arenoparrella Mexicana,* and *Haplophragmoides wilberti* (Culver et al., 2006) (Table 3). Furthermore, Culver et al. (2006) described four sequences in deposits on Pea Island; sequence 1 and 4, consisting of well-sorted mobile sand, were barren of foraminifera except for a few specimens of *Elphidium excavatum.* Sequence 2 contained a normal marine assemblage of *Elphidium excavatum, Elphidium subarcticum*, *Elphidium mexicanum*, *Elphidium galvestonense*, *Hanzawaia strattoni*, *Ammonia parkinsoniana*, and *Buccella inusitata*. Sequence 3 also consisted of a normal marine assemblage dominated by *Elphidium excavatum* and *Buccella inusitata*.

Abbene et al. (2006) documented modern foraminiferal assemblages in Pamlico Sound (Figure 4). They identified four biofacies; marsh, estuarine A, estuarine B, and marine (Table 3). Estuarine A biofacies consisted of *Ammotium salsum* (83%), *Ammonia parkinsoniana* (6%), and *Elphidium excavatum* (4%). Estuarine B biofacies consisted of *Elphidium excavatum* (65%), *Ammotium salsum* (15%), and *Ammonia parkinsoniana* (12%). The marine biofacies was composed of 70% *Elphidium excavatum* with several other species of foraminifera that are associated with normal marine or open-shelf species; *Cibicides lobatulus, Cibicides refulgens,*

Elphidium subarcticum, Quinqueloculina lamarckiana, and *Quinqueloculina seminula*. The marsh biofacies was characterized by *Haplophragmoides wilberti, Miliammina fusca, Tiphotrocha comprimata* and *Trochammina inflata*. They concluded, as did Foley (2006), that *Ammotium salsum* is dominant at relative lower salinities and *Elphidium excavatum* is dominant at relative higher salinities in Pamlico Sound. In Chesapeake Bay, Virginia, Cronin et al. (2000), described the relationship between salinity and *Elphidium.* In salinities of 20–30 psu (practical salinity unit) *Elphidium* is most abundant and is absent at salinities of < 10 psu. The salinity range in Chesapeake Bay is comparable to that of Pamlico Sound (salinity ranging from 0.5 psu at the rivers to 36 psu at the inlets; Wells and Kim, 1989; Abbene et al., 2006).

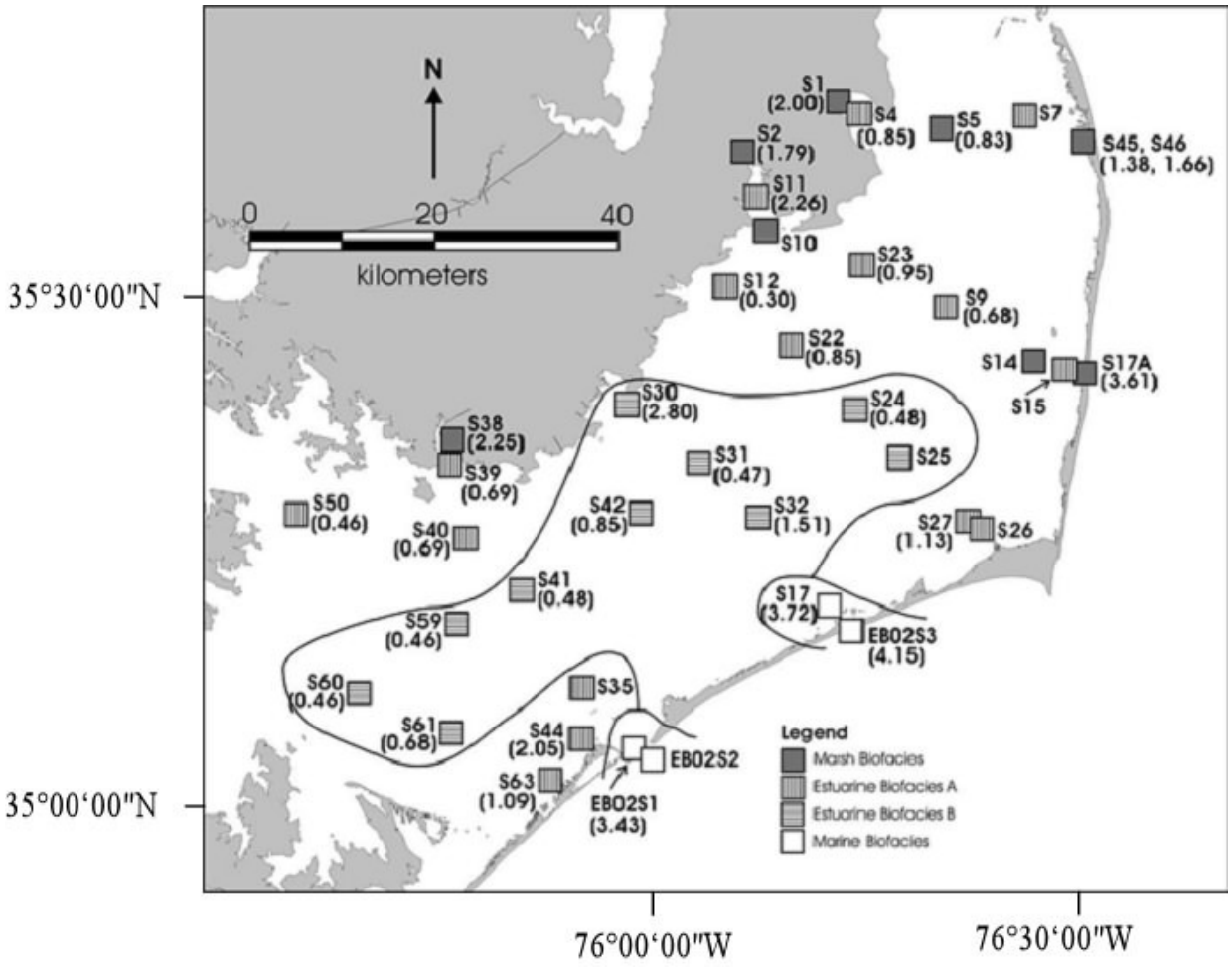

Figure 4: Distribution of four foraminiferal assemblages in Pamlico Sound resulting from cluster analysis of dead foraminifera. Values for Fisher's alpha in parentheses from Abbene et al. (2006).

Rosenberger (2006) defined six paleo-environments (marsh, barrier island/sand flat, inner shelf A, inner shelf B, low energy shelf, and normal salinity/inlet) in the back barrier of Portsmouth Island using lithologic, foraminiferal, geochemical and chronostratigraphic data (Table 3). *Trochammina inflata* and *Haplophragomides willberti* were the dominant foraminifera of the marsh paleo-environment. Barrier island/sand flat paleo-environment were

barren of foraminifera. Inner shelf A contained 30 taxa and was characterized by *Rosalina* species*, Elphidium subarcticum, Planulina mera, Buccella inusitata, Elphidium macellum,* and *Quinqueloculina lamarckiana.* Inner shelf B was less diverse than Inner shelf A and was characterized by *Glabratellina sagrai, Buccella* species*,* and *Elphidium macellum.* The low energy shelf was diverse with 29 taxa and was characterized by *Ammonia tepida, Rosalina* species A*, Bolivina lowmani, Stetsonia minuta,* and *Elphidium subarcticum.* A normal salinity/inlet assemblage was identified in sediments coarser than the other paleo-environments and was characterized by *Quinqueloculina impressa, Quinqueloculina jugosa, Quinqueloculina* sp.*, Quinqueloculina lamarckiana, Stetsonia minuta, Eponides repandus, Textularia* cf. *T. gramen, Miliammina fusca,* and *Elphidium gunteri.*

Twamley (2006) identified six biofacies based on foraminiferal assemblages from 66 samples in 16 vibracores near Hatteras Village, North Carolina; inner shelf, inlet, low energy estuarine, high energy estuarine, marsh, and barrier island (Table 3). The inner shelf assemblage included *Elphidium excavatum, Elphidium subarcticum, Nonionella atlantica,* and *Hanzawaia strattoni*. The inlet biofacies included *Quinqueloculina seminula, Quinqueloculina lamarckiana,* and *Quinqueloculina jugosa*. The low energy estuarine biofacies consisted of *Elphidium excavatum* and *Ammonia parkinsoniana*. The high energy estuarine biofacies was barren of most foraminifera except for a few specimens of *Ammotium salsum*. The marsh assemblage contained *Arenoparrella mexicana, Haplophragmoides wilberti,* and *Trochammina inflata*. The barrier island biofacies was barren of foraminifera.

Vance et al. (2006) identified five biofacies; nearshore marine and inlet, estuarine shoal, estuarine, inner estuarine, and marsh, utilizing cluster analysis of dead foraminifera in Albemarle Sound (Table 3). The nearshore marine and inlet biofacies, was dominated by *Elphidium*

excavatum, Hanzawaia strattoni, Ammobaculites crassus, Elphidium subarcticum, and *Ammonia parkinsoniana.* The estuarine shoal biofacies had low species richness and was dominated by *Ammobaculites crassus* and *Ammotium salsum*. The estuarine biofacies were dominated by *Ammobaculites crassus, Ammotium salsum, Miliammina fusca,* and *Ammobaculites subcatenulatus*. *Ammobaculites subcatenulatus,* and secondary species *Ammotium salsum* and *Miliammina fusca*, were present in the inner estuarine biofacies. *Ammoastuta inepta, Arenoparrella mexicana, Haplophragmoides bonplandi,* and *Trochammina inflata* dominated the marsh biofacies.

Foley (2007) identified four foraminiferal assemblages; low salinity estuary, low-intermediate salinity estuary, high-intermediate salinity estuary, and high salinity estuary in cores from central Pamlico Sound (Table 3). The low salinity estuary assemblage was characterized by *Ammotium salsum.* The low-intermediate salinity estuary was characterized by *Ammotium salsum, Ammonia parkinsoniana,* and *Trochammina inflata.* The high-intermediate salinity estuary was characterized by *Ammotium salsum* and *Ammonia parkinsoniana,* however it had a greater ratio of *Ammonia parkinsoniana* to *Ammotium salsum* than the low-intermediate salinity estuary. The high salinity estuary was dominated by *Elphidium excavatum* and *Ammonia parkinsoniana.*

Hale (2008) examined foraminifera from 63 samples in 17 vibracores along three transects off of Ocracoke Island and identified five biofacies; high energy normal salinity/inlet, low energy normal salinity/inner shelf, flood tide delta, estuarine flat, and marsh (Table 3). The high energy normal salinity/inlet contained 24 calcareous taxa. *Quinqueloculina frigida, Quinqueloculina jugosa, Quinqueloculina seminula, Quinqueloculina lamarckiana, Textularia* cf. *T. gramen, Quinqueloculina* sp., *Asterigerina carinata, Elphidium subarcticum, Buccella*

inusitata, Cibicides lobatulus, Hanzawaia strattoni, Elphidium mexicanum, Nonionella atlantica, Elphidium translucens, Elphidium galvestonense, and *Ammonia parkinsoniana* represent the dominant species of the high energy normal salinity/inlet biofacies. The low energy normal salinity/inner shelf biofacies was characterized by *Elphidium poeyanum, Haynesina germanica, Elphidium excavatum, Elphidium galvestonense, Cibicides lobatulus*, and *Buccella inusitata.* The flood tide delta biofacies was characterized by *Glabratellina lauriei, Elphidium mexicanum, Hanzawaia strattoni, Elphidium* spp., *Elphidium translucens, Quinqueloculina* spp., *Rosalina floridana, Elphidium galvestonense, Cibicides lobatulus, Elphidium gunteri, Elphidium subarcticum, Nonionella atlantica*, and *Textularia* cf. *T. gramen.* The estuarine flats were characterized by *Ammonia parkinsoniana, Elphidium gunteri*, and *Haynesina germanica.* The marsh biofacies was characterized by more agglutinated taxa including *Arenoparrella mexicana, Haplophragmoides wilberti, Haplophragmoides bonplandi, Haplophragmoides manilaensis, Tiphotrocha comprimata, Jadammina macrescens*, and *Trochammina inflata*.

Metger (2009) identified six biofacies; low brackish estuary, high brackish estuary, high brackish with inlet influence, inlet, normal marine, and estuary in seventeen vibracores in Pamlico Sound near Ocracoke Inlet (Table 3). Low brackish estuary was characterized by *Elphidium excavatum* (54.1%), *Ammonia parkinsoniana* (34.4%), and *Haynesina germanica* (2.9%). The high brackish estuary had 88.3% *Elphidium excavatum* and 9.4% *Ammonia parkinsoniana* and differed from the high brackish estuary with inlet influence that had 48.1% *Elphidium excavatum*, 22.2% *Ammonia parkinsoniana*, and 20.3% *Quinqueloculina* spp. The inlet assemblage consisted of 65.5% *Elphidium excavatum* with *Ammonia parkinsoniana, Elphidium galvestonense, Elphidium mexicanum, Hanzawaia strattoni, Nonionella atlantica,* and *Quinqueloculina seminula* as secondary taxa. The normal marine assemblage had 71.1%

Elphidium excavatum and 12.2% *Ammonia parkinsoniana* with secondary taxa consisting of *Elphidium* sp., *Hanzawaia strattoni*, and planktonics. The estuarine biofacies consisted of only one taxon, *Elphidium excavatum*.

Pruitt et al. (2010) studied estuarine foraminifera in Core Sound and identified three estuarine biofacies (Table 3). Two (biofacies A and B) were identified as high salinity and one (biofacies C) as low salinity. Biofacies A consisted of *Ammonia parkinsoniana, Elphidium mexicanum,* and *Quinqueloculina* spp. Biofacies B consisted of *Ammonia parkinsoniana, Elphidium excavatum,* and *Quinqueloculina* spp. Biofacies A was located along the eastern side of Core Sound and Biofacies B was located in central Core Sound. Biofacies C, located adjacent to the mainland, consisted of agglutinated species *Ammotium salsum* as well as the calcareous species *Ammonia parkinsoniana* and *Elphidium gunteri*.

Grand Pre et al. (2011) conducted an in-depth analysis of a single core PS-03 located between Hatteras and Ocracoke Inlets in Pamlico Sound (Figure 1a). Six cluster-groups (F1-F6) were recognized from 404 contiguous samples and dominant foraminifera were identified and associated with depositional environments (Table 2). Foraminiferal assemblage F6 was typical of high brackish areas, F5 and F2 had open shelf foraminifera as well as planktonic foraminifera which are typical in shelf assemblages (Schnitker, 1971), F3 had assemblages similar to low-medium brackish areas, and F1 had a medium-high brackish estuarine assemblage. F4 had an assemblage that was indeterminate but probably estuarine.

Table 2: Down-core cluster groups of foraminifera in PS-03 and associated environments (Grand Pre et al., 2011).

Cluster Group	Depth	Characteristic foraminifera		Environment
F1	0.00–0.62	*Elphidium excavatum*	55.6%	medium-high brackish estuary
		Ammotium salsum	25.5%	
		Ammonia parkinsoniana	13.7%	
F2	0.62–1.82	*Elphidium excavatum*	73.6%	open shelf
		Ammonia parkinsoniana	15.8%	
		Ammonia tepida	3.3%	
		Ammotium salsum	2.6%	
F3	1.82–2.66	*Ammotium salsum*	46.7%	low-medium brackish estuary
		Trochammina ochracea	33.0%	
		Elphidium excavatum	20.0%	
F4	2.66–4.38	*Elphidium excavatum*	83.6%	indeterminate (probably estuarine)
		Ammonia parkinsonian	11.0%	
F5	4.38–5.38	*Elphidium excavatum*	64.2%	open shelf
		Ammonia parkinsoniana	23.0%	
		Ammonia tepida	3.3%	
		Elphidium mexicanum	3.0%	
F6	5.38–6.20	*Elphidium excavatum*	80.5%	high brackish estuary
		Ammonia parkinsoniana	16.7%	
		Ammonia tepida	1.7%	

Peek et al. (2013) identified five biofacies based on foraminifera cluster analysis in the Hatteras Flats and Buxton Woods area of North Carolina; low salinity estuary, high salinity estuary, normal marine salinity/flood-tide delta/shoal, normal marine/shoreface, and barrier island (Table 3). The low salinity estuary was dominated by foraminiferal species *Ammotium salsum, Elphidium excavatum,* and *Reophax bacillaris*. The high salinity estuary was characterized by *Elphidium excavatum, Ammonia parkinsoniana,* and *Haynesina germanica*. In both normal marine biofacies (normal marine salinity/flood-tide delta/shoal and normal marine/shoreface*) Elphidium excavatum* and *Ammonia parkinsoniana* were dominant. However, they differed in lithology; normal marine salinity/flood-tide delta/shoal consists of shelly muddy

sand, shelly sand, and shelly sandy mud; normal marine/shoreface consists of shelly sand. The barrier island biofacies was typically barren of foraminifera, however, when foraminifera were present, *Elphidium excavatum*, *Ammonia parkinsoniana*, and *Elphidium gunteri* were the only species that occurred.

Smith (2016) examined the Ocracoke Flood-Tide Delta (OFTD) and identified four biofacies; proximal OFTD, intermediate OFTD, distal OFTD, and paleo-valley (Table 3). The proximal OFTD biofacies contained 27 taxa with *Elphidium excavatum* (67%), *Elphidium mexicanum* (8%), and *Ammonia parkinsoniana* (7%) as the most abundant. The intermediate OFTD biofacies contained 22 taxa with *Elphidium excavatum* (56%), *Ammonia parkinsoniana* (25%), and *Ammonia tepida* (6%) as the most abundant. The distal OFTD contained nine rotaliid taxa with *Elphidium excavatum* (87%) and *Ammonia parkinsoniana* (12 %) as the most abundant. The paleo-valley contained few specimens of one taxon, *Elphidium excavatum.*

Table 3: Foraminifera in biofacies defined in studies from eastern North Carolina.

Author/Year	Location	Biofacies/ Environment	Dominant Species	Secondary Species
Grossman and Benson, 1967	Core Sound	Open Sound	*Ammobaculites* species *Ammotium* species *Elphidium* species	
		Saltwater Lagoon	*Elphidium gunteri* *Elphidium tumidum*	
		Estuarine	*Ammobaculites* species *Miliammina* species *Ammotium* species	
		Marsh	*Haplophragmoides* species *Trochammina* species *Miliammina* species	
		Tidal Delta	*Elphidium galvestonense* *Quinqueloculina* species *Triloculina* species	
Schnitker, 1971	Atlantic Coastal Shelf	Nearshore Shelf	*Elphidium excavatum*	
		Central Shelf	*Hanzawaia strattoni* *Reophax atlantica* *Peneroplis proteus* *Quinqueloculina seminula* *Asterigerina carinata*	
		Shelf Edge	*Lenticulina orbicularis* *Cibicides pseudoungerianus* *Amphistegina carinata*	
Workman, 1981	Nags Head	Inner Shelf - Low Diversity	*Elphidium excavatum*	*Elphidium gunteri* *Eggerella advena* *Quinqueloculina seminula* *Ammonia tepida* *Rosalina floridina*
		Inner Shelf - High Diversity	*Quinqueloculina* species	*Elphidium excavatum* *Elphidium gunteri* *Elphidium limatulum* *Ammonia parkinsoniana*
Culver et al., 2006	Pea Island	Nearshore Estuarine	*Ammobaculites dilatatus*	

		Marsh	*Trochamma inflata* *Miliammina fusca* *Tiphotrocha comprimata* *Jadammina macrescens* *Arenoparrella mexicana* *Haplophragmoides wilberti*	
		Normal Marine	*Elphidium excavatum* *Elphidium subarcticum* *Hanzawaia strattoni* *Buccella inusitata*	
Abbene et al., 2006	Pamlico Sound	Marsh	*Haplophragmoides wilberti* *Miliammina fusca* *Tiphotrocha comprimata* *Trochammina inflata*	*Ammoastuta inepta* *Haplophragmoides bonplandi*
		Estuarine A	*Elphidium excavatum* *Ammotium salsum*	*Ammobaculites dilatatus* *Textularia earlandi*
		Estuarine B	*Elphidium excavatum* *Ammotium salsum*	*Elphidium mexicanum*
		Normal Marine	*Cibicides lobatulus* *Elphidium galvestonense* *Elphidium mexicanum* *Elphidium subarcticum* *Hanzawaia strattoni* *Quinqueloculina seminula*	*Cibicides refulgens* *Quinqueloculina lamarckiana* *Quinqueloculina* species
Rosenberger, 2006	Portsmouth Island	Marsh	*Trochammina inflata* *Haplophragomides willberti*	
		Barrier Island	Barren	
		Inner Shelf A	*Rosalina* species *Elphidium subarcticum* *Planulina mera* *Buccella inusitata* *Elphidium macellum* *Quinqueloculina lamarckiana*	
		Inner Shelf B	*Glabratellina sagrai* *Buccella* species *Elphidium macellum*	
		Low Energy Shelf	*Ammonia tepida* *Rosalina* species A *Bolivina lowmani* *Stetsonia minuta* *Elphidium subarcticum*	

		Normal Salinity	*Quinqueloculina impressa* *Quinqueloculina jugosa* *Quinqueloculina* species *Quinqueloculina lamarckiana* *Stetsonia minuta* *Eponides repandus* *Textularia* cf. *T. gramen* *Miliammina fusca* *Elphidium gunteri*	
Twamley, 2006	Hatteras Village	Inner Shelf	*Elphidium excavatum* *Elphidium subarcticum* *Nonionella atlantica* *Hanzawaia strattoni*	
		Inlet	*Quinqueloculina seminula* *Quinqueloculina lamarckiana* *Quinqueloculina jugosa*	
		Low Energy Estuarine	*Elphidium excavatum* *Ammonia parkinsoniana*	
		High Energy Estuarine	*Ammotium salsum*	
		Marsh	*Arenoparrella mexicana* *Haplophragmoides wilberti* *Trochammina inflata*	
		Barrier Island	Barren	
Vance et al., 2006	Albemarle Sound	Nearshore Marine/Inlet	*Elphidium excavatum* *Hanzawaia strattoni* *Ammobaculites crassus* *Elphidium subarcticum* *Ammonia parkinsoniana*	
		Estuarine Shoal	*Ammobaculites crassus* *Ammotium salsum*	
		Estuarine	*Ammobaculites crassus* *Ammotium salsum* *Miliammina fusca* *Ammobaculites subcatenulatus*	
		Inner Estuarine	*Ammobaculites subcatenulatus*	*Ammotium salsum* *Miliammina fusca*
		Marsh	*Ammoastuta inepta* *Arenoparrella mexicana* *Haplophragmoides bonplandi* *Trochammina inflata*	

Foley, 2007	Pamlico Sound	High - Intermediate Salinity Estuary	*Ammonia parkinsoniana* *Ammotium salsum*	*Ammotium salsum* *Arenoparrella mexicana* *Elphidium excavatum* *Haplophragmoides wilberti* *Jadammina macrescens* *Quinqueloculina* species *Trochammina* species
		High Salinity Estuary	*Elphidium excavatum* *Ammonia parkinsoniana*	*Ammonia tepida* *Ammotium salsum* *Arenoparrella mexicana* *Elphidium galvestonense*
		Low salinity Estuary	*Ammotium salsum*	
		Low - Intermediate Salinity Estuary	*Ammotium salsum* *Trochammina inflata*	*Ammonia parkinsoniana* *Arenoparrella mexicana* *Elphidium excavatum* *Jadammina macrescens* *Trochammina* species *Deuterammina ochracea* *Thurammina* species
Hale, 2008	Ocracoke Island	High Energy Normal Salinity/Inlet	*Quinqueloculina frigida* *Quinqueloculina jugosa* *Quinqueloculina seminula* *Quinqueloculina lamarckiana* *Textularia* cf. *T.gramen* *Quinqueloculina* species *Asterigerina carinata* *Elphidium subarcticum* *Buccella inusitata* *Cibicides lobatulus* *Hanzawaia strattoni* *Elphidium mexicanum* *Nonionella atlantica* *Elphidium translucens* *Elphidium galvestonense* *Ammonia parkinsoniana*	
		Low energy Normal Salinity/Inner Shelf	*Elphidium poeyanum* *Haynesina germanica* *Elphidium excavatum* *Elphidium galvestonense* *Cibicides lobatulus* *Buccella inusitata*	

		Flood Tide Delta	*Glabratellina lauriei* *Elphidium mexicanum* *Hanzawaia strattoni* *Elphidium* species *Elphidium translucens* *Quinqueloculina* species *Rosalina floridana* *Elphidium galvestonense* *Cibicides lobatulus* *Elphidium gunteri* *Elphidium subarcticum* *Nonionella atlantica* *Textularia* cf. *T. gramen*	
		Estuarine Flat	*Ammonia parkinsoniana* *Elphidium gunteri* *Haynesina germanica*	
		Marsh	*Arenoparrella mexicana* *Haplophragmoides wilberti* *Haplophragmoides bonplandi* *Haplophragmoides manilaensis* *Tiphotrocha comprimata* *Jadammina macrescens* *Trochammina inflata*	
Metger, 2009	Pamlico Sound near Ocracoke Inlet	Low Brackish estuary	*Elphidium excavatum* *Ammonia parkinsoniana* *Haynesina germanica*	
		High Brackish Estuary	*Elphidium excavatum* *Ammonia parkinsoniana*	
		High Brackish with Inlet Influence	*Elphidium excavatum* *Ammonia parkinsoniana* *Hanzawaia strattoni* *Quinqueloculina* species	
		Inlet	*Elphidium excavatum*	*Ammonia parkinsoniana* *Elphidium galvestonense* *Elphidium mexicanum* *Hanzawaia strattoni* *Nonionella atlantica* *Quinqueloculina seminula*
		Normal Marine	*Elphidium excavatum* *Ammonia parkinsoniana*	*Elphidium* species *Hanzawaia strattoni* planktonics
		Estuary	*Elphidium excavatum*	

Pruitt et al., 2010	Core Sound	High Salinity A (East)	*Ammonia parkinsoniana* *Elphidium mexicanum* *Quinqueloculina* species	
		High Salinity B (Central)	*Ammonia parkinsoniana* *Elphidium excavatum* *Quinqueloculina* species	
		Low Salinity (West)	*Ammotium salsum* *Ammonia parkinsoniana* *Elphidium gunteri*	
Grand Pre et al., 2011	Between Hatteras and Ocracoke Inlet	Marsh	*Elphidium excavatum* *Ammotium salsum* *Ammonia parkinsoniana*	
		Open Shelf	*Elphidium excavatum* *Ammonia parkinsoniana* *Ammonia tepida* *Ammotium salsum* *Elphidium mexicanum*	
		Low - Medium Brackish	*Ammotium salsum* *Trochammina ochracea* *Elphidium excavatum*	
		Indeterminate (Probably Estuarine)	*Elphidium excavatum* *Ammonia parkinsonian*	
		High Brackish	*Elphidium excavatum* *Ammonia parkinsoniana* *Ammonia tepida*	
Peek et al., 2013	Hatteras Flat/Buxton Woods	Low Salinity Estuary	*Ammotium salsum* *Elphidium excavatum* *Reophax bacillaris*	
		High Salinity Estuary	*Elphidium excavatum* *Ammonia parkinsoniana* *Haynesina germanica*	
		Normal Marine Salinity/Flood - Tide Delta/Shoal	*Elphidium excavatum* *Ammonia parkinsoniana*	
		Normal Marine/Shoreface	*Elphidium excavatum* *Ammonia parkinsoniana*	
		Barrier Island	Barren	

Smith, 2016	Ocracoke flood-tide delta	Proximal Ocracoke Flood - Tide Delta	*Elphidium excavatum* *Elphidium mexicanum* *Ammonia parkinsoniana*	
		Intermediate Ocracoke Flood - Tide Delta	*Elphidium excavatum* *Ammonia parkinsoniana* *Ammonia tepida*	
		Distal Ocracoke Flood - Tide Delta	*Elphidium excavatum* *Ammonia parkinsoniana*	
		Paleo - valley	*Elphidium excavatum*	

Several generalities can be derived from the foregoing studies. Common marsh biofacies consist of *Trochammina inflata, Miliammina fusca, Haplophragmoides wilberti, Arenoparrella mexicana,* and *Jadammina macrescens* (Culver et al., 2006; Abbene et al., 2006; Rosenberger, 2006; Twamley, 2006; Vance et al., 2006; Hale, 2008). There are high salinity and low salinity estuarine biofacies where *Elphidium excavatum, Ammotium salsum,* and *Ammonia parkinsoniana* are present. However, the higher the salinity, the greater the percentage of *Elphidium excavatum;* conversely the lower the salinity, the greater the percentage of *Ammotium salsum* (Cronin et al., 2000; Abbene et al., 2006; Twamley, 2006; Foley, 2007; Metger, 2009; Pruitt et al., 2010; Grand Pre et al., 2011; Peek et al., 2013). An inlet biofacies consists of *Quinqueloculina* spp. and *Elphidium excavatum* (Twamley, 2006; Metger, 2009). Normal marine biofacies include, *Elphidium excavatum, Elphidium subarcticum, Hanzawaia strattoni, Haynesina germanica, Cibicides lobatulus, Ammonia parkinsoniana,* and *Quinqueloculina* spp. (Culver et al., 2006; Abbene et al., 2006; Vance et al., 2006; Hale, 2008; Metger, 2009; Grand Pre et al., 2011; Peek et al., 2013). An inner shelf biofacies, consists primarily of *Elphidium subarcticum, Elphidium excavatum, Quinqueloculina* spp., *Haynesina germanica,* and *Hanzawaia strattoni* (Schnitker, 1971; Workman, 1981; Rosenberger, 2006; Twamley, 2006). Normal marine and inner shelf biofacies are similar; however, they are more diverse than estuarine biofacies. Barrier Island biofacies are typically barren of foraminifera (Culver et al., 2006, Twamley 2006; Peek et al., 2013) but where foraminifera are present they include *Elphidium excavatum*, *Ammonia parkinsoniana*, and *Elphidium gunteri* (Peek et al., 2013).

2.4 Sedimentology

Numerous studies have focused on Pamlico Sound organic-rich muds and sands (Wells and Kim, 1989; Riggs et al., 1993; Riggs, 1996; Riggs and Ames, 2003; Peek et al., 2013, Smith, 2016; Zaremba et al., 2016). Organic material from erosion and flushing of swamp forests and marsh shorelines are introduced into Pamlico Sound through two major tributaries, the Neuse River and Tar-Pamlico River (Riggs et al., 1993; Riggs and Ames 2003). Additional sediment sources to the APES include shoreline erosion, continental shelf (via inlets and overwash), and autochthonous biogenic production (Wells and Kim, 1989). While sand in the west side of Pamlico Sound originates from the mainland and discharged into the sound through rivers, the sand from the central and eastern portions of Pamlico Sound are sourced from the barrier islands and offshore (Duane, 1964; Wells and Kim, 1989). Sand occurs on the perimeter of the APES and decreases towards the center of the basin. Within the APES there are four sediment types: sand, peat, organic-rich mud, and organic-poor mud. Sediments within Pamlico Sound were 35.9% inorganic sand, 2.9% organic sand, 53.8% inorganic mud, and 7.4% organic-rich mud, as a percentage of the total bottom area of the basin (Riggs et al., 1993).

Wells and Kim (1989) studied the sediments of Pamlico Sound in terms of the grain-size, mineralogy, and sedimentary structures. They described the sand sediments in Pamlico Sound as well sorted, negatively skewed when subjected to winnowing, and positively skewed when not subjected to waves and currents. The mineral content of the coarse sand fraction of the APES show that quartz (60–90%) is the dominant mineral, with heavy minerals (1–15%) , shell and wood fragments (2–20%), and mica (up to 10%) part of the sand fraction. They also found that in the basins of the APES, that a thin layer of mud is deposited over sand sheets during periods

of high sedimentation and that the sand and mud can become suspended again during storm events.

Peek et al. (2013) described 10 lithofacies from 16 vibracores Hatteras Flats and Buxton area of North Carolina. She identified seven sand lithofacies; sand (S), shelly sand (shS), shelly gravelly sand (shgS), muddy sand (mS), shelly muddy sand (shmS), organic-rich muddy sand (orgmS), and organic-rich sand (orgS), one interbedded lithofacies; shelly interbedded mud and sand (shI), and two mud lithofacies; sandy mud (sM) and shelly sandy mud (shsM). Cores from Buxton Woods consists primarily of sand (S), shelly sand (shS) and organic-rich sand (orgS). The shelly sand (shS) contained up to 10% shell material and comprise the basal sediments in the Buxton Woods cores. Cores from the Hatteras Flats contain all lithofacies except for sand (S). The top of the Hatteras Flats cores is interpreted to represent the modern estuarine depositional environment which consists of muddy sand (mS) or organic muddy sand (orgmS). The top of the Buxton cores is interpreted as the modern shoreface deposit consisting of a moderately-well sorted (0.43–0.90 ϕ) slightly fine skewed (-0.34–0.15 ϕ), organic-rich sand (orgS) that has a medium to fine (1.18–2.36 ϕ) sand mean grain-size. Furthermore, Peek et al. (2013) interpreted five environmental facies from lithofacies and biofacies data; low-salinity estuary, higher-salinity estuary, normal marine salinity/large FTD/submarine shoal, normal marine salinity/upper shoreface, and barrier island sands (Table 4).

Table 4: Environmental facies descriptions (Peek et al., 2013).

Environmental Facies (EF)	Lithology	Biofacies	Common Foraminiferal Species	Depth Range Relative to MSL (m)	Location; No. of Cores
I. Lower-salinity estuary	Organic and muddy sand	E	*Ammotium salsum* *Elphidium excavatum*	–2 to –6.5	Hatteras Flats; 15
II. Higher-salinity estuary	Shelly mud and sand	D	*Elphidium excavatum* *Ammonia parkinsoniana*	–2 to –9	Hatteras Flats; 6
III. Normal marine salinity/ large FTD/submarine shoal	Shelly sand	A, B, C	*Elphidium excavatum* *Ammonia parkinsoniana* *Hanzawaia strattoni*	–1.5 to –8.5	Hatteras Flats; 16
IV, Normal marine salinity/ upper shoreface	Shelly sand	A, B, C	*Elphidium excavatum* *Ammonia parkinsoniana* *Elphidium gunteri*	2.5 to –5.8	Buxton beach ridges; 6
V, Barrier island sand	Organic and shelly sand	A, B, C	*Ammonia parkinsoniana* *Elphidium gunteri*	4.0 to –4.8	Buxton beach ridges; 7

Smith (2016) described lithologies in five vibracores from the Ocracoke Flood-Tide delta (OFTD). She identified eight sand lithofacies; sand (S), gravelly sand (gS), slightly gravelly sand ((g)S), muddy sand (mS), organic-rich muddy sand (mS-org), gravelly muddy sand (gmS), organic-rich gravelly muddy sand (gmS-org), and slightly gravelly muddy sand ((gmS), six mud lithofacies; mud (M), organic-rich mud (M-org), sandy mud (sM), organic-rich sandy mud (sM-org), organic-rich gravelly sandy mud (gsM-org), and slightly gravelly sandy mud ((g)sM), and one other lithofacies; peat (P). The sand fraction of the lithofacies are fine-very fine sands (2.08–3.11 ϕ), well-very well sorted (0.32–0.50 ϕ), and skewness ranges from very fine skewed to very coarse skewed (0.39 to -0.34 ϕ) throughout the samples. Utilizing the lithofacies and biofacies Smith (2016) interpreted six environmental facies; high energy normal marine salinity FTD, low energy normal marine salinity FTD, High salinity estuarine, undetermined estuarine (mid-high salinity), sand flat/shoal, and freshwater riverine swamp forest (Table 5).

Table 5: Environmental facies descriptions and characteristics (Smith, 2016). Mbsl- meters below sea level, and mbsf- meters below seafloor.

EF	Lithologies & Associated Characteristics	Biofacies	Foraminiferal Species (listed decreasing in abundance)	Approximate Depth Range (mbsl)	Cores (VC) & Surface (S) Samples Present In (mbsl)	Cores (VC) & Surface Samples (S) that contain Planktonic Species (mbsl)	Location/ Presence of Foraminiferal Core (VC) & Surface (S) Samples	Barren Samples
I. High Energy Normal marine salinity FTD	Gravelly sand and sand: shells, mottling, mud burrows, & laminations	A	*Elphidium excavatum, Elphidium mexicanum, Ammonia parkinsoniana, Elphidium galvestonense, Hanzawaia strattoni, Elphidium gunteri, Cibicides lobatulus, Quinqueloculina seminula, Haynesina germanica, Nonionella atlantica, Elphidium* sp., *Elphidium translucens, Quinqueloculina* sp., *Elphidium subarcticum, Trifarina angulosa, Quinqueloculina lamarckiana, Ammonia tepida, Elphidium poeyanum, Rosalina floridina, Buccella inusitata, Rosalina* sp., *Trochammina* sp., *Miliolinella subrotunda, Asterigerina carinata, Quinqueloculina jugosa, Valvulineria* sp., *Guttulina lacteal*	4.70–1.50; VC5A: 2.64–1.50; VC8A: 4.70–4.30	VC5A: (2), VC8A: (1); S (13): S1, S2, S3, S4, S5, S6, S7, S8, S11, S14, S16, S17, S22 (top of VC5A)	S14, S16, S17; VC5A (2.60–2.57)	Intermediate & Proximal OFTD	
II. Low Energy Normal marine salinity FTD	Gravelly muddy sand & muddy sand; shells, mottling, mud burrows, laminations, & charcoal & wood debris	B	*Elphidium excavatum, Ammonia parkinsoniana, Ammonia tepida, Elphidium galvestonenese, Elphidium gunteri, Elphidium mexicanum, Cibicides lobatulus, Nonionella atlantica, Hanzawaia strattoni, Elphidium poeyanum, Haynesina germanica, Bolivina lowmani, Elphidium* sp., *Valvulineria* sp., *Quinqueloculina seminula, Guttulina lactea, Rosalina* sp., *Buccella inusitata, Rosalina floridana, Elphidium subarcticum, Trifarina angulosa, Quinqueloculina jugosa*	6.70–3.0; VC3B: 6.70–3.30; VC8A: 5.30–3.30	VC3B: (6), VC8A: (3); S (2): S12, S18 (top of VC3B)	VC3B (4.44–4.42, 5.18–5.16, 5.69–5.67); VC8A (4.05–4.02, 4.90–4.87)	Intermediate OFTD	
III. High salinity estuarine	Sandy mud, muddy sand, & gravelly muddy sand; charcoal, wood, & shell fragments	C	*Elphidium excavatum, Ammonia parkinsoniana, Elphidium galvestonenese, Hanzawaia strattoni, Elphidium* sp., *Elphidium mexicanum, Ammonia tepida, Buccella inusitata, Haynesina germanica*	9.50–3.0; VC1: 9.50–4.0; VC3B: 7.40–6.70; VC8A: 3.30–3.0	VC1: (13), VC3B: (1); S (4): S9, S13, S19 (top of VC1), S21 (top of VC8A)	S19, S21	Distal OFTD; S21 exception-intermediate OFTD	
IV. Undetermined estuarine (mid-to high salinity)	Muddy sand with rare charcoal & wood debris	D	*Elphidium excavatum*	8.20–7.40; VC1	VC1: (3)		Distal OFTD	

EF	Lithologies & Associated Characteristics	Biofacies	Foraminiferal Species (listed decreasing in abundance)	Approximate Depth Range (mbsl)	Cores (VC) & Surface (S) Samples Present In (mbsl)	Cores (VC) & Surface Samples (S) that contain Planktonic Species (mbsl)	Location/ Presence of Foraminiferal Core (VC) & Surface (S) Samples	Barren Samples
V. Sand Flat/Shoal	Slightly gravelly sand, & sand; shells, shell fragments, mud mottling	N/A	*Elphidium excavatum, Ammonia parkinsoniana, Elphidium gunteri*	3.70–1.20; VC2B	VC2B: (2); S (2): S10, S15		Distal OFTD	VC2B: (2.88–2.85); S20 (top of VC2B)
VI. Freshwater Riverine Swamp Forest	Peat & Mud; charcoal & wood debris	N/A	Barren	9.60–9.50; VC1	VC1: (2)		Distal OFTD	VC1: (9.52–9.50, 9.60–9.58)

Zaremba et al. (2016) studied the lithologies between seismic horizons within the Pamlico Sound basin (Table 6). They determined that there were six Holocene units which are predominantly homogenous mud to muddy sand with burrows. The Pleistocene deposits that they describe vary from muddy shell fragments to sandy gravel and can be stained red or orange. Unit 1 (0.5–1.5 m thick) has an approximate age of >8000 cal yr. BP and consists of fluvial channel deposits of the lowstand systems tract. Unit 2 (0.5–1.5 m thick), with an age of approximately 8000–7000 cal yr. BP, is characterized by tidal or bayhead delta deposits within a fetch-limited system. Unit 3 (0–4 m thick), with an age of approximately 7000–4000 cal yr. BP is characterized by sandy mud (mud with fine-grained sand composed of quartz, mica, and shell material) and mud (mud with fine-grained sand composed of quartz, mica, shell fragments and *in-situ* material). Unit 4 (3–5 m thick) with an age of approximately 4000–1200 cal yr. BP exhibits a decrease in the sand/mud ratio as a result of the formation of barrier islands, restricting the influx of sand. Unit 5 (1–1.6 m thick), with an age of approximately 1200–500 cal yr. BP, shows an increase in sand content in Pamlico Sound. Unit 6 (0.4–1.2 m thick) represents the last ca. 500 years, and exhibits an increase in the amount of mud.

2.5 Geophysics

Geophysical data from ground penetrating radar (GPR), chirp seismic, and boomer data have been used to define the stratigraphic framework and interpret the geological history of the Pamlico Sound region (Sager and Riggs, 1998; Mallinson et al., 2005; Culver et al., 2007; Metger, 2009; Mallinson et al., 2010; Grand Pre et al., 2011; Zaremba, 2014). Mallinson et al. (2010, 2011) mapped paleo-inlet channels along the Outer Banks using GPR. These data showed that greater inlet activity occurred during the Medieval Climate Anomaly (MCA) and Little Ice

Age (LIA), and corroborates observations of greater barrier segmentation during the MCA as recognized by Culver et al. (2007) and Grad Pre et al. (2011) based on foraminiferal assemblages.

Zaremba et al. (2016) collected 470 km of chirp seismic data and correlated the data to vibracores. Nine seismic reflections and eight stratigraphic units were identified within Pamlico Sound (Table 6). Many of Zaremba's reflections are used in this study. Geophysical data were crucial to understanding the antecedent topographic controls on the modern morphology of the APES, and in correlating units throughout the region to understand paleo-environmental change during the Holocene (Zaremba et al., 2016; Mallinson et al., 2017).

Table 6: Summary of seismic reflections and seismic units (SU); interpretations based on seismic data combined with core logs, grain-size analysis, and radiocarbon age estimates (Zaremba et al. 2016).

Reflector	SU	Approximate age (cal yr. BP)	Characteristics	Interpretation
H_{SF}		modern		Modern sediment/water interface
	6	500–0	Transparent, delineated by H_{500} and H_{SF}, 0.4–1.2 m thick.	Increased barrier island continuity allowed for deposition of muddy deposits
H_{500}		ca. 500	Medium amplitude, high continuity within the northern basin, low amplitude low continuity within the southern basin.	Delineates top of the 500–1200 cal yr. BP unit; acoustic impedance is a result of finer-grained mud deposits on top of the sandier unit 5.
	5	1200–500	Transparent, delineated by H_{500} and H_{1000}, 1.0–1.6 m thick.	Extensive segmentation of barrier islands increased hydrodynamics and sand content within the Sound.
H_{1000}		ca. 1200	Low to medium in amplitude, low continuity.	Delineates increase in estuarine hydrodynamics/marine influence.
	4b	2500–1200	Generally transparent, but exhibiting a higher amplitude signal toward the top.	Restricted, reduced salinity lagoonal deposition (sM, M) within the Pamlico Sound
H_{2500}		ca. 2500	Medium amplitude, medium continuity. Limited in extent to the southern basin, and western and southern regions of the northern basin. Locally separates Unit 4 into two subunits (4a and 4b).	A minor increase in estuarine hydrodynamics primarily within the southern basin
	4a	4000–1200	Mostly transparent but sometimes containing multiple discontinuous reflections. Most prominent in the northern basin (3–5 m thick).	Fining upward sequence. Initial increase in marine influence, followed by formation of barrier islands which decreased estuarine hydrodynamics and restricted the influx of sand into the Sound.

Reflector	SU	Approximate age (cal yr. BP)	Characteristics	Interpretation
H_{4000}		ca. 5000–3000	High-medium amplitude, high continuity. Rarely occurs in the southern basin.	Erosional surface; represents an increase in estuarine hydrodynamics likely as a result of an increase in fetch and tidal energy as interfluves are overtopped.
	3	7000–4000	Varies in thickness from 0.0–4.0 m, however, thickest sections are likely not imaged due to gas attenuation.	Restricted, reduced salinity lagoonal deposition (sM, M) within the Pamlico Sound.
H_{RS2}		<8000–0	High amplitude, high continuity, variable relief, amalgamates with multiple surfaces.	Holocene bay ravinement surface, truncates the Pleistocene in most locations.
	2	<8000–7000	Rare in the stratigraphic record, thin deposit 0.5–1.5 m thick and confined to paleo-valleys; clinoforms in data are rare.	Tidal and/or bayhead delta deposition occurring within a fetch-limited system, before sea level rose above the interfluves.
H_{RS1}		<8000–7000	Medium amplitude; confined to paleo-valleys; rarely imaged.	Holocene ravinement, interpreted to be the result of tidal scour, truncates Pleistocene deposits.
	1	>8000	0.5–1.5 m thick, transparent, rare in the stratigraphic record.	Fluvial channel deposits of the lowstand systems tract.
P_{LGM}		>8000	High to medium amplitude, high continuity.	Subaerial unconformity exhibiting incised fluvial valleys. Reworked Pleistocene shells and iron staining, or compacted blue-grey clay characterize the surface in cores.

3. Materials and Methods

3.1 Geophysical Data

Approximately 60 km of chirp seismic data were collected northwest of Hatteras Inlet using an EdgeTech 2–16 kHz sub-bottom profiling system and Discover acquisition software (Figure 5). The towfish was submerged to 2 meters below sea-level (mbsl) and towed at 3–4 knots using East Carolina University's R/V Riggs. Navigation was received via a WAAS-enabled Garmin GPS. Seismic lines were digitized using Kingdom Suite software (v 8.8) and SonarWiz6 software to define the stratigraphic framework of the ridges. Correlation of seismic data to core data used a velocity of 1600 m/s (Mallinson et al., 2010; Zaremba, 2014; Zaremba et al., 2016).

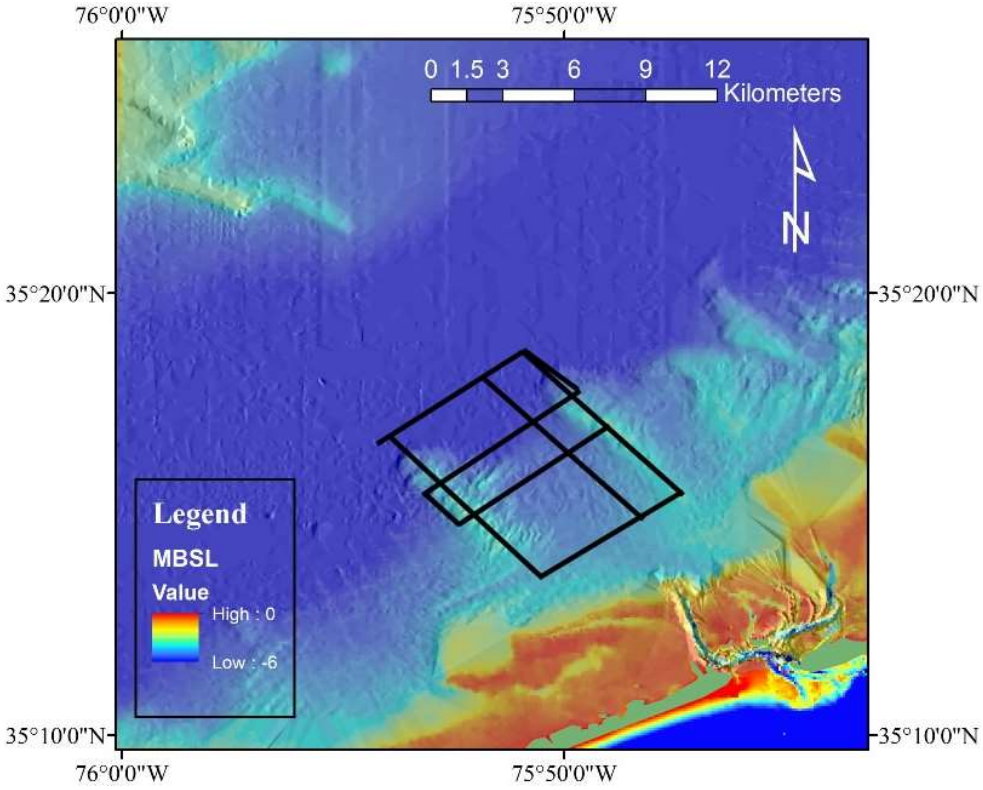

Figure 5: Seismic track along vibracore locations.

3.2 Cores

Six vibracores were obtained from the study area in eastern Pamlico Sound in 2016 (Figure 6). Two additional cores, PS-07 and OCR-07-S203, were acquired by Riggs in 1997, and by Metger in 2007, respectively (Figure 6). PS-07 and OCR-07-S203 were previously analyzed for foraminiferal assemblages, sedimentary facies, and radiocarbon age estimates (Foley, 2007; Metger, 2009; Zaremba et al., 2016). Additionally PS-07 was analyzed for bulk sediment magnetic susceptibility (Zaremba et al., 2016).

Latitude and longitude, depth below sea level, and recovered length were recorded for all cores (Table 7). Vibracores were sectioned at 1.5 m intervals and halved. One half was sealed and bagged for archiving. The other half was used for logging, sampling, and photographing (Appendices A, B).

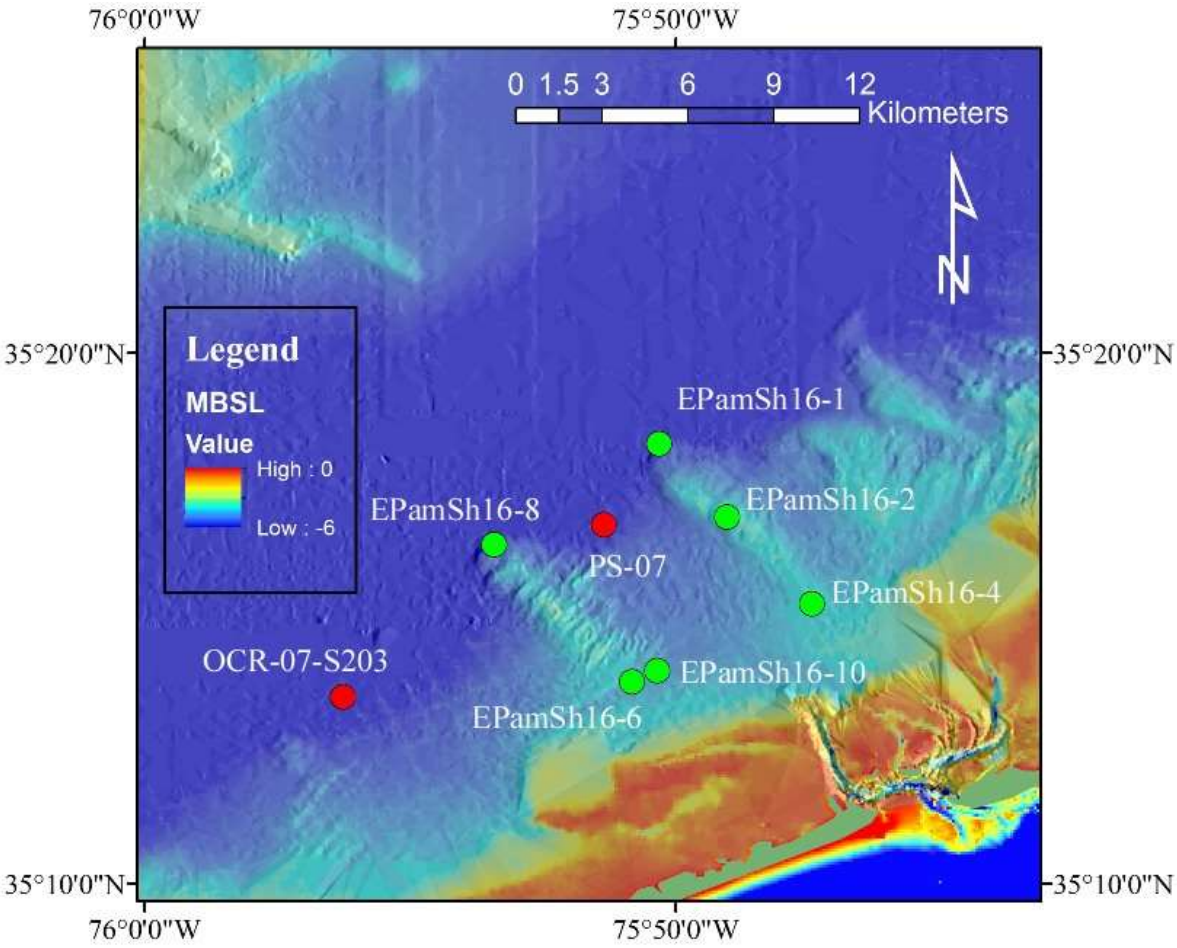

Figure 6: Location of vibracores in this study.

Table 7: Latitude, longitude, water depth, and sediment recovery data for vibracores used in this study.

Core #	Latitude (N)	Longitude (W)	Water depth (m)	Recovered length (m)
PS-07	35°16.760’	75°51.359’	6.50	3.77
OCR-07-S203	35°13.516’	75°56.274’	6.80	8.06
EPamSh16-1	35°18.283’	75°50.324	6.10	6.40
EPamSh16-2	35°16.904’	75°49.038’	3.57	1.12
EPamSh16-4	35°15.267’	75°47.443’	3.72	3.74
EPamSh16-6	35°13.797’	75°50.827’	4.39	3.36
EPamSh16-8	35°16.384’	75°53.424’	4.82	1.37
EPamSh16-10	35°14.009’	75°50.353’	4.60	2.70

3.3 Bulk Sediment Magnetic Susceptibility and Sedimentology

353 samples were acquired at 5 cm intervals from six vibracores and used for grain-size and bulk sediment magnetic susceptibility (BMS) analyses and 210 of the samples were analyzed for grain-size. Samples were dried at 40°C, weighed, and then disaggregated with mortar and pestle. Samples with shell fragments were lightly disaggregated with the mortar and pestle or were not used for BMS based on visual amount of shell material to not interfere with grain size analyses afterwards. 5.5 cm^3 aliquots of sample were analyzed using a Kappabridge MFK1-A by Advanced Geoscience Instruments Company (AGICO). Calibration of the instrument was done using a standard provided by AGICO with a known BMS value. BMS values for the sample holder were measured three times, averaged, and subtracted from the BMS value of each sample. A reference sample (TER15-GC5, 19.2–20.5 cm, Hindes, 2016) was run at the beginning of every sampling session to account for machine drift. The calculated error of the reference samples is 7% (n=30 measurements). Sample measurements were repeated five times to reduce variability and averaged.

After BMS analyses, samples were soaked in 50 ml of 0.05 % sodium hexametaphosphate ($(NaPO_3)_6$), for no less than 24 hours to disaggregate the sediments. A sonicator was used for 4 minutes to further disaggregate the sample. Each sample was then wet sieved over a 4 ϕ sieve to remove the mud fraction. The sand fraction was then placed in an oven at 40 °C overnight to dry. Grain-size distribution of the sand fraction was determined using a Ro-Tap (15 minutes per sample) with nested sieves from -2 ϕ to 4 ϕ at 0.5 ϕ intervals. The average statistics (mean, skewness, sorting, and kurtosis) were calculated using Gradistat

software version 4 (Blott and Pye, 2001). Percent sand was calculated by dividing weight of the dry sand fraction by the total weight of the dry sample minus the weight of the gravel.

3.4 Surface Sample Analysis

Twenty-five surface samples were collected from the estuarine floor using a Shipek grab sampler and latitude and longitude were recorded (Figure 7). Samples were rinsed of salt water and dried in an oven for 24 hours at 40 °C. After drying, samples were disaggregated (if sample was muddy). Approximately 30 g of sample was used for analysis and soaked in sodium hexametaphosphate ($(NaPO_3)_6$) for 24–36 hours then dried again at 40 °C for 24 hours. Samples were then processed identically to samples for core sedimentological analysis.

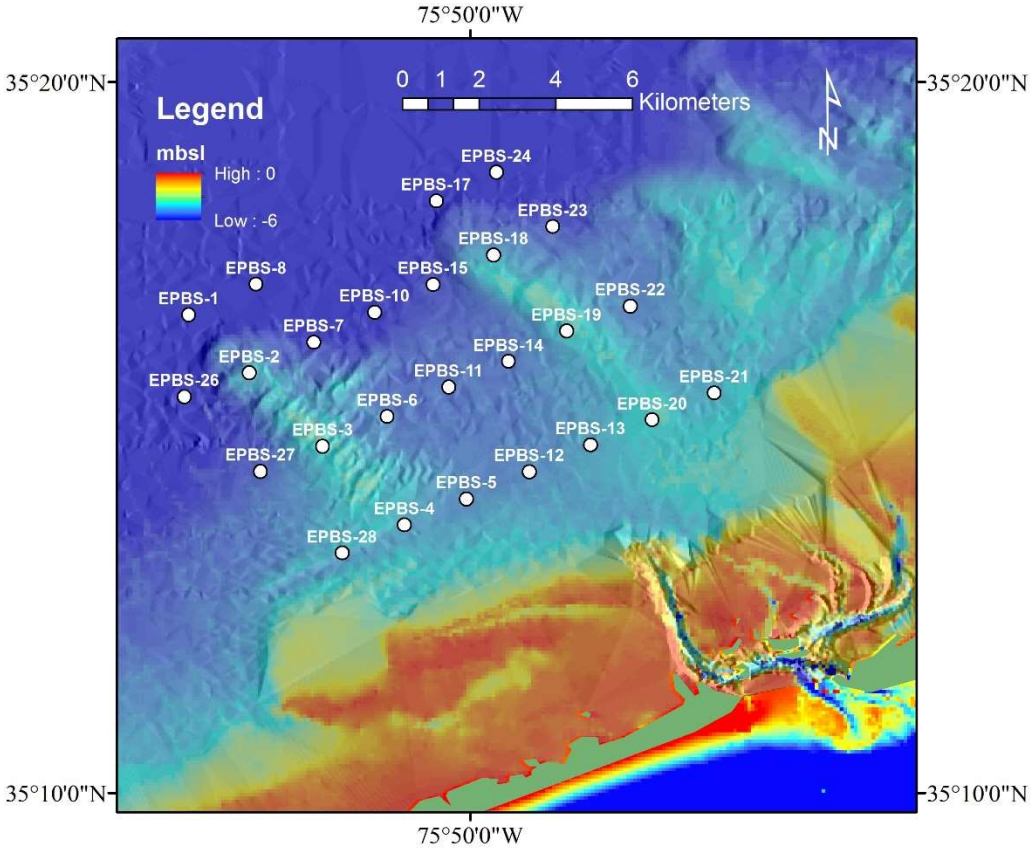

Figure 7: Surface sample locations in Pamlico Sound behind Hatteras Island.

3.5 Foraminiferal Assemblages

Nineteen samples were collected from the six vibracores and processed for benthic foraminifera following the protocol in Culver et al. (2008). Samples were first dried at 40 °C, weighed, and lightly disaggregated with mortar and pestle. Samples were soaked in 0.05 % sodium hexametaphosphate and one tablet of sodium hydroxide for 12–24 hours to facilitate separation of mud and sand grains. Samples were then washed over nested sieves of 710 µm and 63 µm to separate coarse sand and gravel (>710 µm), medium-fine sand (63–710 µm), and mud

(<63 μm) fractions. The >710 μm fraction and 63–710 μm fraction were dried overnight at 40 °C in plastic weigh boats. Once dried, the >710 μm fraction was archived in glass vials.

The 63–710 μm fraction was floated using sodium polytungstate to separate foraminiferal tests from siliciclastic sand grains (Munsterman and Kerstholt, 1996). From the floated portion, samples were spread onto a 45–square picking tray in aliquots of manageable sizes obtained using a micro-splitter. One hundred specimens were picked per sample. If less than 100 specimens were present, the entire sample was picked (Cronin et al., 2000; Grand Pre et al., 2011). Nine species were distinguished and identifications were confirmed by comparison with type and comparative material in the Cushman Collection, Smithsonian Institution, Washington D.C. (Appendix G).

3.6 Geochronology

In-situ articulated mollusk shells were used for radiocarbon dating and sent to National Ocean Science Accelerator Mass Spectrometer (NOSAMS) at Woods Hole, Massachusetts. The sample locations were determined by the availability of material and association with lithological units. Samples were prepared using guidelines provided by the NOSAMS webpage. CALIB 7.00 software and Marine13 (Stuiver and Reimer, 1993) was used to calibrate ages received from NOSAMS. A marine reservoir effect of 102 +/- 70 years (Thomas, 2008) calculated in Beaufort, North Carolina was applied to all age estimates.

4. Results/Interpretations

4.1 Lithofacies

Eleven lithofacies were identified within the cores (Table 8): mud (M), sandy mud (sM), slightly gravelly sandy mud ((g)sM), bioturbated slightly muddy sand (biot (m)S), rooted bioturbated slightly muddy sand (rt-biot (m)S), muddy sand (mS), bioturbated muddy sand (biot mS), mottled bioturbated muddy sand (mot-biot mS), mixed slightly gravelly muddy sand (mxd (g)mS), mixed gravelly muddy sand (mxd gmS), bioclastic gravelly muddy sand (bio gmS). Mud (M) and sandy mud (sM) lithologies have sharp erosional contact with all sand units. There are gradational contacts between each of the sand units. When shell material is greater than 30 % in a sand unit, the gradational contact occurs over a narrower depth range than between sand units of <30 % shell material.

Table 8: Characteristics of lithofacies in vibracores.

Lithofacies	Figure	Color	Sedimentary Structures	% Mud	% Sand	% Gravel	% Bioclasts
mud (M)	8	5Y 3/1	burrowing	94.9 to 98.5	1.5 to 4.9	0.0 to 0.3	0
sandy mud (sM)	9	5Y 5/1	burrowing, shells	55.6 to 96.3	3.7 to 29.6	0.0 to 0.1	1
slightly gravelly sandy mud ((g)sM)	10	5Y 3/1	shells	82.4 to 82.7	15.2 to17.3	0.0 to 2.4	2
bioturbated slightly muddy sand (biot (m)S	11	10YR 6/1 5Y 4/1	burrowing	0.3 to 10.7	87.4 to 99.8	0.0 to 2.0	0
rooted bioturbated slightly muddy sand (rt-biot (m)S)	12	10YR 3/2 5Y 4/1	roots, burrowing	0.1 to 5.4	94.4 to 99.9	0.0 to 1.0	0
muddy sand (mS)	13	5Y 5/1	shells	3.1 to 36.7	63.3 to 96.9	0.0 to 2.4	1–20
bioturbated muddy sand (biot mS)	14	10YR 6/1	burrowing, shells	4.6 to 35.2	64.8 to 95.4	0.0 to 0.3	<1
mottled bioturbated muddy sand (mot-biot mS)	15	5Y 5/1	mottling, burrowing, shells	5.0 to 32.9	67.1 to 94.3	0.0 to 2.5	<1
mixed slightly gravelly muddy sand (mxd (g)mS)	16	5Y 4/1	shells	4.5 to 17.5	82.5 to 94.3	0.1 to 2.5	30–40
mixed gravelly muddy sand (mxd gmS)	17	5Y 5/1	shells	4.5 to 31.1	61.9 to 95.5	0.0 to 7.7	30–40
bioclastic gravelly muddy sand (bio gmS)	18	5Y 5/1	shells	5.5 to 12.3	67.1 to 93.9	0.6 to 20.7	70–95

4.1.1 Mud (M)

The mud lithofacies is grey (5Y 3/1), (Table 8, Figure 8) and is 0.30 m thick. It is composed of mud (95–99 %), well sorted (0.92–1.62 ϕ) very coarse to fine skewed (-0.79–0.27 ϕ) medium sand (0.92–1.62 ϕ, 1–5 %), and bioclasts (*Anadara* sp., unidentifiable shell fragments, 1 %) (Table 9). The mineralogy of the sand is made up of quartz (91 %), feldspars (1 %), micas (3 %), and heavy minerals (5 %). This lithofacies appears in core EPamSh16-1 (0.2–0.6 mbsf: meters below sea floor) basinward of the eastern sand ridge (Appendix B).

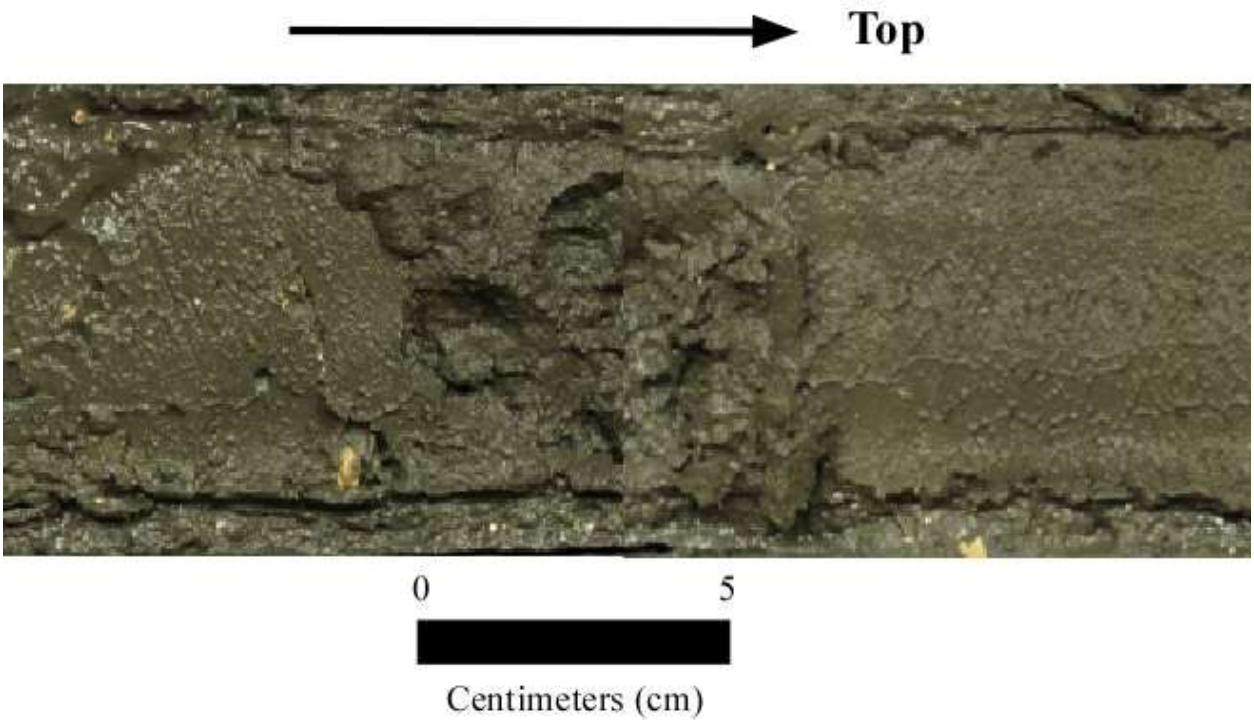

Figure 8: Image of mud (M) lithofacies from EPamSh16-1 at 0.30–0.50 mbsf.

4.1.2 Sandy mud (sM)

The sandy mud lithofacies is light grey (5Y 5/1) (Table 8, Figure 9) and ranges from 0.6–2.8 m thick. It is composed of mud (55–96 %), well sorted (0.24–1.26 ϕ) very coarse to fine skewed (-0.79–0.27) very fine sand (2.59–3.69 ϕ, 4–30 %), and bioclasts (unidentifiable shell fragments, <1 %) (Table 9). The mineralogy of the sand is made up of quartz (84 %), feldspars (1 %), micas (5 %), and heavy minerals (10 %). This lithofacies appears in two cores EPamSh16-1 (0.6–1.2; 1.3–4.1 mbsf) basinward of the eastern sand ridge and EPamSh16-10 (0.8–2.3 mbsf) (Appendix B).

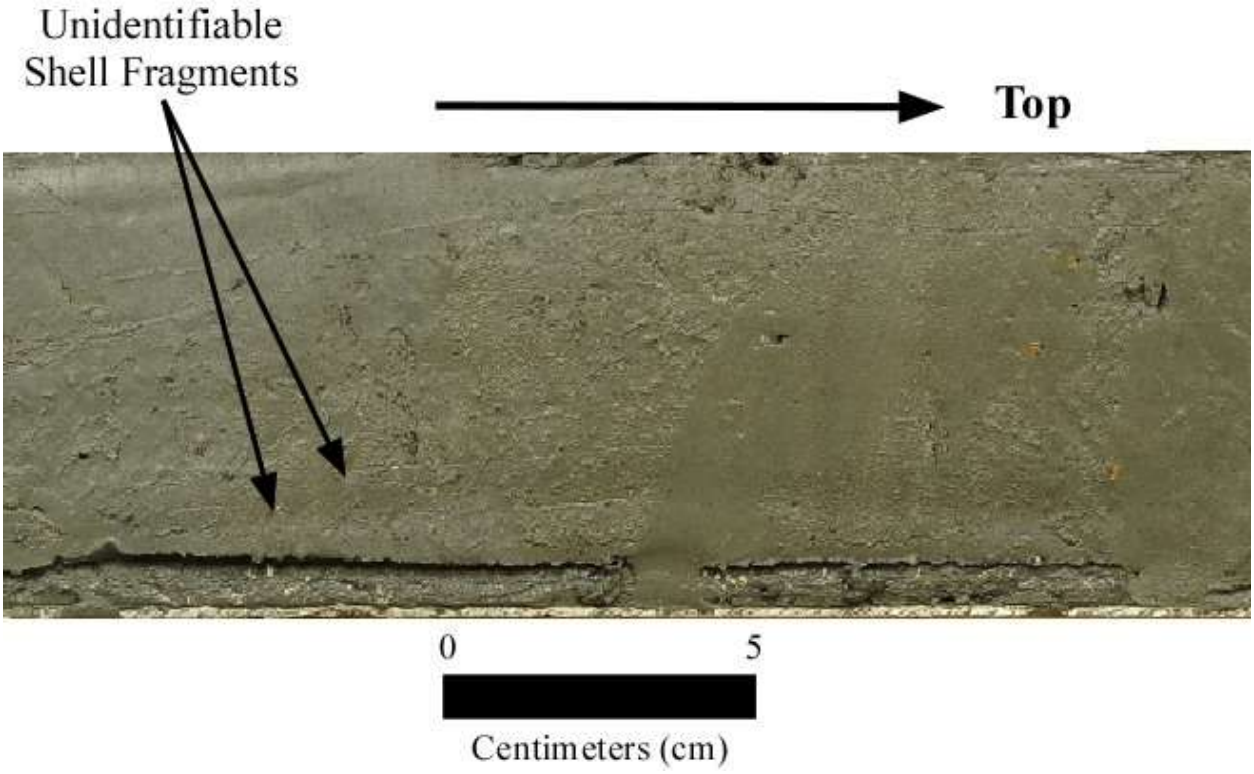

Figure 9: Image of sandy mud (sM) lithofacies in EPamSh16-1 at 2.71–2.91 mbsf.

4.1.3 Slightly gravelly sandy mud ((g)sM)

The slightly gravelly sandy mud lithofacies is light grey (5Y 3/1) (Table 8, Figure 10) and is 0.1 m thick. It is composed of mud (82 %), well sorted (0.27–1.63 ϕ) very coarse to coarse skewed (-0.85 to -0.27 ϕ) very fine sand (2.88–3.66 ϕ, 15–17 %), gravel (3–4 %), and bioclasts (*Cyrtopleura costata, Anadara* sp., unidentifiable shell fragments, 2 %) (Table 9). The mineralogy of the sand is made up of quartz (80 %), mica (5 %), and heavy minerals (15 %). This lithofacies appears in core EPamSh16-1 (1.2–1.3 mbsf) (Appendix B).

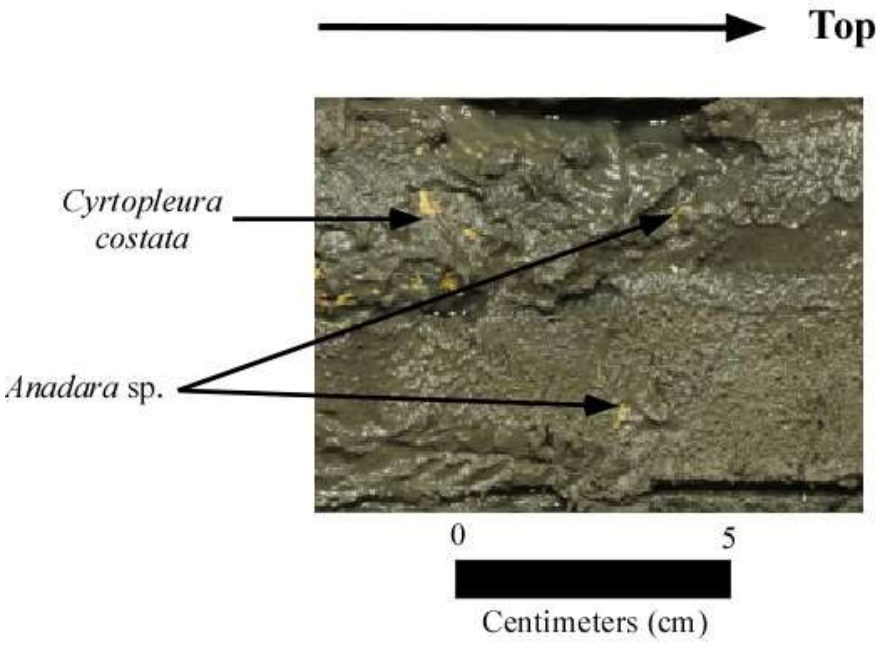

Figure 10: Image of slightly gravelly sandy mud ((g)sM) lithofacies from EPamSh16-1 at 1.3–1.4 mbsf.

4.1.4 Bioturbated slightly muddy sand (biot (m)S)

The bioturbated slightly muddy sand (biot (m)S) lithofacies is slightly orange grey (10YR 6/1) with burrows of light grey (5Y 4/1) (Table 8, Figure 11) that ranges from 1.10–1.40 m in thickness. It is composed of mud (1–10 %) and moderately to well sorted (0.46–0.83 ϕ) symmetrical to very coarse skewed (-0.39–0.08 ϕ) medium sand (1.13–2.05 ϕ, 87–99 %) (Table 9). The mineralogy of the sand is made up of quartz (97–99 %), feldspars (1–2 %), and heavy minerals (1 %). EPamSh16-2 and EPamSh16-8 (on the eastern and western ridge, respectively) consist exclusively of this lithofacies (Appendix B).

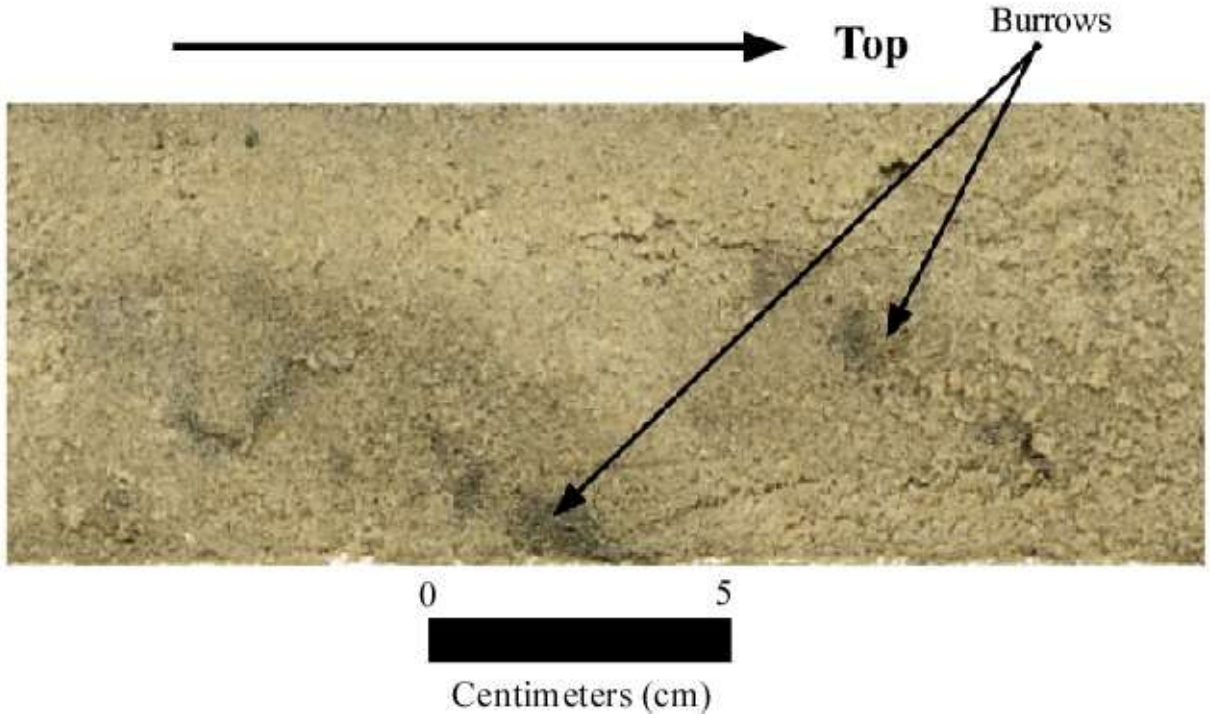

Figure 11: Image of bioturbated slightly muddy sand (biot (m)S) lithofacies. EPamSh16-8, 0.50–0.70 mbsf.

4.1.5 Rooted-bioturbated slightly muddy sand (rt-biot (m)S)

The rooted bioturbated slightly muddy sand lithofacies is burrowed, brown (10YR 3/2) (Table 8, Figure 12) and is approximately 0.7 m thick. It is composed of mud (0–5 %), very well-sorted (0.28–0.96) very coarse to fine skewed (-0.69–0.29 ϕ) medium to fine sand (1.80–2.35 ϕ, 95–99 %), and gravel (0–1 %) (Table 9). The mineralogy of the sand is made up of quartz (93 %), feldspars (5 %), and roots (2 %). Burrows within the lithofacies can be observed by the slightly lighter orangey brown (10YR 6/1) fill. Organic material consists of small wood and root fragments only occurring in EPamSh16-4 from 3.0–3.7 mbsf (Appendix B).

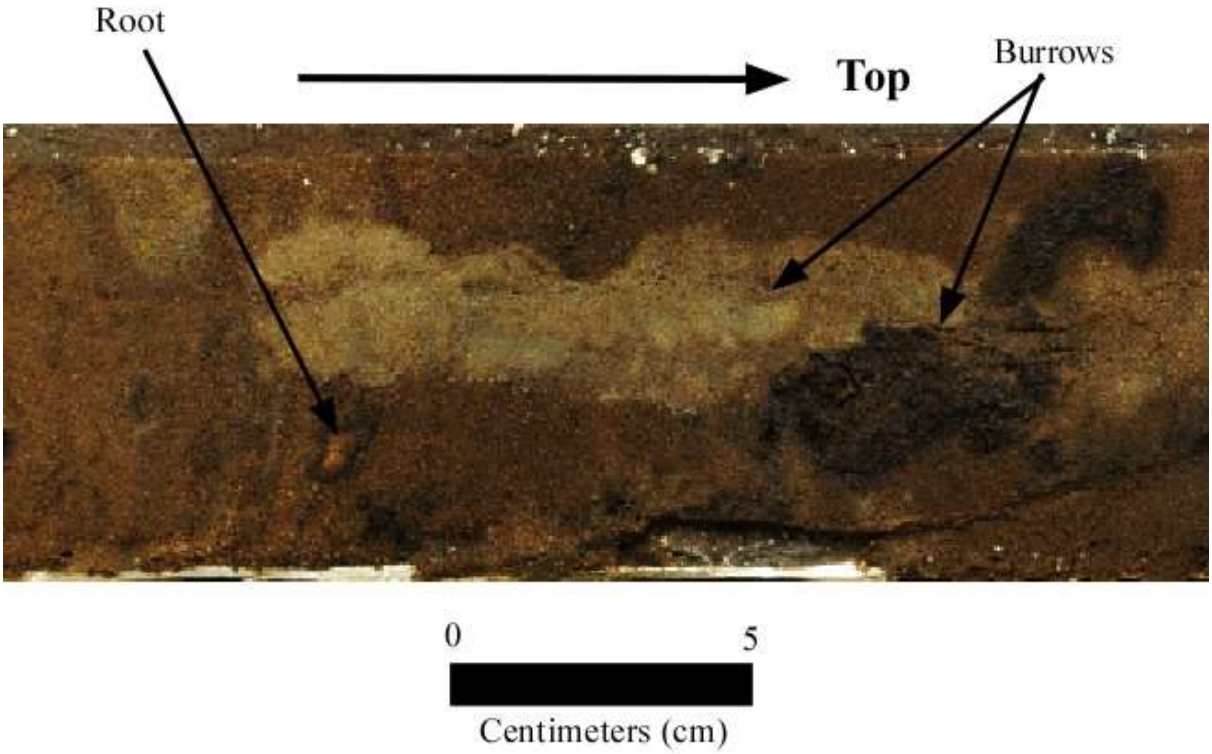

Figure 12: Image of rooted bioturbated slightly muddy sand (rt-biot (m)S) lithofacies. EPamSh16-4, 3.35–3.55 mbsf.

4.1.6 Muddy Sand (mS)

The muddy sand lithofacies is grey (5Y 5/1) (Table 8, Figure 13) and ranges from 0.3–2.0 m thick. It is composed of mud (1–10 %), moderately to well sorted (0.29–1.31 ϕ) very coarse to very fine skewed (-0.38–0.31 ϕ) fine to medium sand (0.67–2.87 ϕ, 63–97 %), gravel (0–2 %), and bioclastics (unidentifiable shell fragments, 1–20 %) (Table 9). The mineralogy of the sand is made up of quartz (96 %), micas (1 %), and heavy minerals (3 %). This lithofacies appears in four cores, EPamSh16-1 (0.0–0.2 mbsf), EPamSh16–4 (0.0–1.0; 1.1–2.1; 2.2–2.7 mbsf), EPamSh16-6 (0.0–0.4; 1.0–3.0 mbsf), and EPamSh16-10 (0.0–0.8 mbsf) (Appendix B).

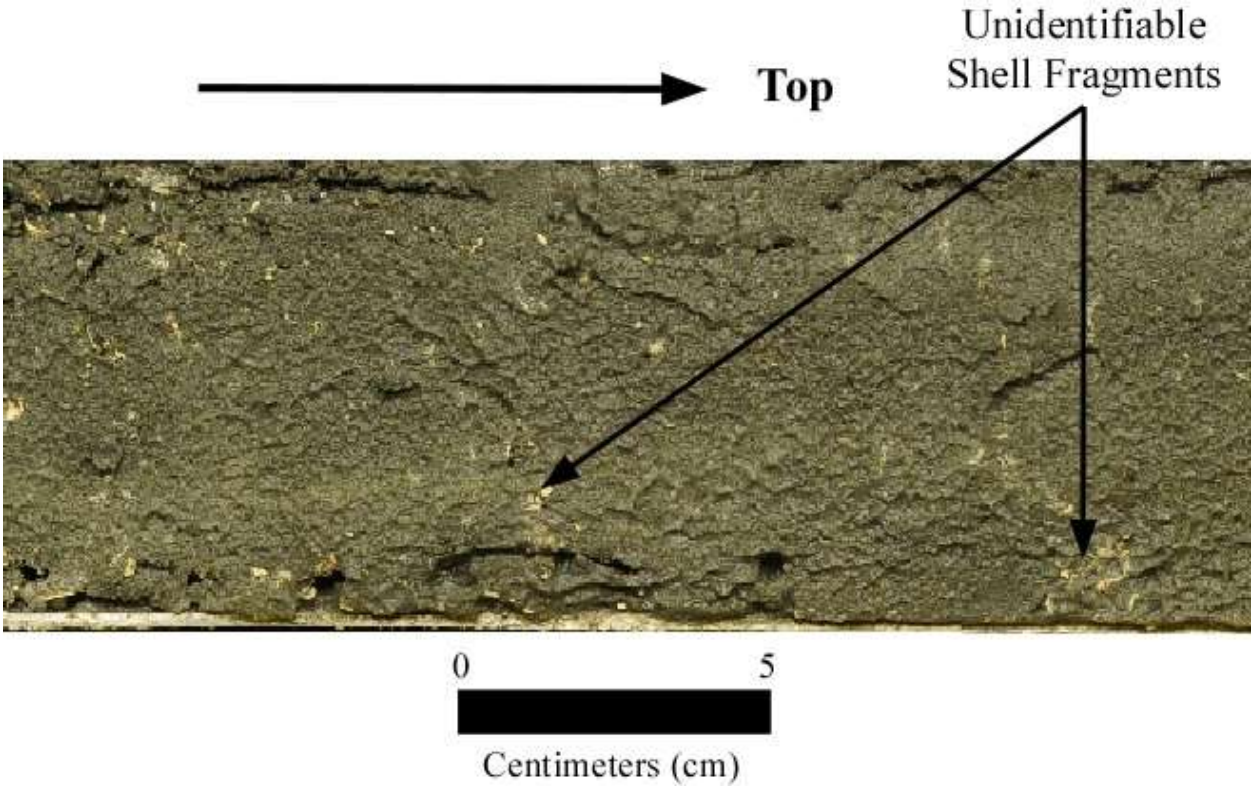

Figure 13: Image of muddy sand (mS) lithofacies. EPamSh16-4, 1.94–2.14 mbsf.

4.1.7 Bioturbated Muddy Sand (biot mS)

The bioturbated muddy sand lithofacies is orangey brown (10YR 6/1) (Table 8, Figure 14) and ranges from 0.2–0.8 m thick. It is composed of mud (5–35 %), very well sorted (0.89 to 1.02 ϕ) symmetrical to very coarse skewed (-0.10 to -0.39 ϕ) medium sand (1.61–1.98 ϕ, 65–95 %), gravel (<1 %), and bioclasts (*Anadara* sp., unidentifiable shell fragments, 1–20 %) (Table 9). The mineralogy of the sand is made up of quartz (97–99 %), feldspars (1 %), and heavy minerals (2 %). This lithofacies appears EPamSh16-1 (4.1–4.9 mbsf) and EPamSh16-4 (2.8–3.0 mbsf) (Appendix B).

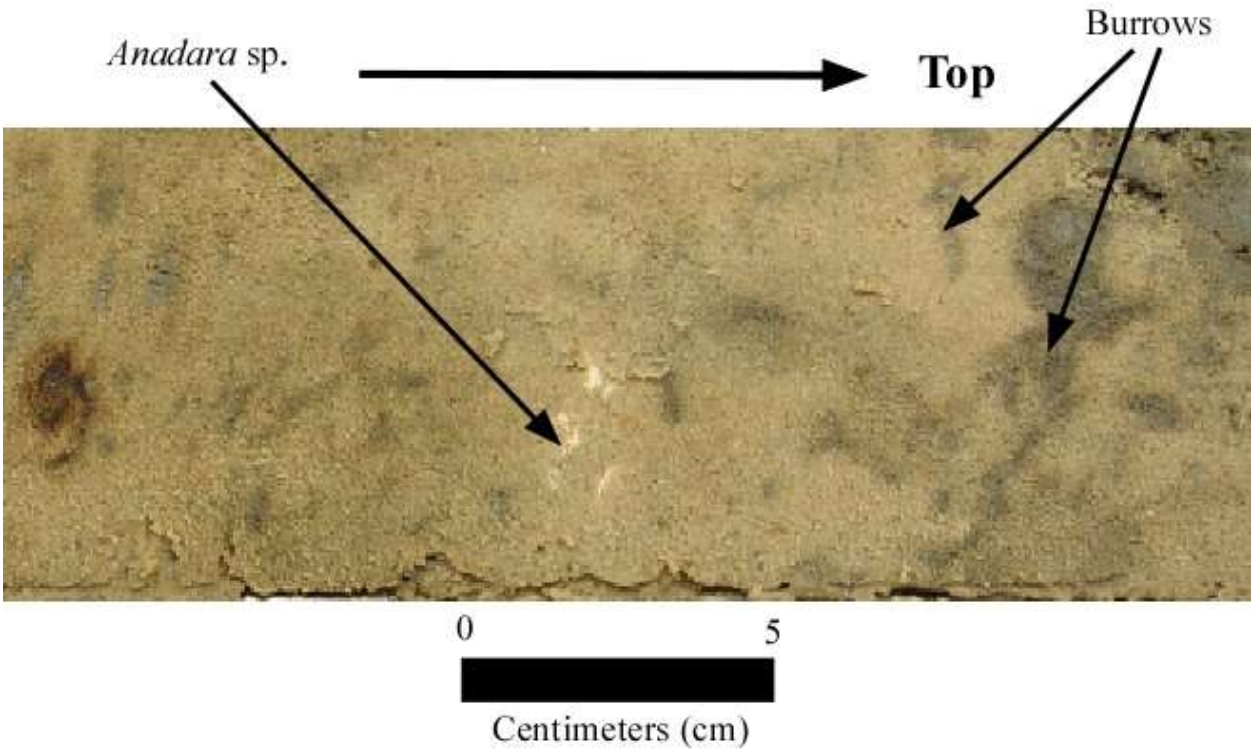

Figure 14: Image of bioturbated muddy sand (biot mS) lithofacies. EPamSh16-4, 2.8–3.0 mbsf.

4.1.8 Mottled bioturbated muddy sand (mot-biot mS)

The mottled bioturbated muddy sand lithofacies is grey (5Y 5/1) and orange brown (10YR 6/1 and 10YR 3/2) (Table 8, Figure 15). There are two variations of this lithofacies; one is dominated by the grey (5Y 5/1) color and is 0.4 m thick, and the other is dominated by the orange brown color (10YR 6/1 and 10YR 3/2) and 0.7 m thick. The facies is composed of mud (5–33 %), very well sorted (0.50–1.00 ϕ) very coarse to very fine skewed (-0.44–2.52 ϕ) medium sand (1.00–2.56 ϕ, 67–94 %), gravel (0–2 %), and bioclasts (unidentifiable shell fragments, <1 %) (Table 9). The mineralogy of the sand is made up of quartz (98 %), feldspars (1%), and heavy minerals (1 %). This lithofacies appears only at the base of EPamSh16-1 at 4.9–6.0 mbsf (Appendix B).

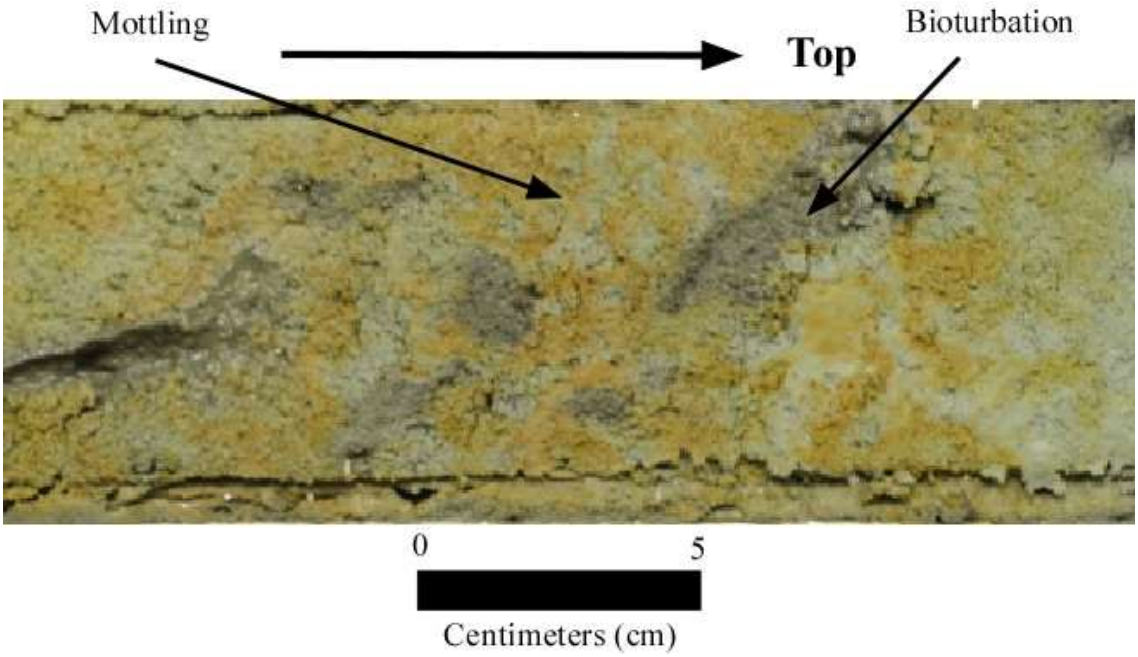

Figure 15: Image of mottled bioturbated muddy sand (mot-biot mS) lithofacies. EPamSh16-1, 5.30–5.50 mbsf.

4.1.9 Mixed slightly gravelly muddy sand (mxd (g)mS)

The mixed slightly gravelly muddy sand lithofacies is grey (5Y 4/1) (Table 8, Figure 16) and ranges from 0.1–0.4 m thick. It is composed of mud (4–17 %), very well sorted (0.54–0.92 ϕ) coarse to symmetrically skewed (-0.30 to -0.04 ϕ) medium sand (1.00–2.61 ϕ, 82–94 %), gravel (0–2 %), and bioclasts (*Anadara* sp., *Mulinia* sp., unidentifiable shell fragments, 30–40 %) (Table 9). The mineralogy of the sand is made up of quartz (92 %), feldspars (5 %), and heavy minerals (3 %). This lithofacies appears in EPamSh16-1 at the base of the core (6.0–6.4 mbsf) and EPamSh16-4 (1.0–1.1; 2.1–2.2; 2.7–2.8 mbsf) on the eastern sand ridge (Appendix B).

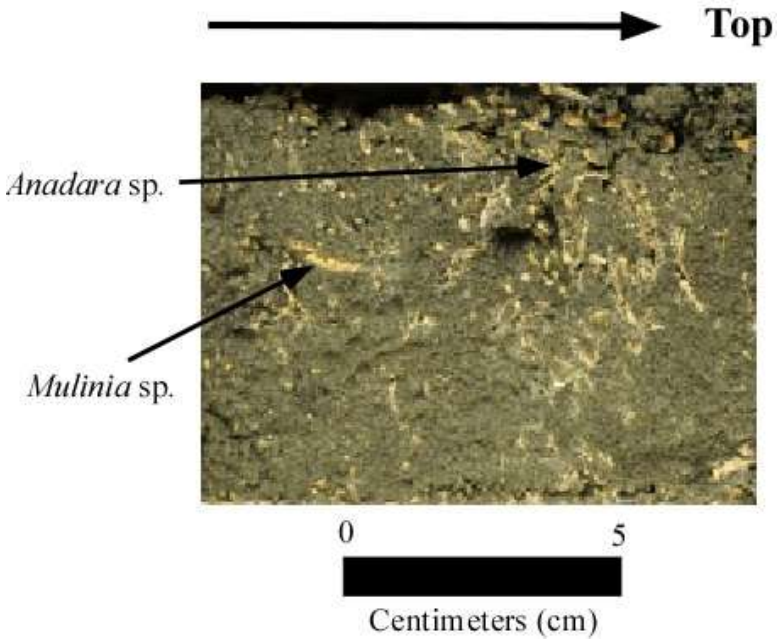

Figure 16: Image of mixed slightly gravelly muddy sand (mxd (g)mS) lithofacies. EPamSh16-4, 2.15–2.25 mbsf.

4.1.10 Mixed gravelly muddy sand (mxd gmS)

The mixed gravelly muddy sand lithofacies is grey (5Y 5/1) (Table 8, Figure 17) and ranges from 0.4–0.6 m thick. It is composed of mud (5–31 %), well sorted (0.45–1.37 ϕ) very coarse to symmetrically skewed (-0.41 to -0.07 ϕ) fine-medium sand (1.67–3.26 ϕ, 62–95 %), gravel (0–8 %), and bioclasts (*Anadara* sp., *Mulinia* sp., unidentifiable shell fragments, 30–40 %) (Table 9). The mineralogy of the sand is made up of quartz (95 %), mica (1 %), and heavy minerals (4 %). This lithofacies appears in EPamSh16-6 (0.4–1.0 mbsf) and EPamSh16-10 at the base of the core (2.3–2.7 mbsf) (Appendix B).

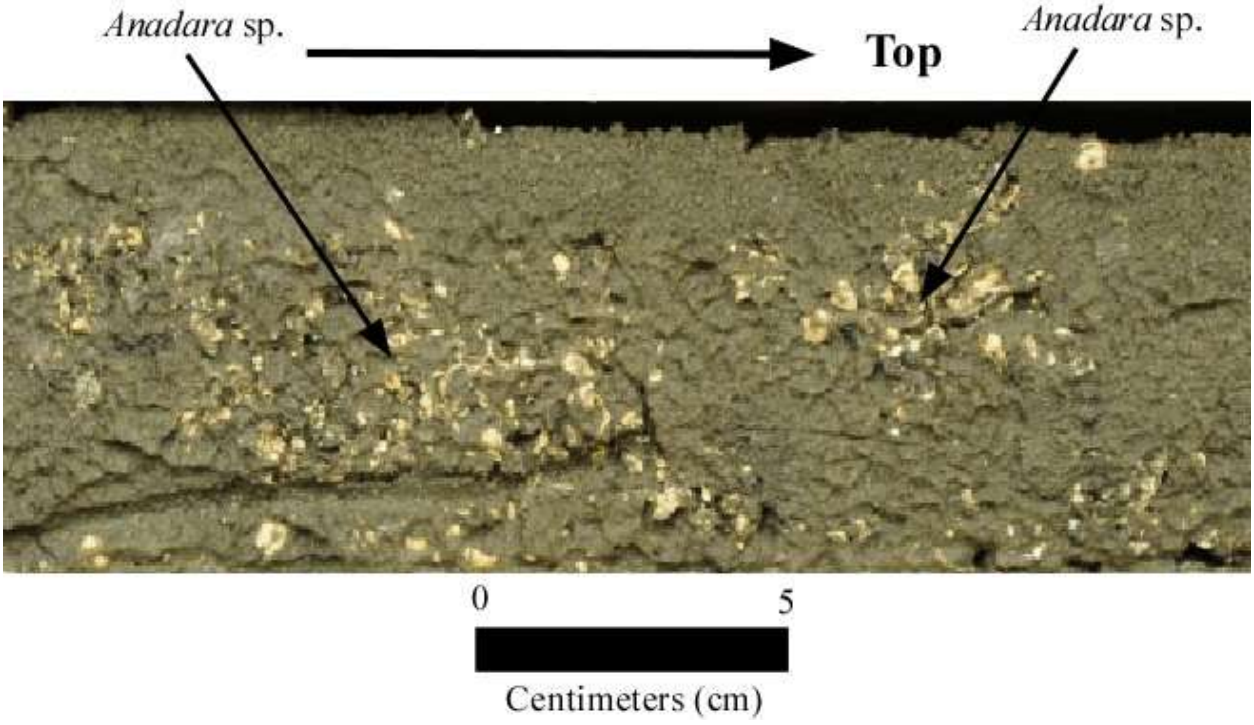

Figure 17: Image of mixed gravelly muddy sand (mxd gmS) lithofacies. EPamSh16-6, 0.45–0.65 mbsf.

4.1.11 Bioclastic gravelly muddy sand (bio gmS)

The bioclastic gravelly muddy sand lithofacies is grey (5Y 5/1) (Table 8, Figure 18) and is greater than 0.4 m thick. It is composed of mud (6–12 %), very well sorted (0.50–1.00 ϕ very coarse to very fine skewed (-0.44–2.52 ϕ) medium sand (0.86–2.56 ϕ, 67–94 %), gravel (1–21+ %), and bioclasts (*Anadara* sp.*, Mulinia* sp.*, Cyrtopleura costata,* unidentifiable shell fragments, 70–95%) (Table 9). The mineralogy of the sand is made up of quartz (95 %), feldspars (3 %), and heavy minerals (2 %). This lithofacies appears only at the base of EPamSh16-6 at >3.0 mbsf (Appendix B).

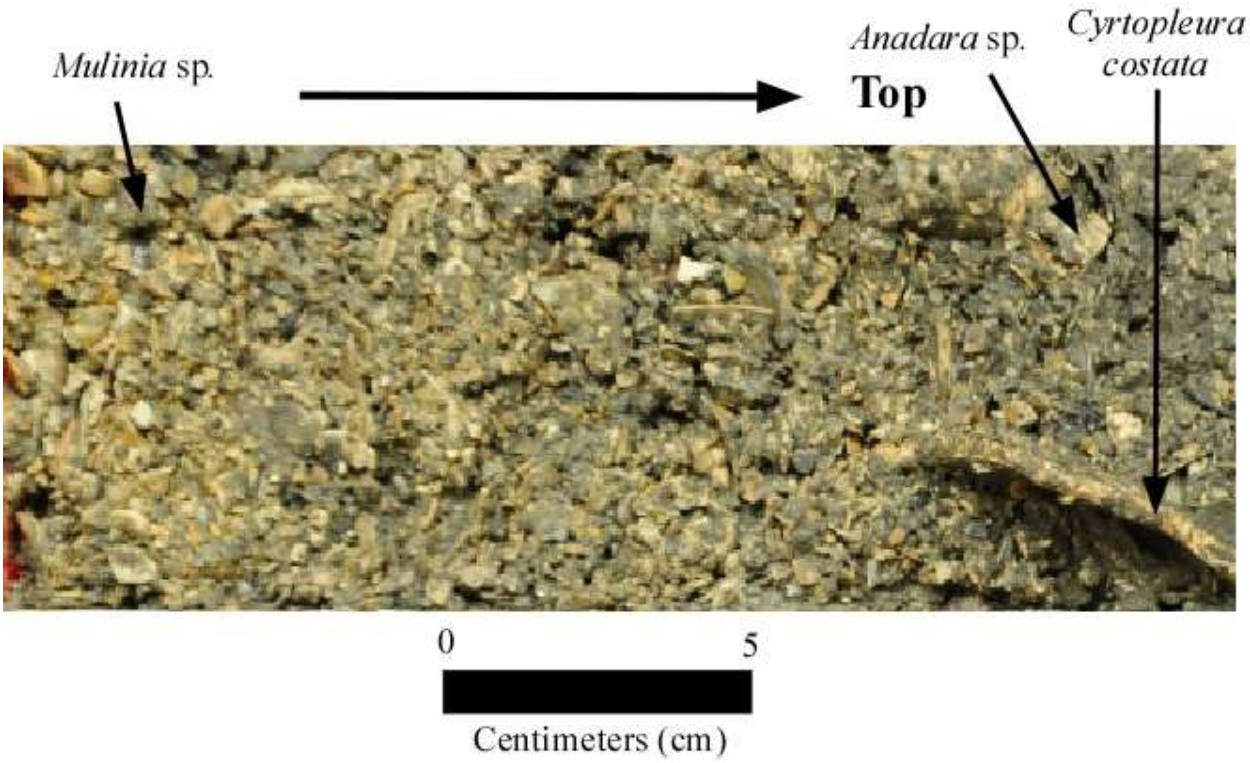

Figure 18: Image of bioclastic gravelly muddy sand (bio gmS) lithofacies. EPamSh16-6, 3.15–3.35 mbsf.

Table 9: Depth of lithofacies and range of sand fraction grain-size statistics.

		Sand Fraction			
Lithofacies	Depth (m)	Grain Size Mean (ϕ)	Sorting (ϕ)	Skewness (ϕ)	Kurtosis (ϕ)
mud (M)	EPamSh16-1; 0.2–0.6	0.98 to 3.24	0.92 to 1.62	-0.79 to 0.27	0.60 to 2.41
sandy mud (sM)	EPamSh16-1; 0.6–1.2, 1.3–4.1 EPamSh16-10; 0.8–2.3	2.59 to 3.69	0.24 to 1.26	-0.79 to 0.10	0.60 to 2.41
slightly gravelly sandy mud ((g)sM)	EPamSh16-1; 1.2–1.3	2.88 to 3.66	0.27 to 1.63	-0.28 to -0.85	1.36 to 4.32
bioturbated slightly muddy sand (biot (m)S	EPamSh16-2; 0.0–1.1 EPamSh16-8; 0.0–1.4	1.13 to 2.05	0.46 to 0.83	-0.39 to 0.08	0.83 to 1.27
rooted bioturbated slightly muddy sand (rt-biot (m)S)	EPamSh16-4; 3.0–3.7	1.80 to 2.35	0.28 to 0.96	0.29 to -0.69	0.93 to 1.39
muddy sand (mS)	EPamSh16-1; 0.0–0.2 EPamSh16-4; 0.0–1.0, 1.1–2.1, 2.2–2.7 EPamSh16-6; 0.0–0.4, 1.0–3.0 EPamSh16-10; 0.0–0.8	0.67 to 2.87	0.29 to 1.31	-0.38 to 0.31	0.78 to 9.47
bioturbated muddy sand (biot mS)	EPamSh16-1; 4.1–4.9 EPamSh16-4; 2.8–3.0	1.61 to 1.98	0.89 to 1.02	-0.10 to -0.39	0.86 to 0.94
mottled bioturbated muddy sand (mot-biot mS)	EPamSh16-1; 4.9–6.0	1.00 to 2.56	0.50 to 1.00	2.52 to 0.44	0.92 to 1.39
mixed slightly gravelly muddy sand (mxd (g)mS)	EPamSh16-1; 6.0–6.4 EPamSh16-4; 1.0–1.1, 2.1–2.2, 2.7–2.8	1.00 to 2.61	0.54 to 0.92	-0.04 to -0.30	-1.26 to 0.93
mixed gravelly muddy sand (mxd gmS)	EPamSh16-6; 0.4–1.0 EPamSh16-10; 2.3–2.7	1.67 to 3.26	0.45 to 1.37	-0.07 to -0.41	0.87 to 2.47
bioclastic gravelly muddy sand (bio gmS)	EPamSh16-6; 3.0–3.4	0.86 to 2.56	0.50 to 1.00	2.52 to -0.44	0.92 to 1.39

4.2 Biofacies

Nineteen vibracore samples were analyzed for foraminiferal assemblages. Seven samples were barren of foraminifera including the entirety of vibracores EPamSh16-2 and EPamSh16-8. Nine taxa were identified from twelve samples (Appendix G). Cluster analysis was not performed due to the high similarity of taxa between all samples. Two groups, High Brackish biofacies A and High Brackish biofacies B, were identified based on diversity of species and environment. Both biofacies were dominated by the foraminifera *Elphidium excavatum*.

4.2.1 High Brackish Biofacies A

The High Brackish biofacies A occur in two samples, EPamSh16-6 at 1.65 mbsf and EPamSh16-10 at 2.45 mbsf. This biofacies is more diverse than the High Brackish biofacies B with eight different taxa. In addition, *Cibicides lobatulus* and *Elphidium subarcticum*, which are commonly found in normal marine shelf conditions, and occur within these two samples (Schnitker, 1971; Culver et al., 2006; Abbene et al., 2006; Rosenberger, 2006; Twamley, 2006; Vance et al., 2006; Hale, 2008). High Brackish biofacies A in EPamSh16-6 in the muddy sand (mS) lithofacies, and in EPamSh16-10 in mixed gravelly muddy sand lithofacies (mxd gmS) (Figure 19, 20, 21).

4.2.1 High Brackish Biofacies B

The High Brackish biofacies B occurs in ten samples. This biofacies is less diverse than the High Brackish biofacies A biofacies with three different. This biofacies consists of 97% *Elphidium excavatum* (Table 10), and occurs in EPamSh16-1 (0.14–0.15, 6.64–0.65, 3.84–3.85, 4.24–4.25, and 4.94–4.95m), EPamSh16-4 (0.24–0.25 and 2.44–2.45m), EPamSh16-6 (0.14–0.15 and 1.64–1.65), and EPamSh16-10 (0.64–0.65, 2.24–2.25, and 2.44–2.45) (Figure 19, 20, 21).

Table 10: Total and percentage of foraminifera in biofacies recognized in vibracores.

	Biofacies			
	High Brackish biofacies A		High Brackish biofacies B	
Taxa	Total	Percentage	Total	Percentage
Ammonia parkinsoniana	12	6.32	15	2.84
Ammonia tepida	2	1.05	0	0
Cibicides lobatulus	1	0.53	0	0
Elphidium excavatum	165	86.84	512	96.97
Elphidium gunteri	2	1.05	1	0.19
Elphidium mexicanum	2	1.05	0	0
Elphidium subarcticum	3	1.58	0	0
Haynesina germanica	3	1.58	0	0

4.3 Seismic Data

SU 1 – (Seismic Unit 1): Seismic unit 1 represents the unit beneath the Pleistocene/Holocene ravinement horizon (Table 11, Figures 19, 20, 21). The depth to the top of the seismic unit is variable, ranging from 5.5–17 mbsl. There are southeast dipping clinoforms in the upper portion (0–1 m) of the unit (Figure 19, Panel C). SU 1 includes rooted bioturbated slightly muddy sand (rt-biot (m)S) in EPamSh16-4 (>6.7 mbsl) and mottled bioturbated muddy sand (mot-biot-mS) from 11.0–12.1 mbsl, and mixed slightly gravelly muddy sand (mxd (g)mS) at >12.1 mbsl in EPamSh16-1.

***P* –** (Pleistocene): This reflector is a high to medium amplitude, continuous surface, and is imaged at 5.5–17 mbsl (Table 11, Figures 19, 20, 21). The reflector is interpreted as a sequence boundary separating the Pleistocene unit (SU1) from the Holocene units. Parts of the reflector define channel structures. In some areas this reflector is obscured by gas pockets or masked by the bottom multiple. Southeast dipping clinoforms occur below this horizon (Figure 19, Panel C). This reflector is present in cores EPamSh16-1, EPamSh16-4, and PS-07; no other cores penetrated this reflector (Table 11).

***H_{RS}* –** (Holocene Ravinement surface): This is a medium to high amplitude reflector and is observed at 5.5–10.5 mbsl (Table 11, Figures 19, 20, 21). This reflector appears to be amalgamated with the Pleistocene (P) horizon across antecedent highs (Table 11).

SU 2 – (Seismic Unit 2): Seismic unit 2 is bounded by the P/H_{RS} and H_{2500} (Table 11, Figures 19, 20, 21). This unit is approximately 0–2.5 m thick at 9.5–10.5 mbsl and exhibits no internal structure. SU2 is identified in core EPamSh16-1 associated with bioturbated muddy

sand (biot mS) from 10.2–11.0 mbsl, EPamSh16-4 associated with mixed slightly gravelly muddy sand (mxd (g)mS) and bioturbated muddy sand (biot mS) from 6.4–6.6 mbsl, and EPamSh16-10 associated with mixed slightly gravelly muddy sand (mxd (g)mS) from 7.0–7.3 mbsl.

H_{2500} **–** (Holocene reflector ca. 2500 years BP): This reflector is medium amplitude, has moderate continuity and occurs from 5.5–9.5 mbsl (Table 11, Figure 19, 20, 21). The age of this reflector is constrained by radiocarbon dates in PS11-VC1 (Zaremba, 2014). This reflector is present in core EPamSh16-1.

SU 3 – (Seismic Unit 3): Seismic unit 3 is bounded by H_{2500} and H_{1000}. This unit is approximately 0.25–2.5 m thick at 4–7 mbsl (Table 11, Figure 19, 20, 21). There are northwest dipping clinoforms basinward of the western ridge (Figures 20, Panel C). SU 3 is identified in EPamSh16-1, EPamSh16-2, EPamSh16-4, and EPamSh16-6. Sandy mud (sM) is associated with SU 3 in EPamSh16-1. Muddy sand (mS) in EPamSh16-4 and EPamSh16-6 is associated with SU 3. In EPamSh16-2, bioturbated slightly muddy sand (biot (m)S) is associated with SU 3.

H_{1000} **–** (Holocene reflection ca. 1000 years BP): This reflector is low to medium amplitude, low continuity, and occurs between 3.5–3.0 mbsl (Table 11, Figures 19, 20, 21). This reflector is constrained by radiocarbon age estimates in cores PS-05, PS11-VC1, PS-09, PS12-VC2, PS11-03, and PS-03 (Culver et al., 2007, Grand Pre et al., 2011, Zaremba, 2014; Zaremba et al., 2016). This reflector is identifiable in EPamSh16-4 as mixed slightly gravelly muddy sand (mxd (g)mS) and slightly gravelly muddy sand ((g)mS) in EPamSh16-1 (Table 11, Figure 22).

In EPamSh16-6 this reflector should be present at the bottom of the mxd gmS lithofacies between 4.8–5.4 mbsl.

SU 4 – (Seismic Unit 4): Seismic unit 4 is bounded by H_{1000} and H_{500} (Table 11, Figures 19, 20, 21). This unit is approximately 0.25–1.5 m at 4.5–5.5 mbsl. Lithofacies within SU 4 include mud (M) in EPamSh16-1, bioturbated slightly muddy sand in EPamSh16-2 and EPamSh16-8, and muddy sand (mS) in EPamSh16-4 and EPamSh16-6.

H_{500} – (Holocene reflector ca. 500 years BP): This reflector is characterized by medium amplitude, high continuity, and occurs between 3.5–5.5 mbsl in all vibracores (Table 11, Figures 19, 20, 21). Zaremba et al. (2016) used this reflector to define the upper boundary of the ridge sands in this study. Radiocarbon age estimates from cores PNP-5, OCK-5, PS-05, PS-06, and PS-09 are used to constrain the age of this reflector to 500 cal yr. B.P. (Zaremba, 2014; Zaremba et al., 2016). This reflector is present in all cores.

SU 5 – (Seismic Unit 5): Seismic unit 5 is bounded by H_{500} and H_{SF} (modern seafloor) (Table 11, Figures 19, 20, 21). SU 5 is approximately 0–0.5 m thick above the H_{500} horizon and present in all cores. In EPamSh16-1, EPamSh16-4, EPamSh16-6, and EPamSh16-10 SU 5 is a muddy sand (mS) and a bioturbated muddy sand (biot mS) in EPamSh16-2 and EPamSh16-8.

H_{SF} – (Holocene modern seafloor): This high amplitude horizon is the modern seafloor surface located between 3–6.5 mbsl (Table 11, Figures 19, 20, 21).

Table 11: Summary of seismic reflections and seismic units (SU). Interpretations based on radiocarbon age estimates, lithofacies, foraminiferal data, and seismic data.

Reflection	SU	Approximate age (cal. yr. BP)	Characteristics	Lithofacies Units	Interpretation
H_{SF}		modern			Modern sediment/water interface
	5	0–500	Transparent, delineated by H_{500} and H_{SF}, 0–2.4 m thick.	mS, biot mS, sM	Decrease in marine influence; continued sand ridge deposition.
H_{500}		ca. 500	Medium amplitude and high continuity. Occurs 0.0–0.5 mbsf.		Defines the top of the 1200–500 cal. yr. BP deposit; an increase in inlet activity increased marine influence; acoustic impedance is result of increase in bioclasts.
	4	1200–500	Transparent, delineated by H_{1000} and H_{500}, 0.25–1.5 m thick.	mxd (g)mS, biot (m)S, mS, M, sM	Flooding of normal marine conditions in southern Pamlico Sound; continued sand ridge deposition.
H_{1000}		ca. 1200	Low to medium amplitude low continuity. Occurs 1.0–1.5 mbsf.		Defines a decrease in marine influence; increase in bioclasts.
	3	2500–1200	Transparent, delineated by H_{2500} and H_{1000}, 0.25–2.5 m thick. Northwest dipping clinoforms.	mxd (g)mS, sM, mS, biot (m)S	Increase in marine influence; initial sand ridge formation.
H_{2500}		ca. 2500	Medium amplitude and moderate continuity. Occurs 2.0–4.0 mbsf.		Defines the top of 4000–2500 cal. yr. BP deposit; increase in bioclasts.
	2	>2500	Transparent, delineated by H_{2500} and H_{rs} or P, 0–2.5 m thick, rare.	mot-biot mS, mxd (g)mS, biot mS	Decrease in marine influence. Beginning of overtopping of interfluves.
H_{RS}		depends on elevation	Medium to high amplitude. Occurs 1.0–6.0 mbsf and usually amalgamated to P reflection except near paleo-channel.		Ravinement surface caused by tidal and wave scour.
P		ca 22,000	High to medium amplitude and continuous. Occurs 1.0–11.0 mbsf.		Subaerial unconformity
	1	> ca 22,000	Less transparent from Holocene SU units. Southwest dipping clinoforms throughout.	rt-biot (m)S, mxd (g)mS	Undifferentiated environments

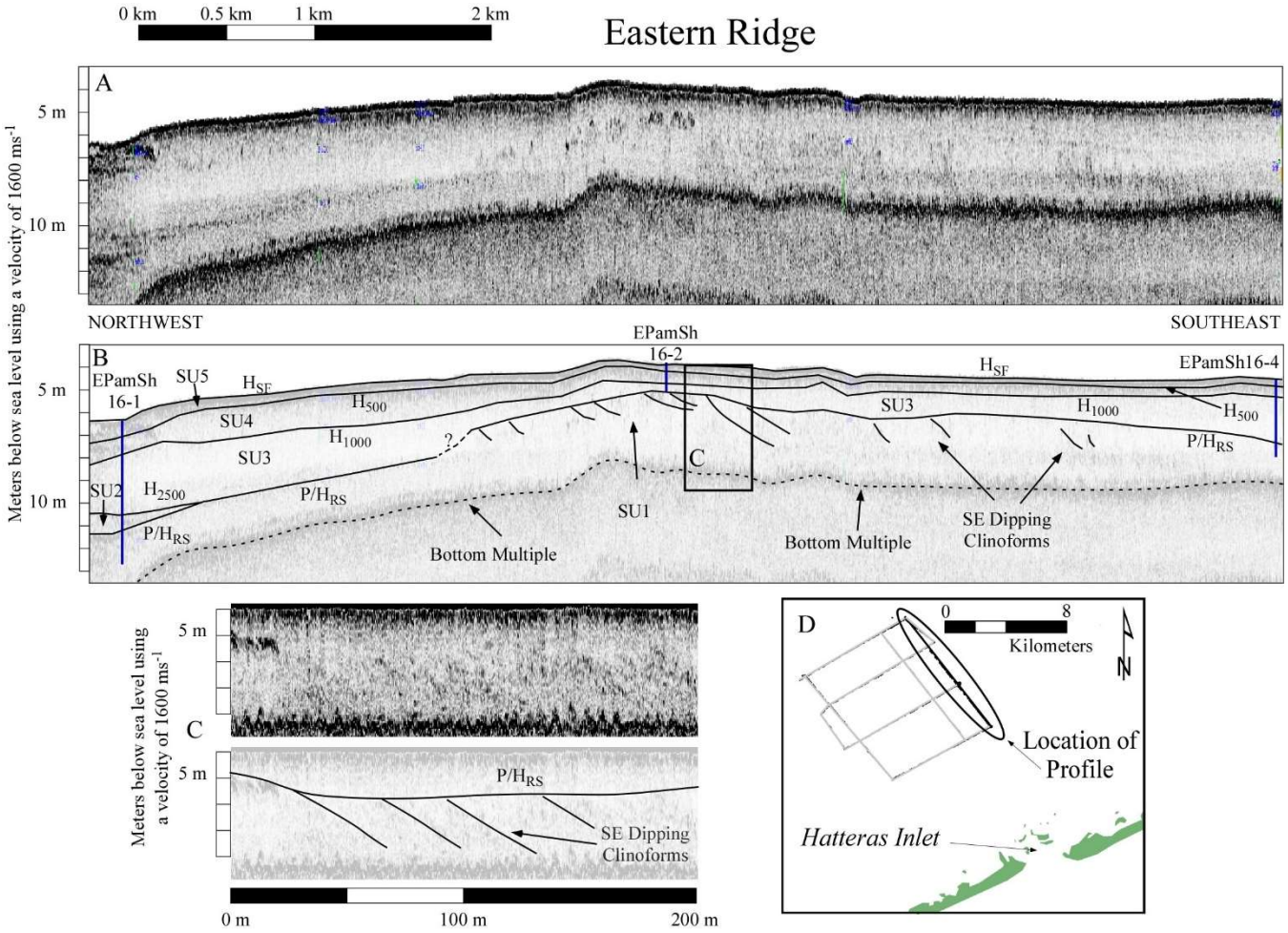

Figure 19: Chirp seismic (panel A) and interpreted stratigraphic features (panel B) located along the eastern ridge of the sand ridges northwest of Hatteras Inlet. Panel C shows southeast dipping clinoforms below the P/H_{RS} reflector. The profile location is indicated by ellipse along survey lines in panel D.

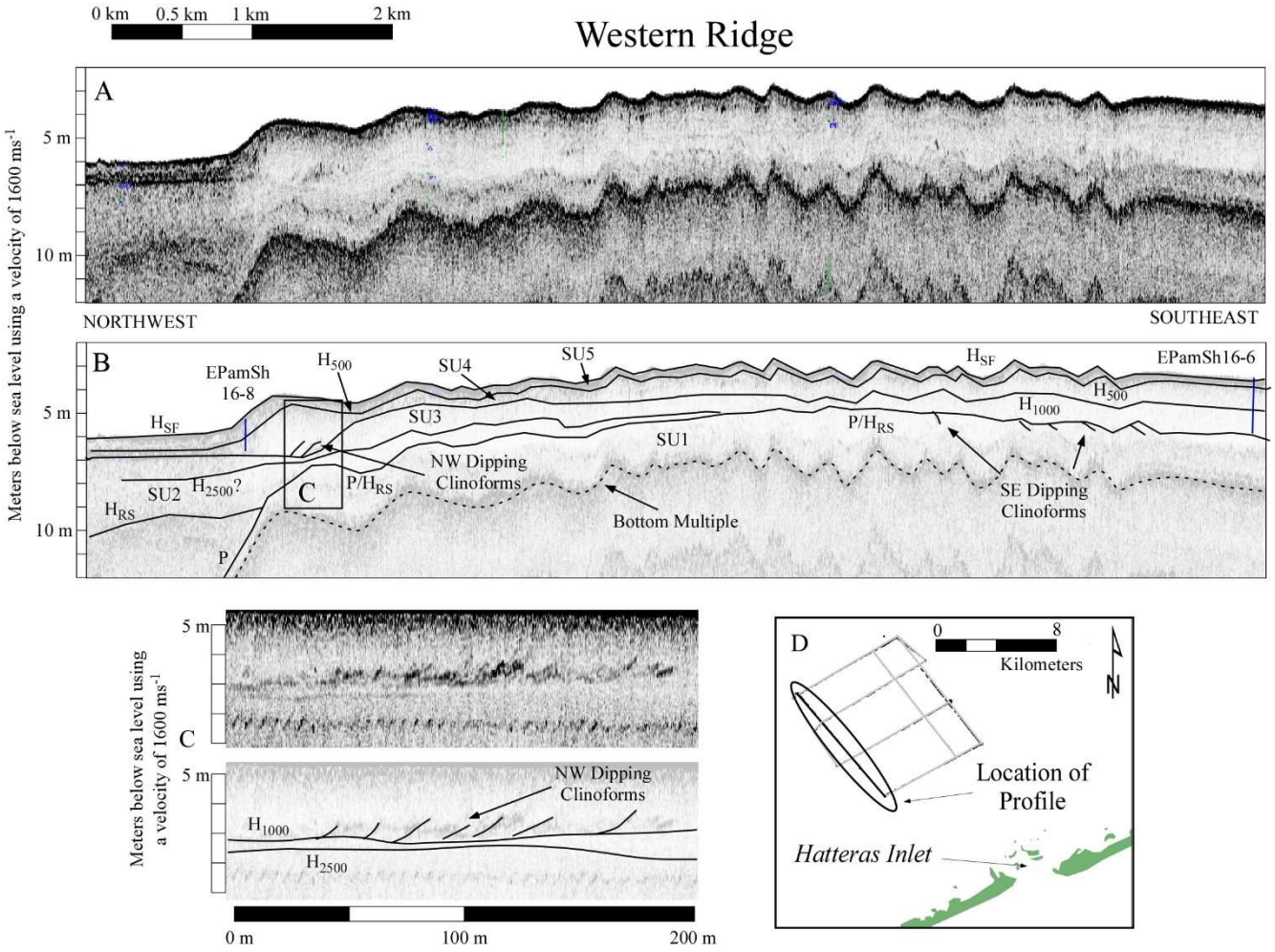

Figure 20: Chirp seismic (panel A) and interpreted stratigraphic features (panel B) located along the western ridge of the sand ridges northwest of Hatteras Inlet. Panel C shows northwest dipping clinoforms above the P/H_{RS} reflector and possibly the H_{2500} reflector. The profile location is indicated by ellipse along survey lines in panel D.

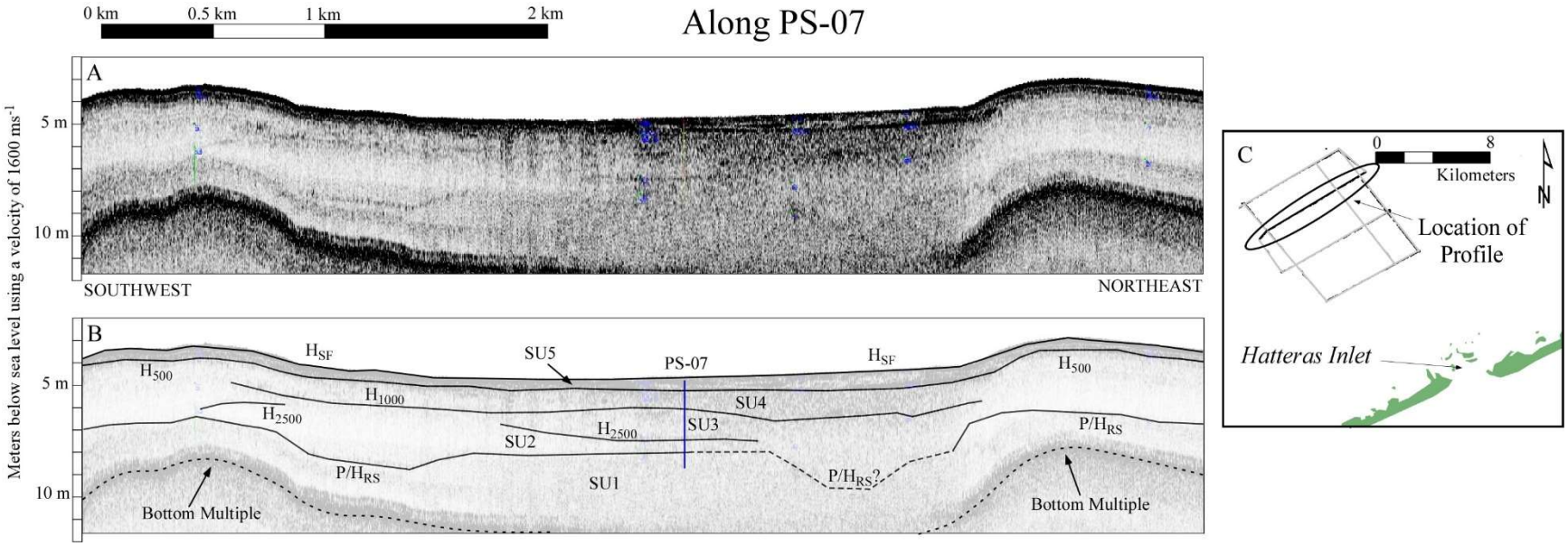

Figure 21: Chirp seismic (panel A) and interpreted stratigraphic features (panel B) located along transect including PS-07 (Zaremba, 2014; Zaremba et al., 2016) between the sand ridges northwest of Hatteras Inlet. The profile location is indicated by ellipse along survey lines in panel C.

4.4 Geochronology

Twelve radiocarbon age estimates combined with four previously acquired age estimates; (Zaremba, 2014; Zaremba et al., 2016; Table 12), are used to derive the chronostratigraphic framework. Ages range from modern to 6664–6547 cal yr. BP. No useable material was available for dating in EPamSh16-2 and EPamSh16-8. In EPamSh16-6, two age estimates were acquired (146–1 cal yr. BP at 2.64 mbsl and 4735–4550 cal yr. BP at 2.97 mbsl) and constrained SU 5. In EPamSh16-1, two mollusks (273–93 cal yr. BP at 2.44 mbsl and 334–143 cal yr. BP at 3.01 mbsl) and one mollusk in EPamSh16-10 (413–265 cal yr. BP at 2.97 mbsl) constrain SU 4. SU 3 was constrained in EPamSh16-4 using mollusks (1033–864 cal yr. BP at 3.13 mbsl, 2134–1943 cal yr. BP at 4.17 mbsl, and 2485–2279 cal yr. BP at 4.66 mbsl) and in EPamSh16-6 (2269-–2061 cal yr. BP at 4.99 mbsl). Root material (wood) was dated to 6664–6547 cal yr. BP at 5.99 mbsl in EPamSh16-4 corresponding to SU 1. No datable material was found in SU 2.

Table 12: Radiocarbon age estimates for this study (top) and previously acquired age estimates (Zaremba, 2014).

Core	Material	mbsl	Depth in Core (m)	Conventional age	Age Error	$\delta^{13}C$	Calibrated Age Range
EPamSh16-1	Mollusk	6.54	0.44	655	30.00	-1.90	273–93
EPamSh16-1	Mollusk	7.11	1.01	725	20.00	-0.06	334–143
EPamSh16-4	Mollusk	4.85	1.13	1,490	15.00	-0.02	1033–864
EPamSh16-4	Mollusk	5.89	2.17	2,510	20.00	-0.56	2134–1943
EPamSh16-4	Mollusk	6.38	2.66	2,770	20.00	-1.47	2485–2279
EPamSh16-4	Plant/Wood	7.71	3.99	5,800	45.00	-26.27	6664–6547
EpamSh16-6	Mollusk	5.03	0.64	580	15.00	-0.80	146–1
EPamSh16-6	Mollusk	5.36	0.97	4,560	20.00	-0.42	4735–4550
EPamSh16-6	Mollusk	7.38	2.99	2,590	30.00	-0.16	2269–2061
EPamSh16-10	Mollusk	6.42	1.82	780	20.00	-0.34	413–265
OCR-07-S203	Foraminifera	10.13	3.33	3,130	20.00	-1.75	2873–2727
PS-07	Foraminifera	6.90	0.40	20	15.00	-2.00	modern
Previously acquired dates (Zaremba, 2014)							
PS-07	*Mulinia*	7.35	0.85	2,280	30.00	-0.94	1948–1571
PS-07	*Mulinia*	7.73	1.23	445	25.00	-0.97	modern
PS-07	*Mulinia*	8.11	1.61	2,620	25.00	0.14	2340–1985
PS-07	Bruised *Nassa*	8.76	2.26	2,430	25.00	0.90	2140–1762

4.5 Environmental Facies

Four Environmental Facies (EF I–IV) were interpreted using lithofacies, biofacies, and correlation to seismic data. Pleistocene, High-Energy Estuary >30 % shell, and High-Energy Estuary <30 % shell are fine-medium sands. The Pleistocene Environmental Facies (EF I) is correlated to the base of paleo-Pamlico Creek. High-Energy Estuary (>30 % Shell) Environmental Facies (EF III) is differentiated by a greater percent shell and High Brackish biofacies A from High-Energy Estuary (<30 % Shell) Environmental Facies (EF IV) with lesser percent shell and High Brackish biofacies B. Low-Energy Estuary/Channel Environmental Facies (EF II) is differentiated by lithofacies consisting of muds.

4.5.1 Environmental Facies I: Pleistocene

Environmental Facies I (EF I) is interpreted as Pleistocene based on the mottled appearance, occurrence of Fe-oxides, roots, and correlation to the Pleistocene unit defined within seismic data (Zaremba et al., 2016). The actual depositional environment is not interpreted here. EF I is recognized at the base of EPamSh16-1 from 4.9–6.4 m and EPamSh16-4 from 3.0–3.7 m (Figure 22, 23, 24). EF I is barren of foraminifera and consists of rooted bioturbated slightly muddy sand in EPamSh16-4, mottled bioturbated muddy sand, and mixed slightly gravelly muddy sand in EpamSh16-1.

4.5.2 Environmental Facies II: Low-Energy Estuary/Channel

Environmental Facies II (EF II) represents a low-energy estuarine environment. EF II is recognized in EPamSh16-1 from 0.3–4.1 m and in EPamSh16-10 from 0.8–2.4 m (Figure 22, 23, 24). EF II is characterized by High-Brackish biofacies B dominated by *Elphidium excavatum* and *Ammonia parkinsoniana.* Lithofacies in EF II consists of well sorted, finely skewed, sandy

mud and mud. In EF II there is bioturbation with <5 % shells fragments characterizing periods of relatively low hydrodynamic energy.

4.5.3 Environmental Facies III: High-Energy Estuary (>30 % shell)

Environmental Facies III (EF III) represents a high-energy estuarine environment. EF III is recognized in EPamSh16-1, EPamSh16-4, EPamSH16-6, and EPamSH16-10. EF III occurs in EPamSh16-1 from 1.1–1.2 m, 4.1–4.9 m, and 6.0–6.4 m; in EPamSh16-4 from 1.0–1.1 m, 2.1–2.2 m, and 2.7–3.0 m; in EPamSh16-6 from 0.8–1.0 m and 3.0–3.4; and in EPamSh16-10 from 2.4–2.7 m (Figure 22, 23, 24). EF III contains both biofacies or barren of foraminifera and a variety of lithofacies (slightly gravelly sandy mud, bioturbated muddy sand, mixed slightly gravelly muddy sand, mixed gravelly muddy sand, and bioclastic gravelly muddy sand). Shells (>30 %) commonly occur in EF III and suggest periods of relatively high hydrodynamic energy based on their coarse and fragmented characteristics.

4.5.4 Environmental Facies IV: High-Energy Estuary (<30 % shell)

Environmental Facies IV (EF IV) represents the sand ridge environment. EF IV is recognized in all six vibracores. This environmental facies occurs in EPamSh16-1 from 0.0–0.3 mbsf, EPamSh16-2 from 0.0–1.1 m, EPamSh16-4 from 0.0–1.0 m; 1.1–2.1m; 2.2–2.7 m, EPamSh16-6 0.0–0.8 m; 1.0–3.0 m, EPamSh16-8 0.0–1.4 m , and EPamSh16-10 from 0.0–0.8 m (Figure 22, 23, 24). EF IV contains both biofacies barren of foraminifera and lithofacies muddy sand or bioturbated slightly muddy sand. Shells (<5%) also commonly occur throughout EF IV.

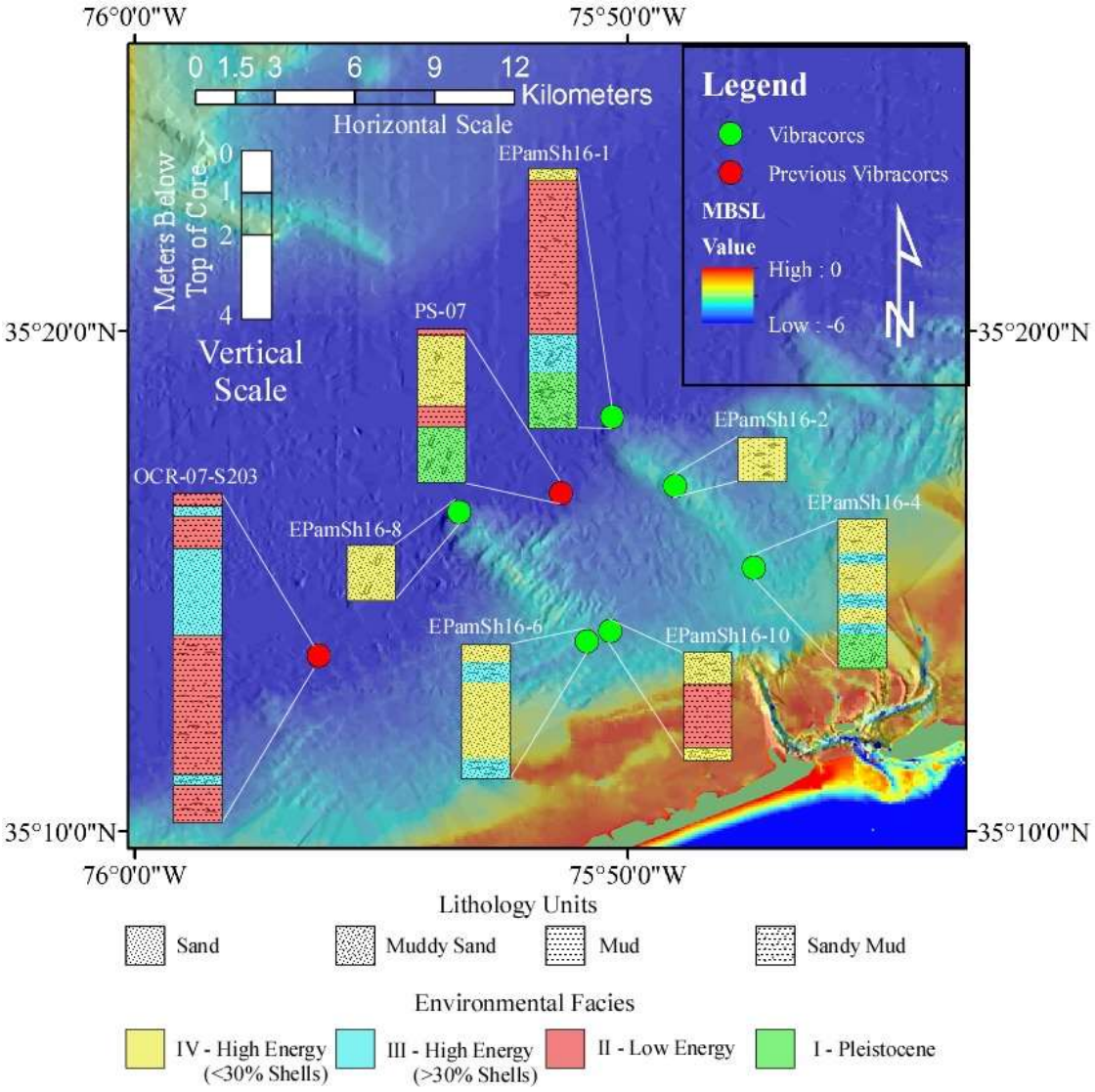

Figure 22: Lithology and Environmental Facies within the study area. PS-07 and OCR-07-S203 are from Foley (2007) and Metger (2009), respectively.

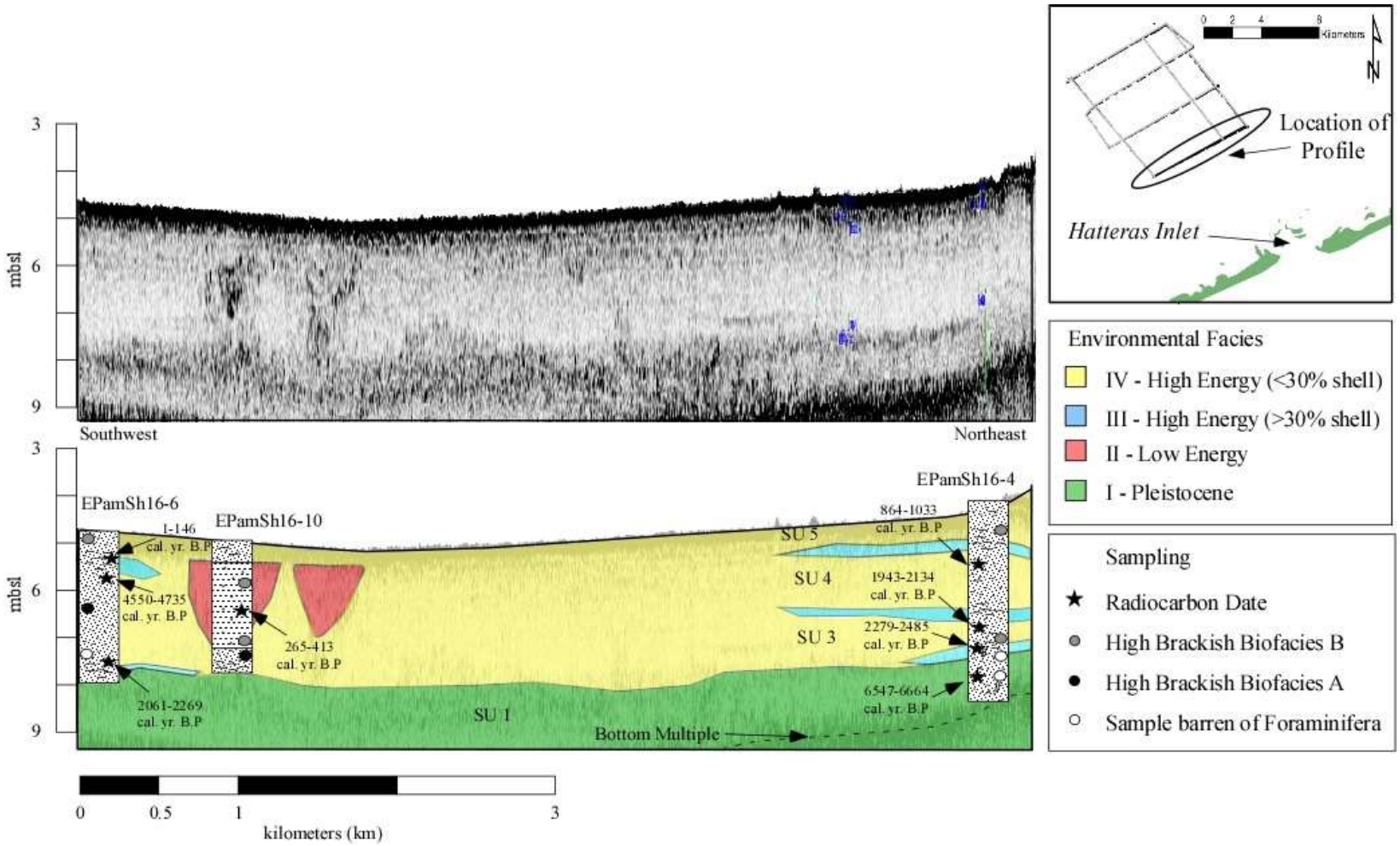

Figure 23: Transect from EPamSh16-6 to EPamSh16-4 between the sand ridges. Core logs are shown with lithologies. Environmental units are overlain on seismic data for reference and profile, location of foraminifera sampling with related biofacies, and radiocarbon age estimates.

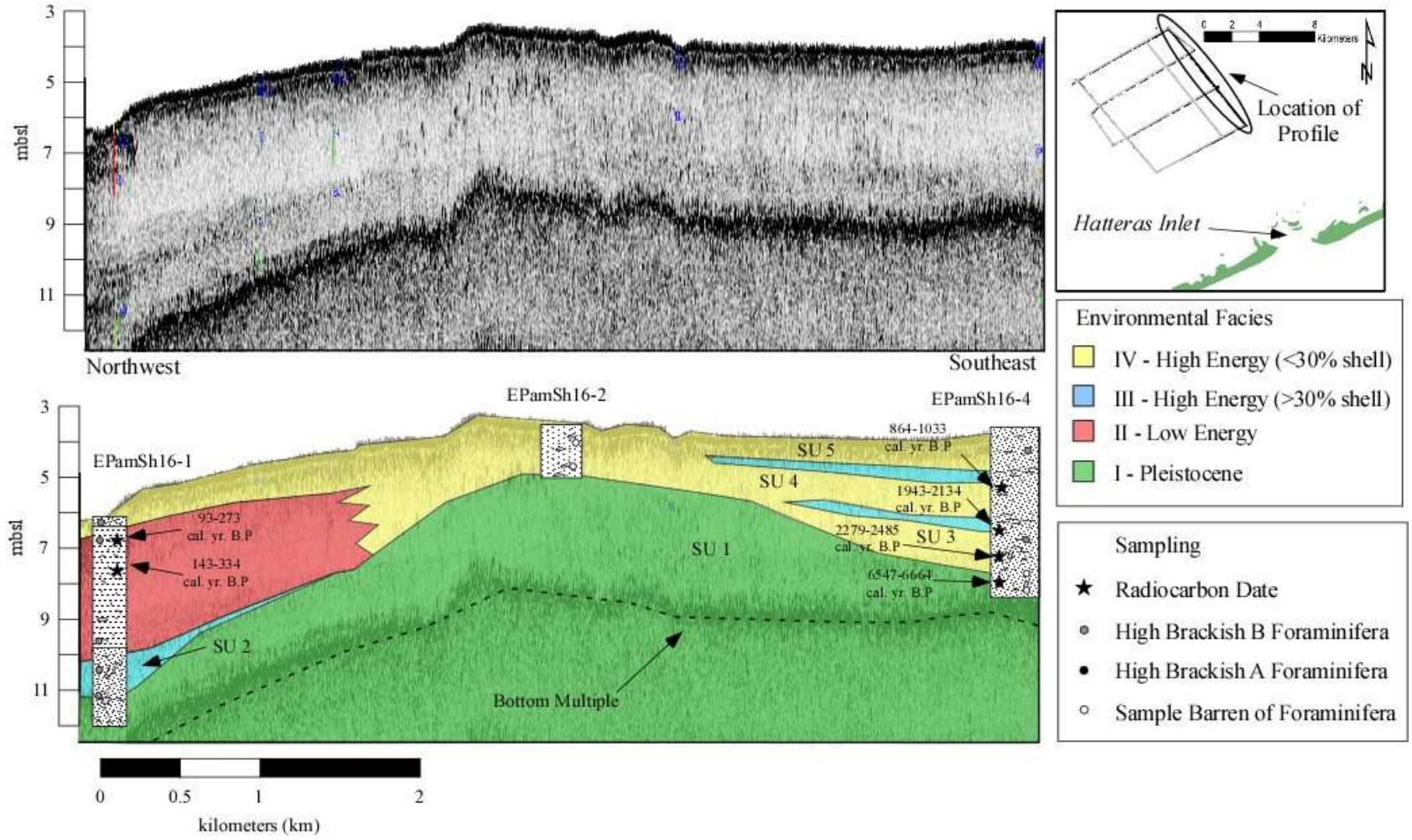

Figure 24: Transect from EPamSh16-6 to EPamSh16-4 along the eastern sand ridge. Core logs are shown with lithologies. Environmental units are overlain on seismic data for reference and profile, location of foraminifera sampling with related biofacies, and radiocarbon age estimates.

4.6 Bulk Magnetic Susceptibility (BMS)

The BMS data from six cores are presented in Figures 25, 26, and Appendix H. The BMS data ranges from 3.446 x10^{-8} k(si) in EPamSh16-8 at 1.05 mbsf to 4.553 x 10^{-5} k(si) in EPamSh16-1 at a depth of 3.60 mbsf (Figure 25). The following are general trends of BMS values.

BMS values at the base of EPamSh16-1, between approximately 6.15 mbsf and 4.8 mbsf show a general up-core increase, but with significant variability. Values fluctuate between approximately 1.0 x 10^{-5} k(si) and 4.3 x 10^{-5} k(si). At 4.75 mbsf, values decrease slightly from 3.5 x 10^{-5} k(si) to 2.0 x 10^{-5} k(si). At 4.0 mbsf values increase again from 2.1 x 10^{-5} k(si) to 3.8 x 10^{-5} k(si). Above 4.0 mbsf, values fluctuate around a mean of approximately 3.8 x 10^{-5} k(si) until decreasing significantly, at 0.2 mbsf, to approximately 1.5 x 10^{-5} at 0.2 mbsf (Figure 25; Appendix H).

BMS values at the base of EPamSh16-2 (1.10 mbsf) are approximately 4.8 x 10^{-6} k(si), and are somewhat constant up-core, until 0.45 mbsf, where a peak value of 1.0 x 10^{-5} k(si) occurs. Above this peak, values decrease to approximately 5.0 x 10^{-6} k(si) at the top of core (Figure 25; Appendix H).

BMS values at the base of EPamSh16-4 (3.70 mbsf) are approximately 1.6 x 10^{-5} k(si), but then show a sudden decrease to 1.3 x 10^{-6} k(si) at 3.5 mbsf. Values then increase to 2.1 x 10^{-5} k(si) at 0.75 mbsf, before decreasing again to 4.5 x 10^{-6} at the top of the core (Figure 25; Appendix H).

BMS values at the base of EPamSh16-6, between 3.10 mbsf and 2.1 mbsf, exhibit minor fluctuations around a mean of approximately 1.5 x 10^{-5} k(si). At 2.1 mbsf, values decrease to 6.6 x 10^{-6} k(si), then exhibit minor fluctuations between 1.1 x 10^{-5} k(si) and 6.7 x 10^{-6} k(si) until 0.95 mbsf. Values then increase to a peak of 2.4 x 10^{-5} k(si) at 0.45 mbsf, and then decrease to 1.3 x 10^{-5} k(si) at the top of the core (Figure 25; Appendix H).

BMS values in EPamSh16-8, between 1.15 mbsf and 0.2 mbsf fluctuate around a mean of approximately 1.3 x 10^{-6} k(si). At 0.2 mbsf, values increase abruptly to 1.3 x 10^{-5} k(si) (Figure 25; Appendix H).

BMS values at the base of EPamSh16-10 (2.60 mbsf) are approximately 1.2 x 10^{-5} k(si). Values increase up-core to 4.2 x 10^{-5} at 2.35 mbsf, then decrease, with minor fluctuations, to 3.2 x 10^{-5} k(si) at 0.90 mbsf. Values then decline abruptly to approximately 1.8 x 10^{-5} k(si) between 0.8 and 0.5 mbsf. From 0.5 to 0.35 mbsf, values increase to 3.6 x 10^{-5}, then decrease to 2.7 x 10^{-5} k(si) at the top of the core (Figure 25; Appendix H).

EPamSh16-1 between 4.10 mbsf to 0.25 mbsf and EPamSh16-10 between 2.35 mbsf to 0.35 mbsf have high percent mud (>80 %) and high BMS value (Figure 25). There is an apparent good positive correlation between BMS and percent mud, and between BMS and grain size (Figure 26). Both correlations are mainly driven by two clusters of data: large (mean of 2.0-3.0 ϕ) grain-size and low percent mud represent one cluster, and small (mean of 5.0-6.0 ϕ) grain-size and high percent mud represent the second cluster. Within these clusters (Figure 26, A1; Figure 26, B1) the correlation equations differ from the whole dataset but they are still evident. The details of these two clusters remains to be further investigated.

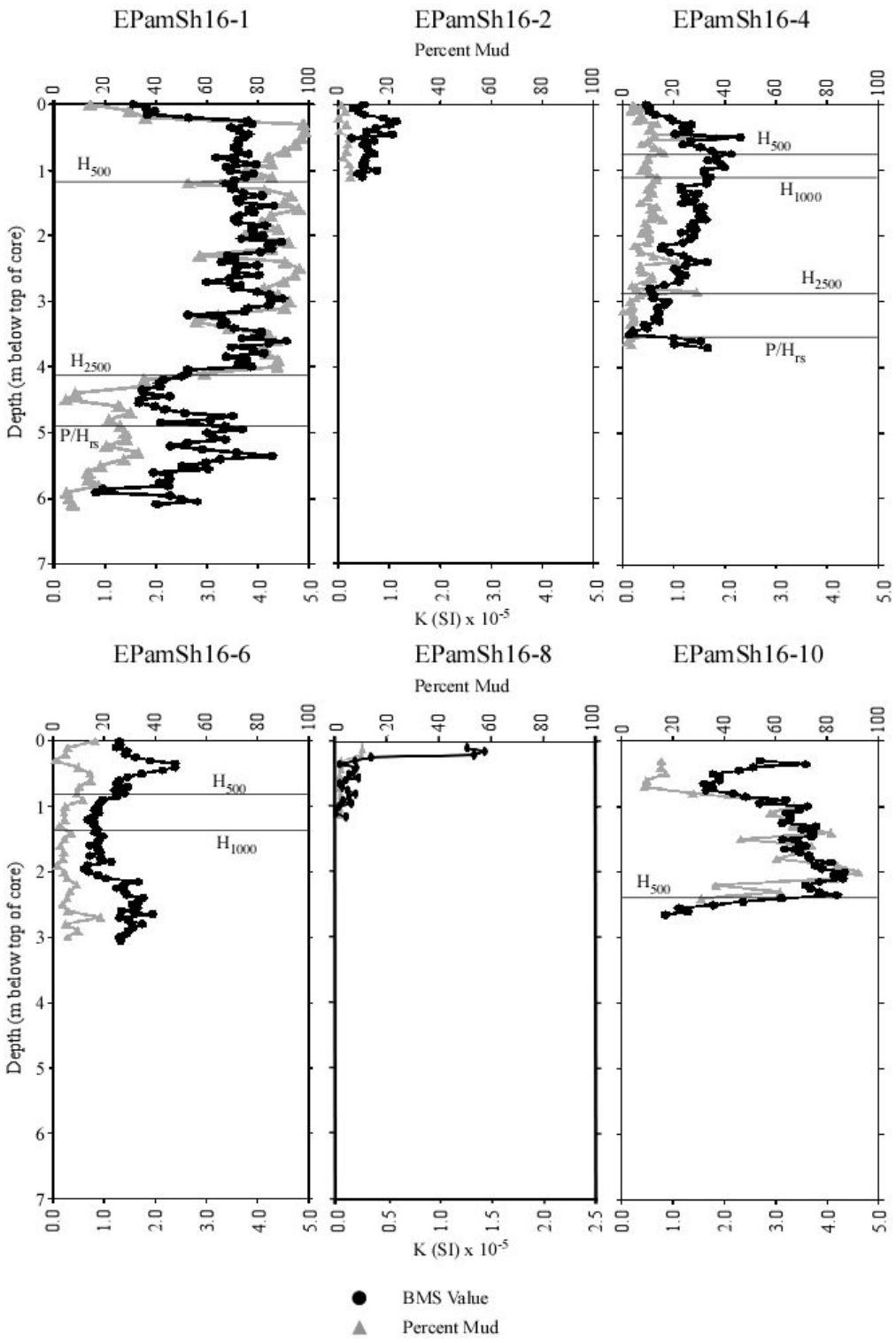

Figure 25: BMS values (k(si) x 10^{-5}) compared to percent mud correlated to seismic horizons.

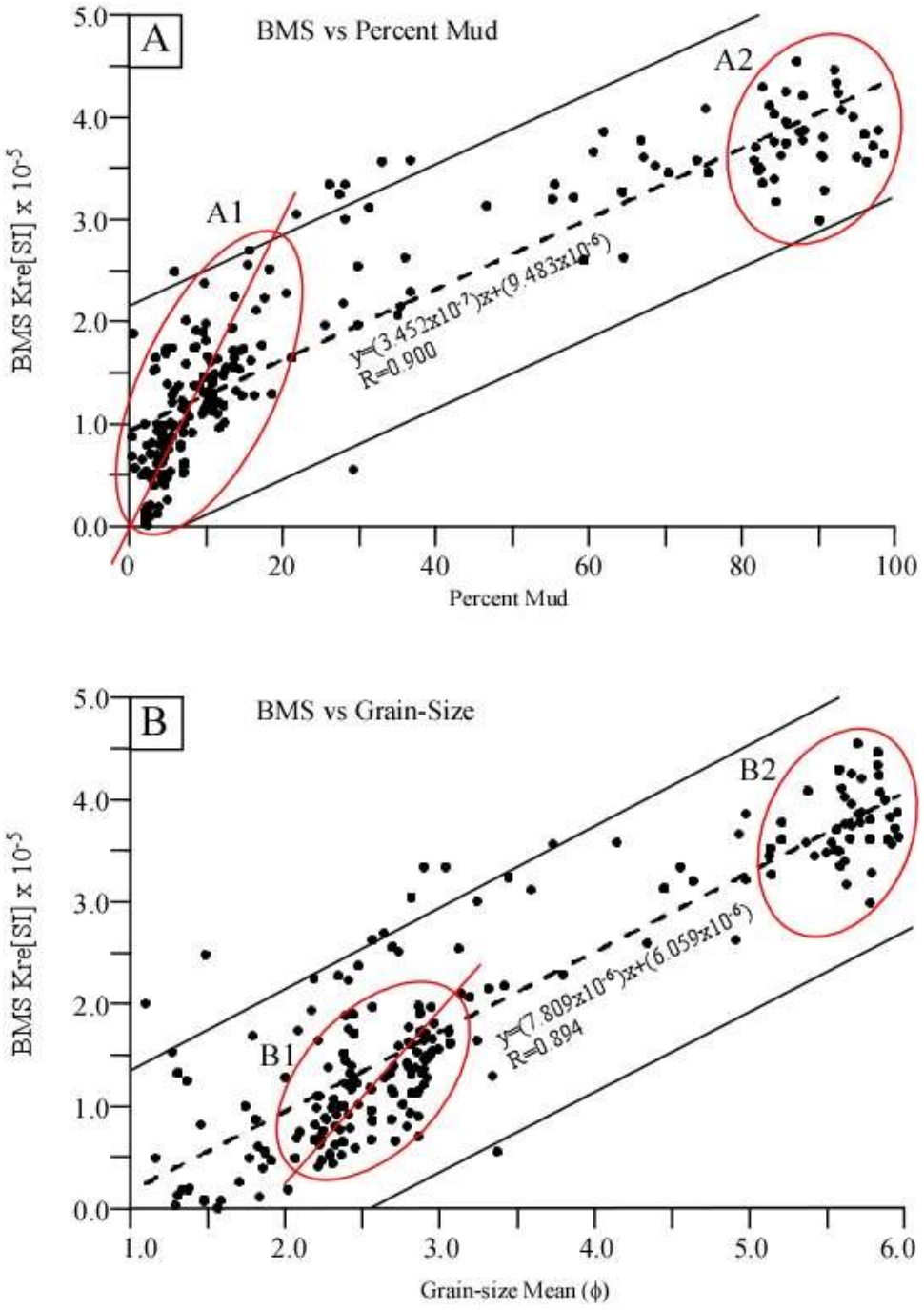

Figure 26: Panel A compares mean BMS values to percent mud and panel B compares mean BMS values to grain-size of all samples (n=210). Dashed line indicates trend line and solid line indicates 90% confidence. A1 and B1 represent one cluster and A2 and B2 represent a second cluster.

4.7 Surface Sample Analysis

Twenty-eight surface samples were collected in the study area and analyzed for grain-size characteristics (Figure 27, Appendix D). The surface samples (EPBS 2, EPBS 3, EPBS 4, EPBS 18, EPBS 19, and EPBS 20) were located on the two ridges dominated by sand with <10% mud, grain-size mean of 2.0 ϕ (medium sand), and sorting of greater than 1.0 ϕ (well sorted) (Figure 28, Panel B and D). Percent mud increase, and the mean grain-size decreases rapidly toward the north and to the west of the ridges. The trough between the two ridges contains a maximum of 44.3 % mud (Figure 28, Panel A). In the trough, the mean grain-size is finer, skewness is greater, and sediments are more poorly sorted than the sand ridges. The surface samples on the sand ridges are finely skewed and skewness coarsens to the west (Figure 28, Panel C, and Appendix D).

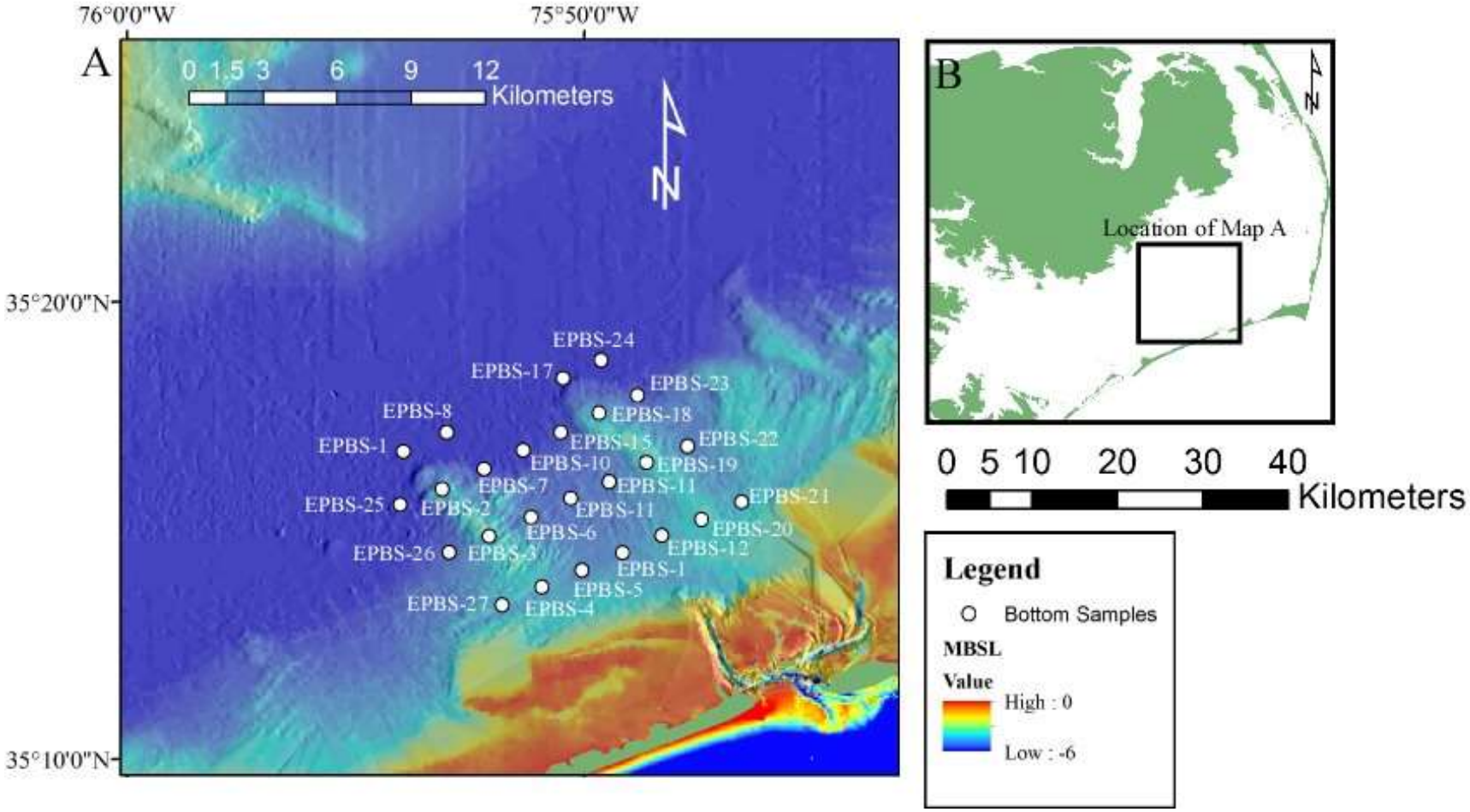

Figure 27: Location of surface samples used for grain-size analysis.

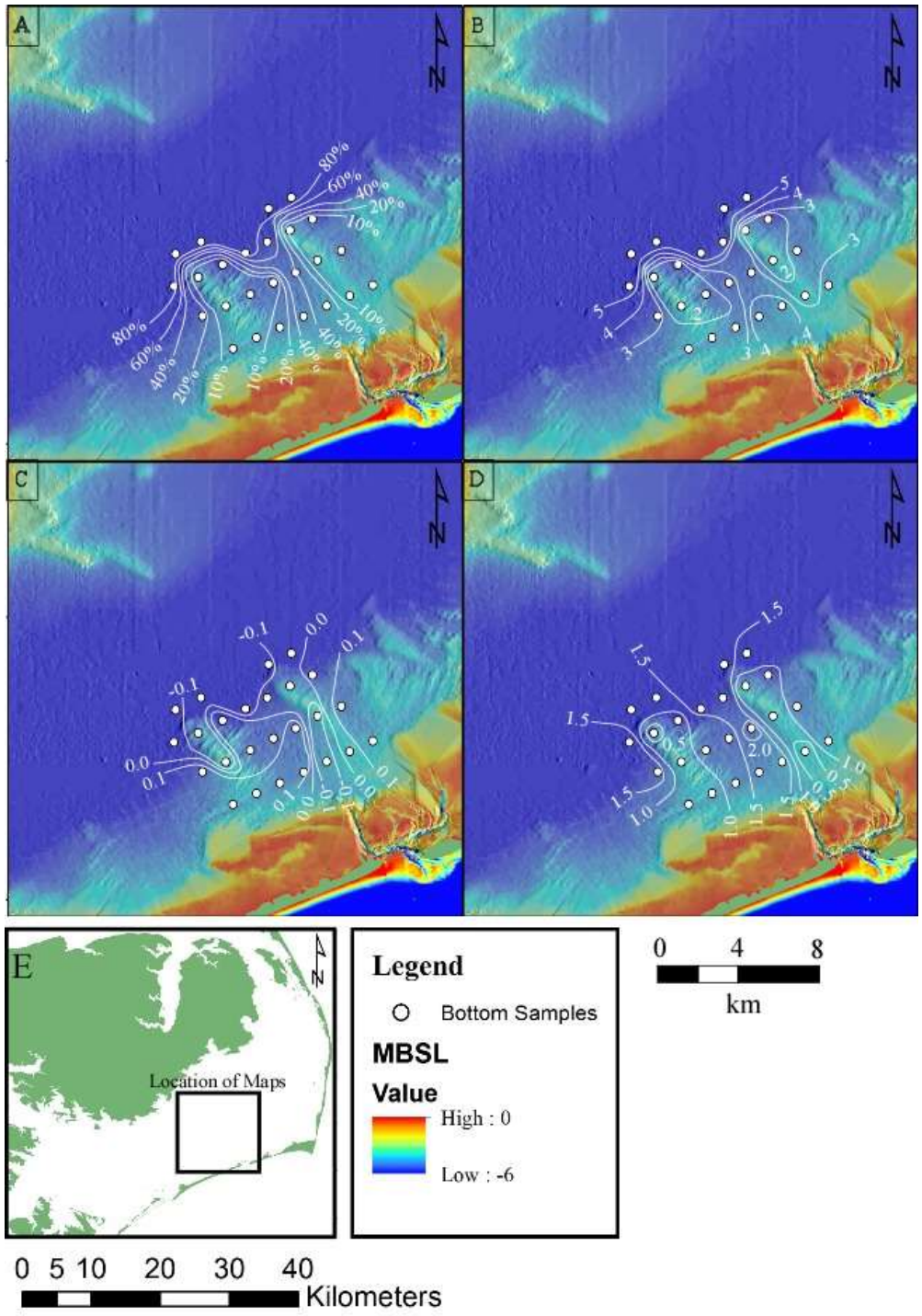

Figure 28: Location (Panel E) of surfaces sample grain-size statistics. Panel A is percent mud, Panel B is mean grain-size, Panel C is skewness, and Panel D is sorting (based on Blott and Pye, 2001). Note units in Panel B, Panel C, and Panel D are in ϕ (Folk and Ward, 1957; Folk, 1974).

5. Discussion

5.1 Evolution of Pamlico Sound

5.1.1 Pre 4000 cal yr. BP

The antecedent topography of Pamlico Sound affects modern estuarine conditions, providing 'new' sediments during storm events and areas of erosion and deposition (Riggs et al., 1995). The antecedent topography, associated with the late Pleistocene, was exposed during the Last Glacial Maximum (LGM) (Riggs et al., 1995). River drainage systems associated with the Neuse River, Tar-Pamlico River, and paleo-Pamlico Creek are incised into the Pleistocene surface (Figure 29; Riggs et al., 1995; Mallinson et al., 2010; 2017). These incised valleys were inundated and filled with sediment from 7500–4000 cal yr. BP, and foraminiferal data indicate the existence of estuarine conditions during that time interval (Culver et al., 2007; Grand Pre et al., 2011). In the study area, seismic data image two antecedent highs (Figure 30) that were cored at the base of EPamSh16-1 and EPamSh16-4. These highs are on the west side of the Hatteras Flats Interstream Divide (HFID), occur between ca. 7 and 5 mbsl, and underlie the modern sand ridges. They occur between small incised channels which are likely tributaries to Pamlico Creek, thus they represent interfluves. Data from Zaremba et al. (2016), suggest that the interfluves were overtopped between 5000–4000 cal yr. BP which resulted in increased hydrodynamic energy in the estuary such as increased wave and tidal energy. Data from Kopp et al. (2015) suggests that these interfluves were overtopped between 6000–5000 cal yr. BP.

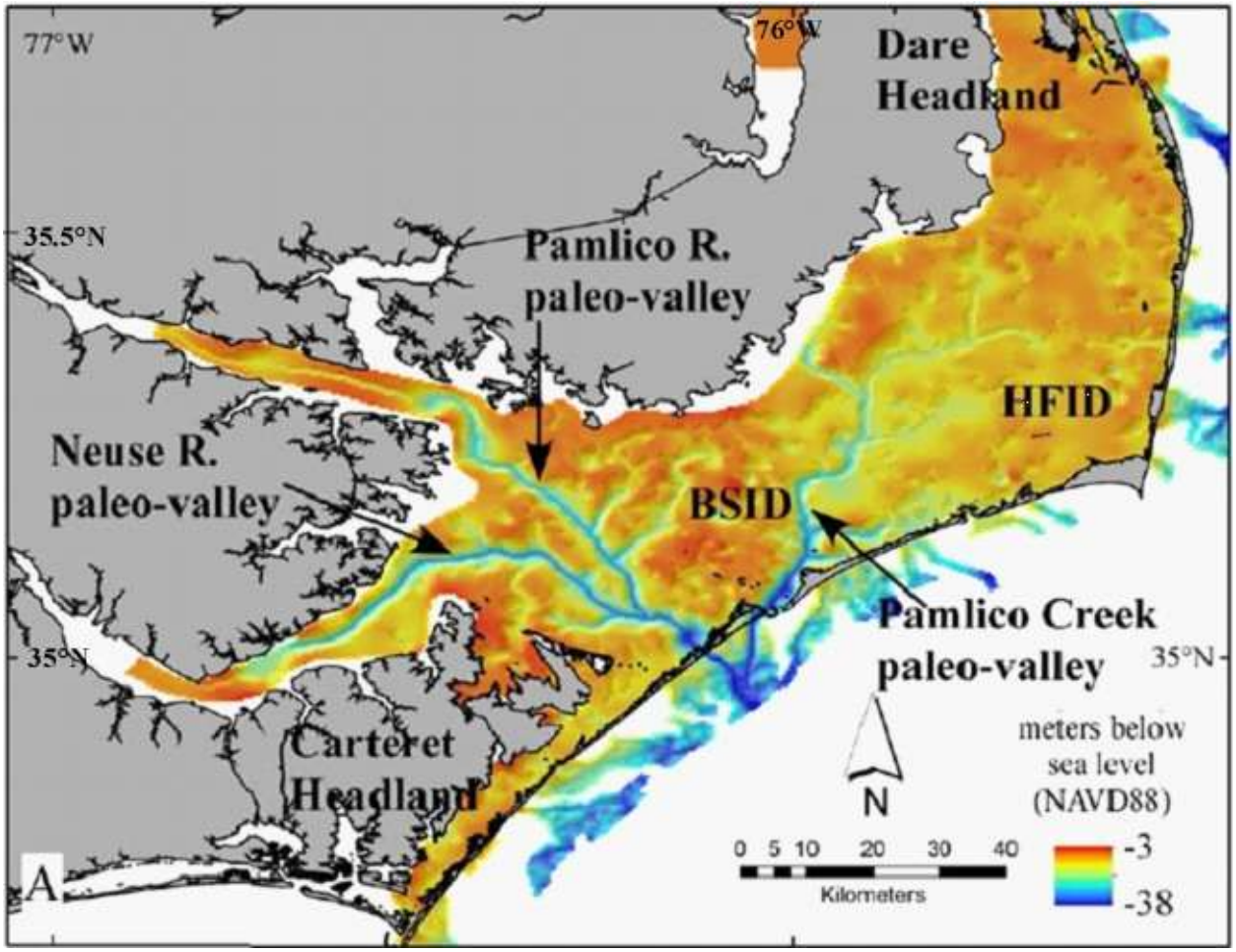

Figure 29: Map showing Pleistocene paleotopographic surface based on seismic data (modified from Mallinson et al., 2010; 2017). Note the Pamlico River, Neuse River, and Pamlico Creek paleo-valleys incised into the Pleistocene surface. BSID is the Bluff Shoal interstream divide and HFID is the Hatteras Flats interstream divide.

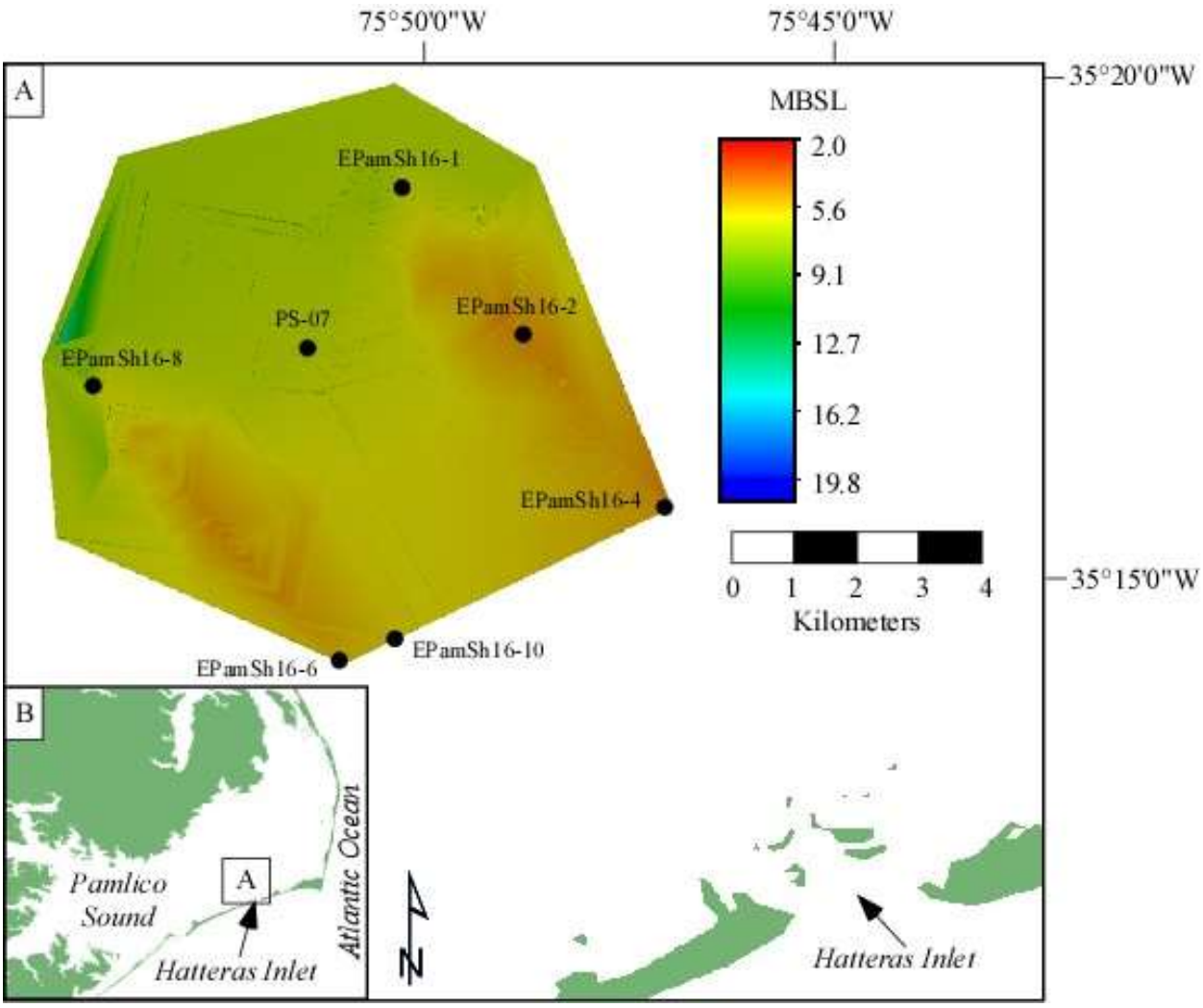

Figure 30: Pleistocene surface in study area. Note color scale begins 2.0 m below sea-level.

In the Hatteras Flats region, Smith et al. (2009) identified relict flood tide delta and estuarine deposits dating from 6000–4000 cal yr. BP which suggests the presence of barrier islands during that time period. Within the study area of this investigation, deposits in EPamSh16-4 from 3.7–3.0 mbsf (7.4–6.7 mbsl) consist of EF I, composed entirely of rooted bioturbated slightly muddy sand lithofacies, and occur below the interpreted H/P boundary based on correlation to the chirp seismic data (Figures 23, 24, 25) . The rooted bioturbated slightly muddy sand is barren of foraminifera and dated to 6664–6547 cal yr. BP using a root found in

EF I. The root provides a minimum age as it must post-date the deposition of the sediments in which it occurs. Its occurrence indicates the subaerial exposure of the overlying surface and provides a terrestrial sea-level limiting point of approximately -7.0 m at ~6500 cal yr. BP, in good agreement with Kopp et al. (2015). In addition to a reworked mollusk dated to 4735–4550 cal yr. BP in EPamSh16-6 at 0.97 mbsf indicates no preserved *in situ* deposits during this interval and extending to 2500 cal yr. BP.

The sand fraction in EF I has a mean grain-size ranging from 1.80–2.35 ϕ, which is similar to shoreface and inlet sands of Peek et al. (2013) and coarser than flood tide delta sands of Smith (2016). Southeast dipping clinoforms (6–8 mbsl) and grain-size data suggest that this may be associated with a prograding shoreface that was active during a Pleistocene highstand (Figure 32). The Pleistocene lithological unit (rooted bioturbated slightly muddy sand) has roots and is similar to the Pleistocene unit (organic sand) found by Peek et al. (2013) without roots beneath the Hatteras Flats. The H/P boundary from EPamSh16-4 is only slightly shallower (6.4 mbsf) than that cored by Twamley (2006) (7.5 mbsf) near Hatteras Village on the edge of Hatteras Flats, likely due to the Pleistocene high under the sand ridges. Beneath the Hatteras Flats behind the Buxton regions (east of the study area) the Pleistocene surface ranges from 8–12 mbsl (Peek et al., 2013).

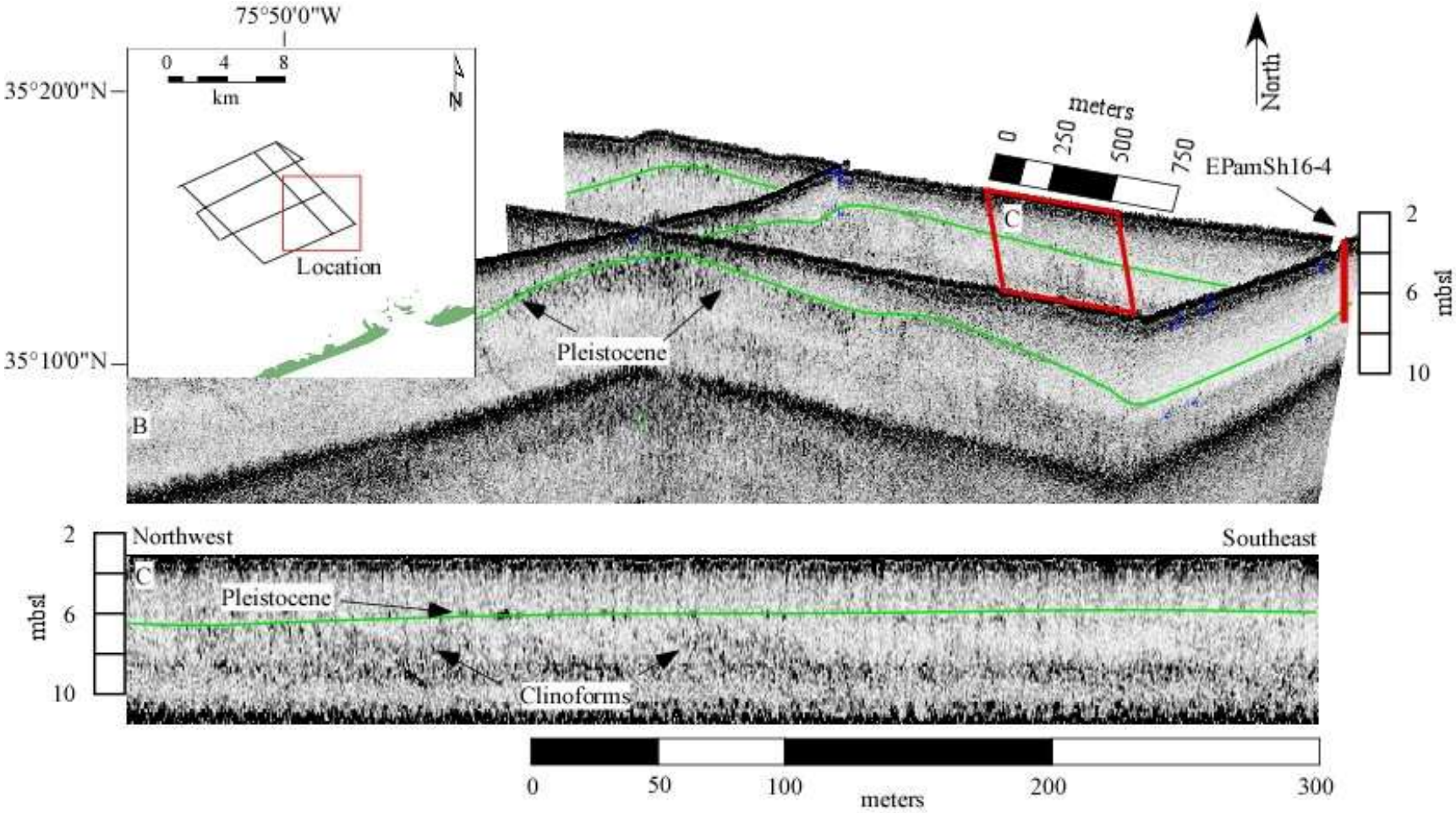

Figure 31: Fence diagram (Panel B) of seismic data in southeast section of study area. Panel C: Close-up of southeast dipping clinoforms below the Pleistocene horizon.

5.1.2 4000–2500 cal yr. BP

From 4000–3500 cal yr. BP, normal marine salinity foraminifera and planktonic foraminifera are observed in southern Pamlico Sound suggesting increased exchange with the Atlantic Ocean (Culver et al., 2007; Metger, 2009; Grand Pre et al., 2011). From 4000–3500 cal yr. BP Pamlico Sound was likely shallower than it is today (Mallinson et al., 2017). From 3500–2500 cal yr. BP, in southern Pamlico Sound, marine influence decreased as barrier islands reformed on shallow shoals and barrier segmentation was reduced (Culver et al., 2007; Grand Pre et al., 2011). The barrier islands in the Cape Hatteras region were likely prograding from 3500–2500 cal yr. BP based on optically stimulated luminescence ages and seismic data across the Hatteras Flats (Mallinson et al., 2017).

Seismic unit 2 is imaged from 4.1–4.9 mbsf (10.2–11.0 mbsl) in EPamSh16-1, and is constrained to 4000–2500 cal yr. BP in age. This unit is not imaged in the rest of the study area. EF III occurs in this location which is consistent with an increase in hydrodynamic energy.

5.1.3 2500–1000 cal yr. BP

From 2500–1000 cal yr. BP, EF IV was being deposited; and was recovered in vibracores EPamSh16-4, EPamSh16-6, and EPamSh16-10 (Figures 22, 23, 24). In EF IV, the increase in the sand fraction grain-size and decrease in percent mud suggests an increase in currents and waves above the H_{2500} horizon near the barrier islands. However, toward the north (EPamSh16-1 region) EF II is present suggesting low current and wave energy conditions during this interval. East of this study area, Peek et al. (2013) and Twamley et al. (2006) identified seaward-dipping clinoforms during this period. Near the northwest limit of the western ridge of the current study

area, there are northwest-dipping clinoforms suggesting sand ridge growth to the northwest (Figure 32).

EF IV occurs proximal to the barrier islands (cores EPamSh16-4, EPamSh16-6, and EPamSh16-10) during this time interval (Figures 22, 23, 24). The occurrence of High Brackish biofacies A in EPamSh16-6 and EPamSh16-10 indicates the influence of normal marine salinity conditions. This may be evidence for the first occurrence of an inlet in the general location of modern Hatteras Inlet. This is in agreement with Rosenberger (2006) and Culver et al. (2007) who indicate greater marine exchange at 2500 cal yr. BP, but only in a limited area near Ocracoke Inlet and North Core Banks. However, in EPamSh16-1 (basinward vibracore) and EPamSh16-4, during this interval, High Brackish biofacies B (low diversity dominated by *Elphidium excavatum*) is present suggesting there was less marine influence. Furthermore, EPamSh16-2 and EPamSh16-8 are barren of foraminifera but the sand fraction has a mean grain-size of 1.5–2.0 ϕ (medium sand) and a percent mud of <5 %, which suggests an increase in current activity. This implies that the study area was in transition from marine-influenced in the south to estuarine-influenced in the north (only EPamSh16-1, northernmost vibracore).

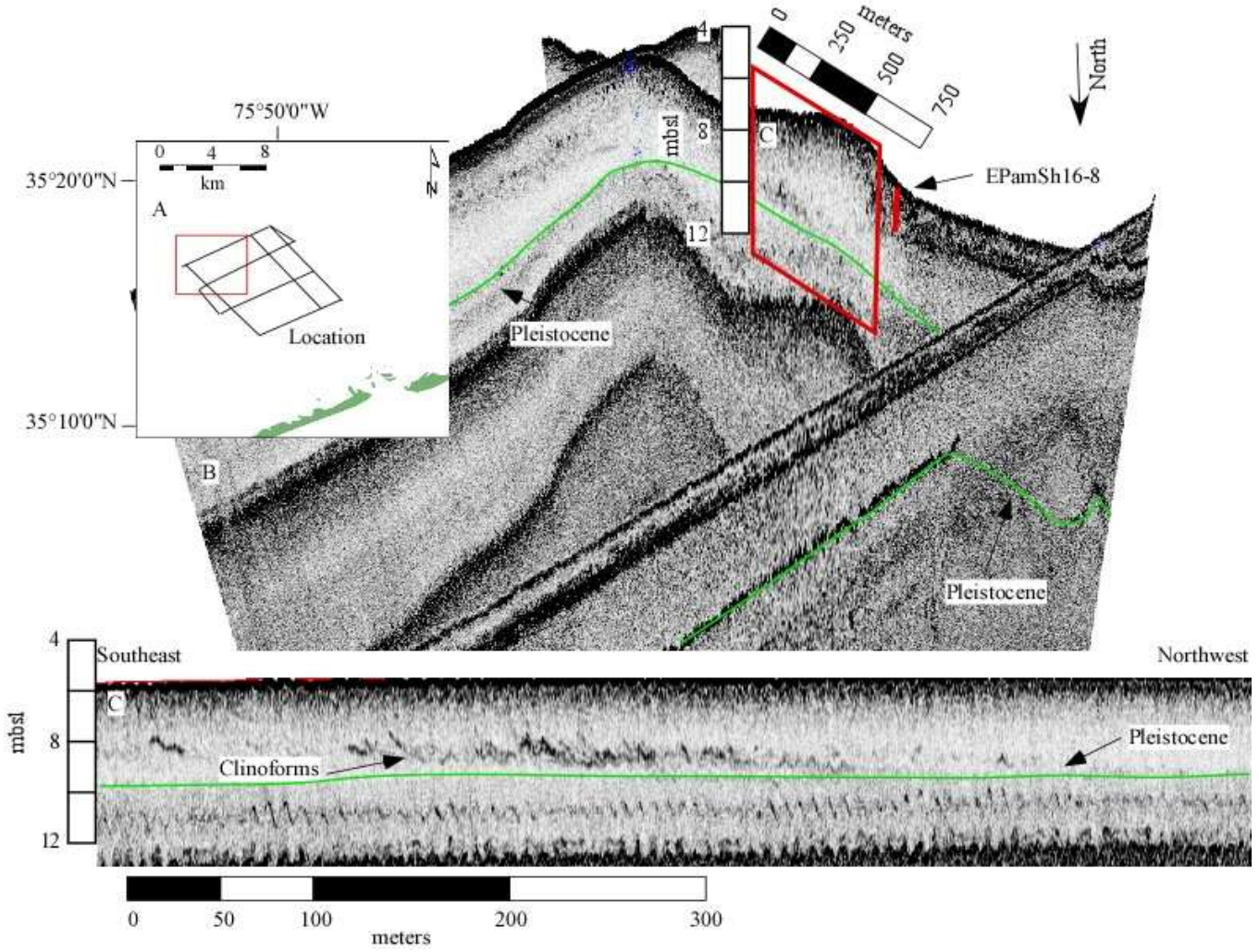

Figure 32: Fence diagram (Panel B) of seismic data in northwest section of study area. Panel C: Northwest dipping clinoforms above the Pleistocene horizon in seismic unit 3 (2500–1000 cal yr. BP).

Along the sand ridge, distal from the barrier islands, the surface sample grain-size is more characteristic of modern shoreface deposits, and proximally grain-size exhibits flood-tide delta characteristics (Peek et al., 2013; Smith, 2016). Peek et al. (2013) examined both shoreface (Hatteras Island) and flood-tide delta (on Hatteras Flats) grain-size and found that shoreface sands averaged 1.51 ϕ and FTD sands averaged 2.6 ϕ. Smith (2016) also recorded grain-size averaging 2.56 ϕ for the OFTD. There is a slight coarsening-up trend from 2500 cal yr. BP to present in the sand fraction; increasing from 1.85–1.14 ϕ in EPamSh16-2 (entire core) and from 1.83–1.19 ϕ in EPamSh16-8 (entire core). In EPamSh16-6 the mean grain-size of the sand also coarsens up-core from 2.81–2.47 ϕ (2.90 mbsf to top of core) (Appendix C). In EPamSh16-4 mean grain-size decreases initially from 2.08–2.84 ϕ (2.70–0.75 mbsf) then increases to 2.26 ϕ. This suggests that the sand ridges were active continually at 2500 cal yr. BP in the areas of EPamSh16-2, EPamSh16-6, and EPamSh16-8. However, in EPamSh16-4, a decrease in mean grain-size suggests that the sand ridge was affected by currents less than EPamSh16-2, EPamSh16-6, and EPamSh16-8 but became more active after the H_{500} horizon.

5.1.4 1000–500 cal yr. BP

Approximately 1000 cal yr. BP, the southern region of Pamlico Sound became dominated by normal marine salinity conditions from the widespread erosion of Ocracoke Barrier Island (Culver et al., 2007; Mallinson et al., 2011; Grand Pre et al., 2011; Peek et al., 2013). The breakdown of the Ocracoke Barrier Island was likely due to an increase in hurricane activity during the Medieval Climate Anomaly (MCA) (Mann et al., 2009; Donnelly et al., 2015), while Culver et al. (2007) suggests alternatively that tsunamis might have caused the breakdown. The ridges in this study were identified by Zaremba et al. (2016) (referred to as the MCA shoals) and

it was suggested that the ridges began forming in response to the breakdown in barrier island continuity. However, based on radiocarbon age dating within the sand unit in this study, we suggest that these ridges were active earlier (beginning ~2500 cal yr. BP) than the MCA (1100–950 cal yr. BP). An increase in shell material is noted within the ridges (EPamSh16-4) that is dated to 1000 cal yr. BP and represents the H_{1000} horizon in the seismic data and suggests an increase in hydrodynamic activity. At the distal portion of the sand ridge it appears that H_{1000} from Zaremba et al. (2016) goes beneath portions of the sand ridge near EPamSh16-8 suggesting sand transport along the ridge during this time.

5.1.5 500 cal yr. BP–present

Post MCA, at 500 cal yr. BP, there is a decrease in water temperature of 4.7°C in Chesapeake Bay, north of APES corresponding with the Little Ice Age (LIA) (Cronin et al., 2003). During the LIA there was significant inlet activity on the Outer Banks (Mallinson et al., 2008, Mallinson et al., 2011). At 500 cal yr. BP, the upper section of all EPamSh16 cores show an increase in mean grain-size of the sand fraction. In EPamSh16-10, a channel was cored and contained EF II (mud), which was dated to 413–264cal yr. BP. This channel is a product of tidal scour related to inlet activity, with mud filling the channel upon a decline in inlet activity. The channel is orientated northwest-southeast between the sand ridges. Throughout much of the Hatteras Flats, to the northeast, Twamley (2006) and Peek et al. (2013) identify similar channels via seismic data trending to the northwest. EF IV was deposited on top of EF II in the last two or three centuries and the presence of the EF IV above the channel fill suggests that the sand ridges are currently active. Radiocarbon age estimates in EPamSh16-1 at 0.4 mbsf (6.5 mbsl) and at 1.0 mbsf (7.4 mbsl), and EPamSh16-10 at 1.8 mbsf (6.4 mbsl) yielded dates of 273–93 cal yr. BP,

334–143 cal yr. BP, and 413–265 cal yr. BP, respectively, in mud and sandy mud lithofacies. Infill of the channels with mud and the presence of High Brackish biofacies B above the H_{500} horizon in all the vibracores suggests that many of the active inlets were closing, returning Pamlico Sound to estuarine conditions, in agreement with the findings of Culver et al. (2007), Grand Pre et al. (2011), and Peek et al. (2013).

Zaremba et al. (2016) noted that there was an increase in BMS values and mud content above the H_{500} horizon which may be an effect of European settlement and subsequent industrialization depositing trace metals within the sediments (Corbett et al., 2007). However, the BMS values in this study increase initially in EPamSh16-6 then decrease above the H_{500} horizon on the sand ridges (Figure 25). In EPamSh16-1 and EPamSh16-10, the BMS values initially remain high due to increased percent mud, then decrease (EPamSh16-1) or increase (EPamSh16-10). EPamSh16-4 also shows a decrease in BMS values after the H_{500} horizon.

5.2 Sand Ridge Origin and Dynamics

Sand ridges are defined as elongate coastal to shelf sand bodies that are larger and longer-lived than subaqueous dunes (Swift 1985; Snedden and Dalrymple 1999). The most commonly modeled type of sand ridge is the shallow-shelf marine sand body (Snedden and Bergman 1999). The model that Snedden and Bergman (1999) described is associated with a transgressive systems tract where the sand ridge occurs above a ravinement surface, the interior of the sand ridge consists of the ridge precursor on a structural high, and the overall shape resembles a dune with lee and stoss sides. In this study, Pleistocene interfluves are structural highs and they influence the modern sand ridges which resemble dunes with lee and stoss sides (Figure 33, panel C). Along the distal (northern) edge of the study area between the two sand ridges, steep

channels are incised into the Pleistocene surface draining into the Paleo-Pamlico Creek drainage system (Figures 33, Panel C and 34). These small scale channels, 2–3 m deep and 50–100 m wide, are similar to what is found on the banks of many rivers in eastern North Carolina. This corroborates the suggestion by Riggs et al. (1995) of submarine headlands, composed of Pleistocene units, influencing the modern shoreface and the geomorphology of the barrier-estuarine system. The sand ridges reside on the west flank of the Hatteras Flats Interstream Divide (HFID; Figure 29), and are similar to Wimble Shoals and Kinnakeet Shoals which occur on the east side of the HFID in that they are likewise interpreted as Pleistocene interfluves (Riggs et al., 1995; Thieler et al., 2015). These geomorphic features affect the energy regime and sediment transport through wave refraction and wave setup, which maintains the sediments within the shoals (Riggs et al., 1995; Gibbons, 2017). The HFID was inundated and eroded at approximately 5000 to 4000 cal yr. BP (Zaremba et al., 2016) and the Pleistocene sands were incorporated into the Holocene sand ridges. Wimble Shoals and Kinnakeet Shoals differ from the sand ridges of this study in that they are on the ocean side of the barrier islands and are influenced more by wave energy and have greater relief. Sediments from Wimble Shoals, Platt Shoals and Kinnakeet Shoals consist of medium to fine sands (Gibbons, 2017) similar to the sediments of the sand ridges of this study.

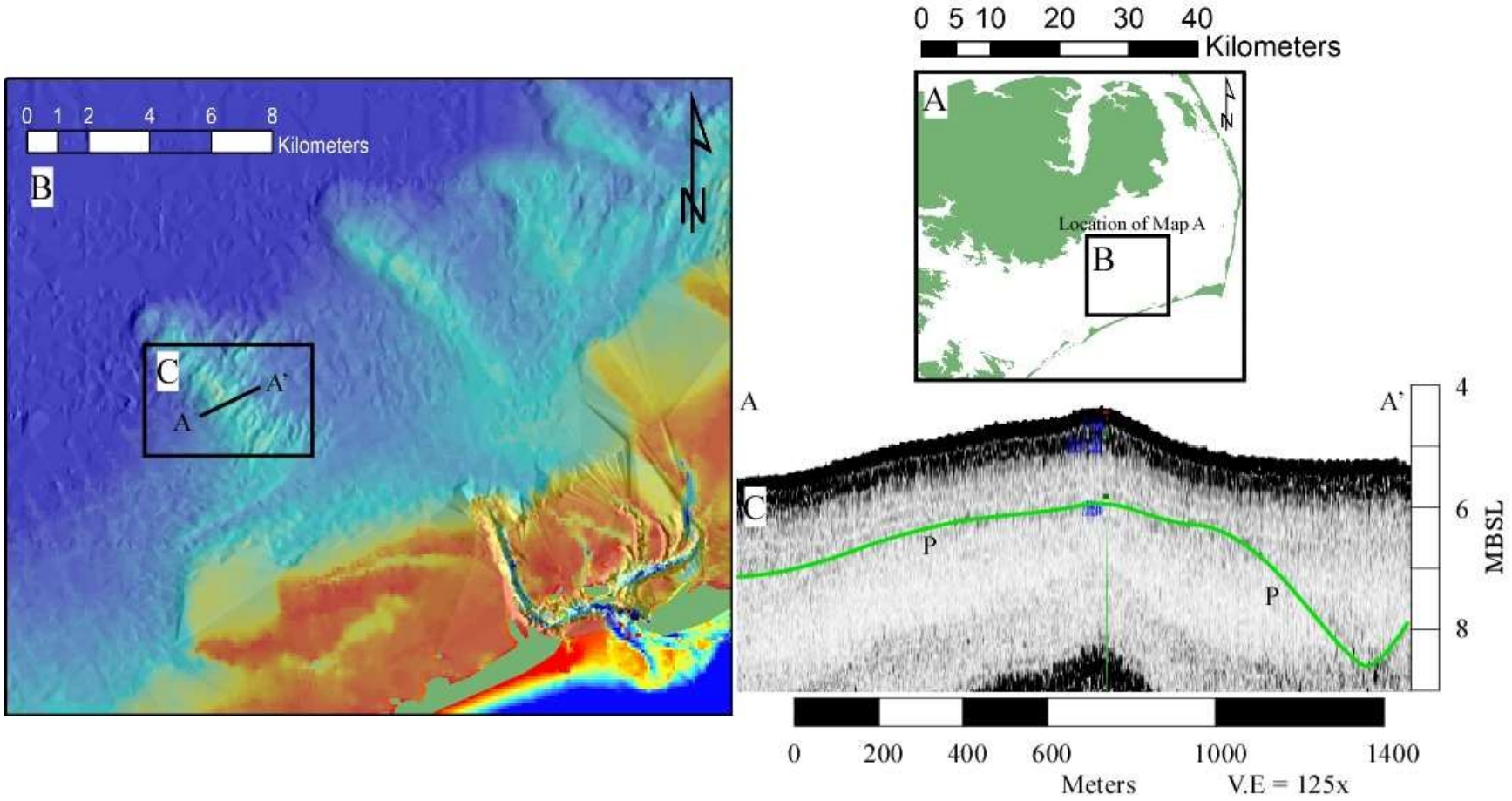

Figure 33: Cross-section (A-A') across the western sand ridge. Panel C displays topographic profile across western sand ridge. Vertical exaggeration is 125x.

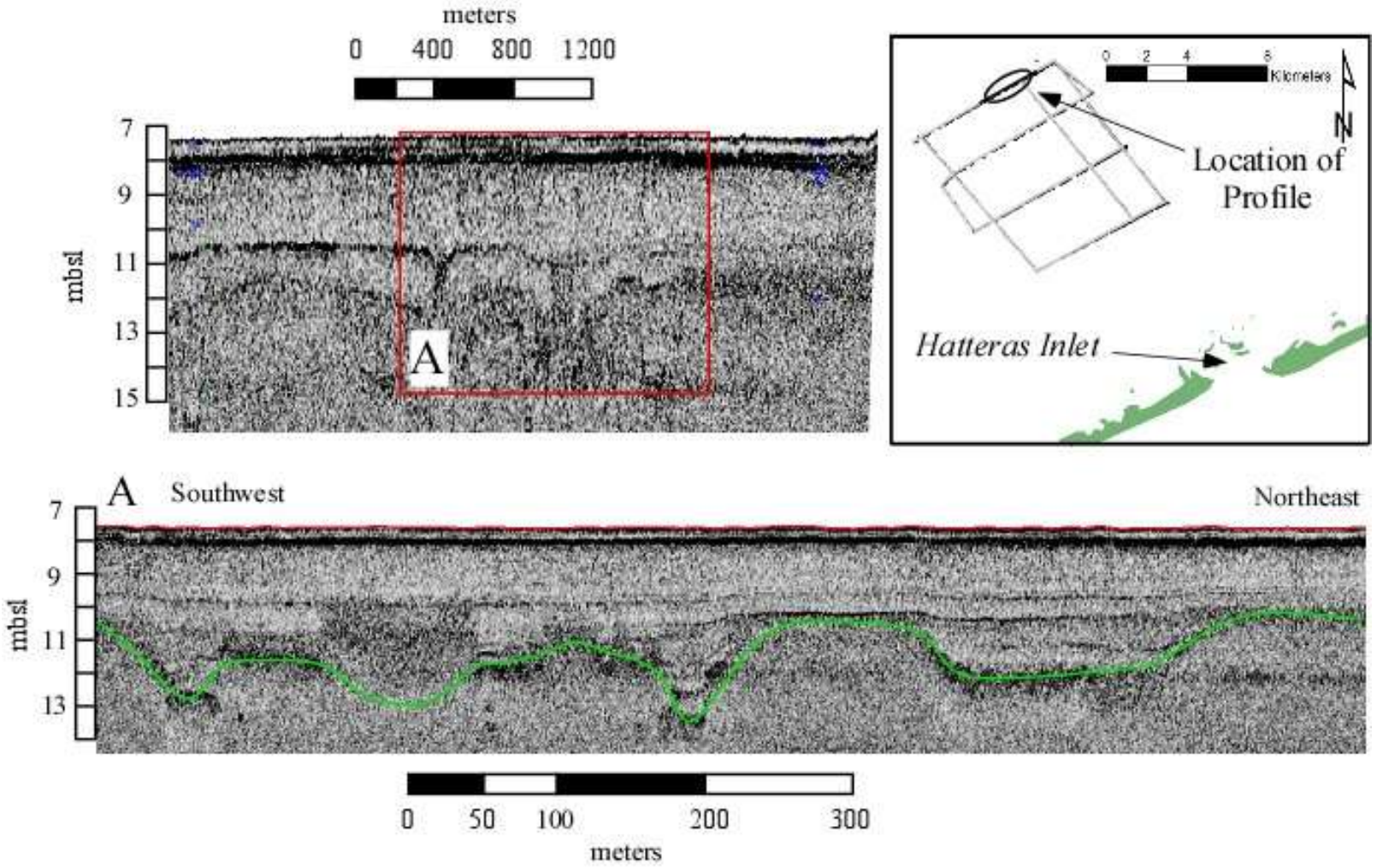

Figure 34: Seismic data (upper panel) of distal channels incised into the Pleistocene surface. Green line represents the Pleistocene surface in magnified portion (bottom panel). Channels are up to 2 m in depth and 50–200 m wide.

Surface sample sediments are finer to the west, away from ridge crests, suggesting that the lee side of the ridges is to the west, the direction of possible migration of the sand ridges, which agrees with the northwest dipping clinoforms on the distal end of the western ridge (Figure 32). The grain-size of the surface samples along the center of the western ridge range from 2.04 ϕ along the lee side of the ridge (EPBS-27, west) to 1.78 ϕ on the crest (EPBS-3) to 1.61 ϕ along the stoss side (EPBS-6, east). This is similar to the eastern ridge but the latter has a lesser magnitude of change from 1.98 ϕ in the trough along the lee side (EPBS-14, west) to 1.84 ϕ on the crest (EPBS-19) to 1.78 ϕ along the stoss side (EPBS-22, east). However, migration of the sand ridges is limited due to reversal of currents at times, depending on the winds and storms, despite the dominant current directed toward the southwest (Figure 35). Clunies et al. (2017) demonstrated that wind direction can affect the velocity and direction of currents within Pamlico Sound. The sand ridges of this study are affected by currents through Hatteras Inlet when winds come from the south and along the estuarine shore side of the barrier islands through Hatteras Flats when winds come from the north (Figure 35).

These sand ridges have similar characteristics to sand ridges characterized by Snedden and Dalrymple (1999). Typically, the lee-side slope is <1° and no more than a maximum of 7° (Table 13; Snedden and Dalrymple, 1999). On the distal edge of the western sand ridge (this study) there are northwest dipping clinoforms at an apparent dip angle of 3°. In the East China Sea, Berné et al. (2002) used high-resolution seismic to identify clinoforms dipping <6° in the direction of the lee face of the ridge. The clinoforms in these ridges are not imaged adequately to identify the true dip direction; but the apparent dip is toward the northwest (toward the lee face).

Snedden and Dalrymple (1999) described three classes of shelf sand ridges (class I, class II, and class III) based on the evolution of a sand ridge (Figure 37). Based on this classification,

the sand ridges in this study are most likely juvenile (Class I) because the Pleistocene high represents the precursor, the deposit post-dates the transgressive ravinement, there is more than one ridge, and the possibility to be buried by mud is moderate to low (Figure 30). However, these ridges are in an estuarine environment, not in a shelf environment, from which the definition of sand ridges is derived.

In the study area, the western sand ridge has sand waves (dunes) superimposed along the ridge whereas the eastern sand ridge does not. The sand waves are visually oriented parallel to slightly oblique to the barrier islands, approximately 0.5 m high, and they average 200 m apart (trough to trough). The orientation of the sand waves suggests that there is sand movement down the axis of the sand ridges, however, the direction of movement is not clear because the orientations of the apparent lee and stoss faces are not consistent. Additionally, farther to the northeast, sand waves occur in association with ridge features near the Hatteras Flats (Figure 1B). The lack of sand waves on the eastern ridge suggests that this ridge is subject to different hydrodynamic conditions than the western ridge or the ridges to the northeast. The eastern ridge is influenced by Hatteras Inlet more than the rest of the sand ridge field (Figures 3, 35, 36).

During storm events, the greatest bed shear stress is along the sand ridges (Figure 3) and there are high surface current velocities through Hatteras Inlet during storm events (Figure 36). Clunies et al. (2017) modeled a velocity of 45 cms^{-1} over Bluff Shoal, the vector shown in figures 35 and 36 through Hatteras inlet is twice as long as the vectors over Bluff Shoal, suggesting a velocity in excess of 45 cms^{-1}. Park et al. (2003) described sand ridges that exhibited no bedforms where velocities were approximately 100 cms^{-1}. Given that the average particle size of the uppermost sand ridge ranges from 1.25–2.50 ϕ, a current velocity of 10–15 cms^{-1} will initiate movement of the sand on the ridges (Wright et a., 1999). Assuming a

conservative fetch of 30 km (from the northwest), an estimate can be made of the current velocity at differing wind speeds. The greatest depth in the study area is 6.10 mbsl at EPamSh16-1 and shallowest is 3.57 mbsl in EPamSh16-2 with the rest of the cores between 4.82–3.72 mbsl. Using those values, and the fetch- and depth-limited wave calculator from Woods Hole Coastal and Marine Science Center (https://woodshole.er.usgs.gov/project-pages/coastal_model/Tools/fetch_limited.html), wave heights and periods were calculated. These were then used in the following equation (Wright et al., 1999) to calculate maximum orbital velocity.

$$\mu_m = \frac{\pi H}{Tsi \quad \frac{2\pi d}{L}}$$

A 20 mph wind generates currents of 16–24 cms^{-1} along the entire ridge which is enough velocity to initiate sand transport across the ridges. Thus, sand transport is likely active along the ridges during typical elevated wind conditions (i.e., it is not necessary to invoke a large storm to activate them). Hurricane Irene (2011) had sustained winds of approximately 70 mph (86 mph at landfall near Cape Lookout, NC) which generated currents from approximately 50 cms^{-1} at 6.1 mbsl to 150 cms^{-1} at 3.57 mbsl easily mobilizing sand to depths below the sand ridges.

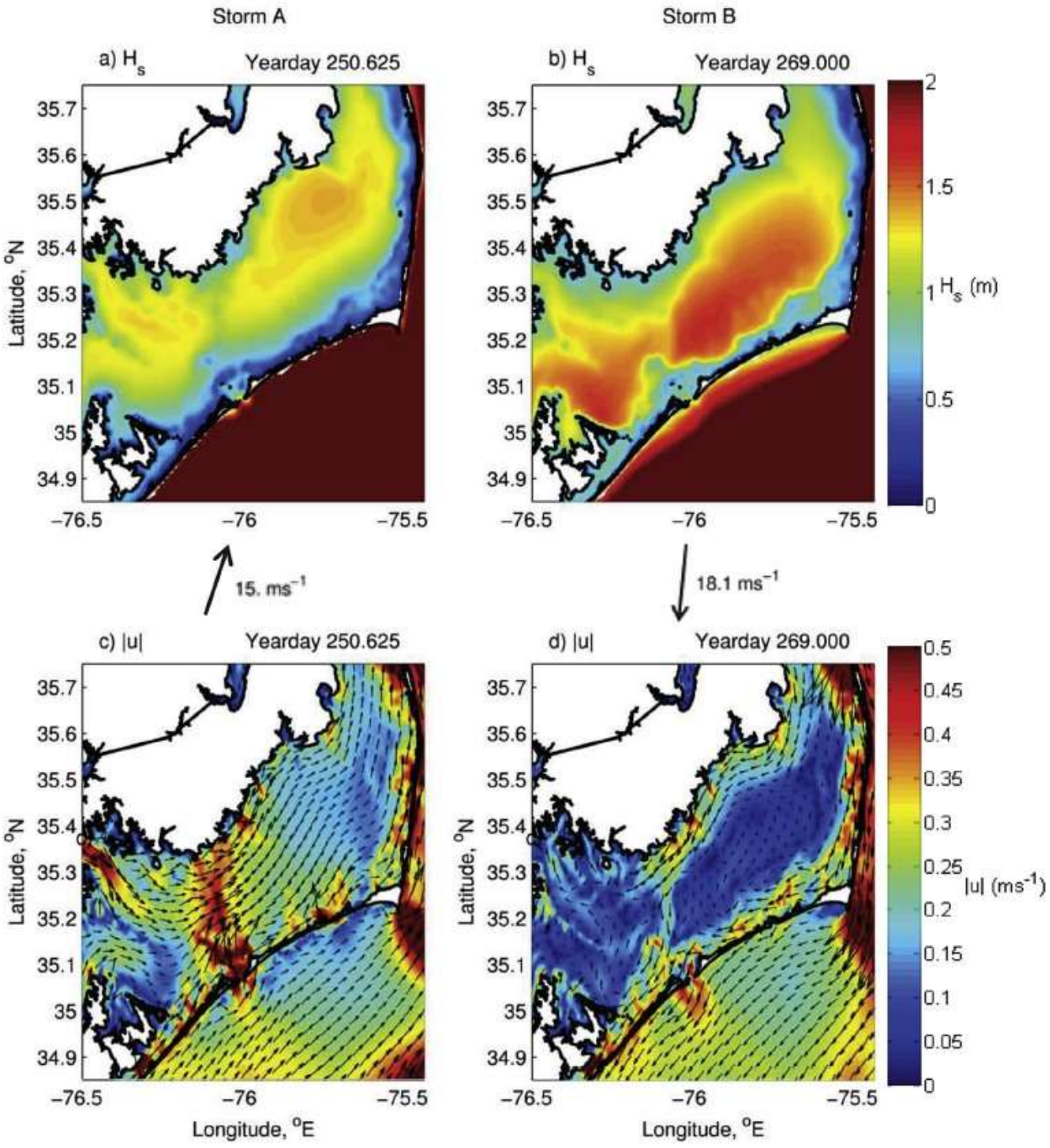

Figure 35: Model results indicating: a) significant wave height (H_s) for the peak conditions of Storm A; b) H_s for the peak conditions of Storm B; c) depth-averaged current velocities for the peak conditions of Storm A; d) depth-averaged current velocities for the peak conditions of Storm B (from Clunies et al., 2017). Arrows indicate wind direction.

On the western sand ridge seismic data show northwest dipping clinoforms internally. These clinoforms suggest the direction of early propagation of the ridge towards the Pamlico Sound basin. EF IV, characterizing the modern environment, includes muddy sand (mS) and bioturbated slightly muddy sand (biot (m)S) lithofacies (containing less than 30% mud), but the sediments are generally 5–15 % mud. Utilizing the H_{SF} (modern surface), H_{2500}, and P/H_{RS} horizons an estimate can be made of an approximate volume of the sand ridges. Beach nourishment projects in North Carolina have utilized approximately 23,000,000 yd^3 of sand from 1966 to 2017 (Gibbons, 2017), with typical nourishment projects ranging from 4,600,000 to 18,500 yd^3. Within the sand ridges of this study, there are approximately 1,275,000 m^3 of sand, assuming an 85% sand average. The grain-size of the ridge sand is slightly smaller (2.28 ϕ) than shoreface and inlet sand (mean of ca. 1.50 ϕ; Peek et al., 2014). This suggests that the sediments within the sand ridges are not ideal for beach nourishment projects near Cape Hatteras, but they remain a possibility if used on a lower energy shore, of if finer sand grains and mud are removed.

Table 13: Modern shelf sand ridge characteristics from Swift (1985); Dalrymple and Hoogendoorn (1997); Snedden and Dalrymple (1999).

Criteria	Characteristics	Sand Ridges of this study
Orientation	Flow-oblique	Flow-oblique
Symmetry	Dominantly asymmetrical	Asymmetrical
Vertical Scale (relief)	5–40 m	0.5–2.5 m
Long axis Length	0.7–8 km	6.5 km
Barform side slopes	Typically <1° to a maximum 7°	0.01–0.08°
Grain Size	Fine to coarse sand	Fine to medium sand
Lateral Trends	Stoss side coarser than lee side	coarser sediments (stoss) to the east of each sand ridge
Superimposed Bedforms	Medium to large 2D and 3D hummocky mega ripples, current ripples	Western ridge appears to have large mega ripples and/or dunes

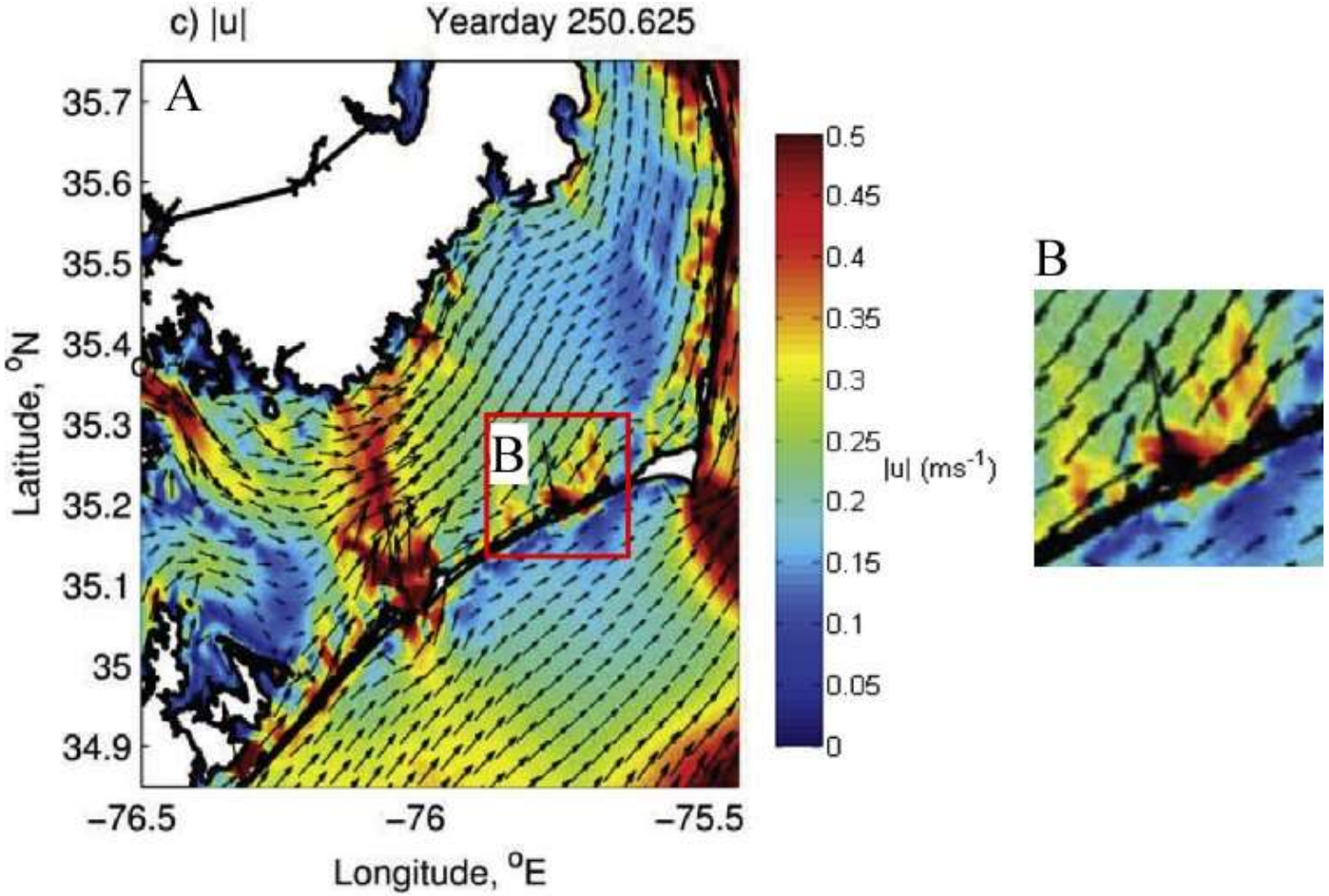

Figure 36: Depth-average current velocities (Panel A) for the peak conditions of Storm A which occurred September 2008 (from Clunies et al., 2017). Hatteras Inlet (Panel B) has high depth-averaged current velocities. Current velocities are relative to winds from the south at 15.0 ms^{-1}.

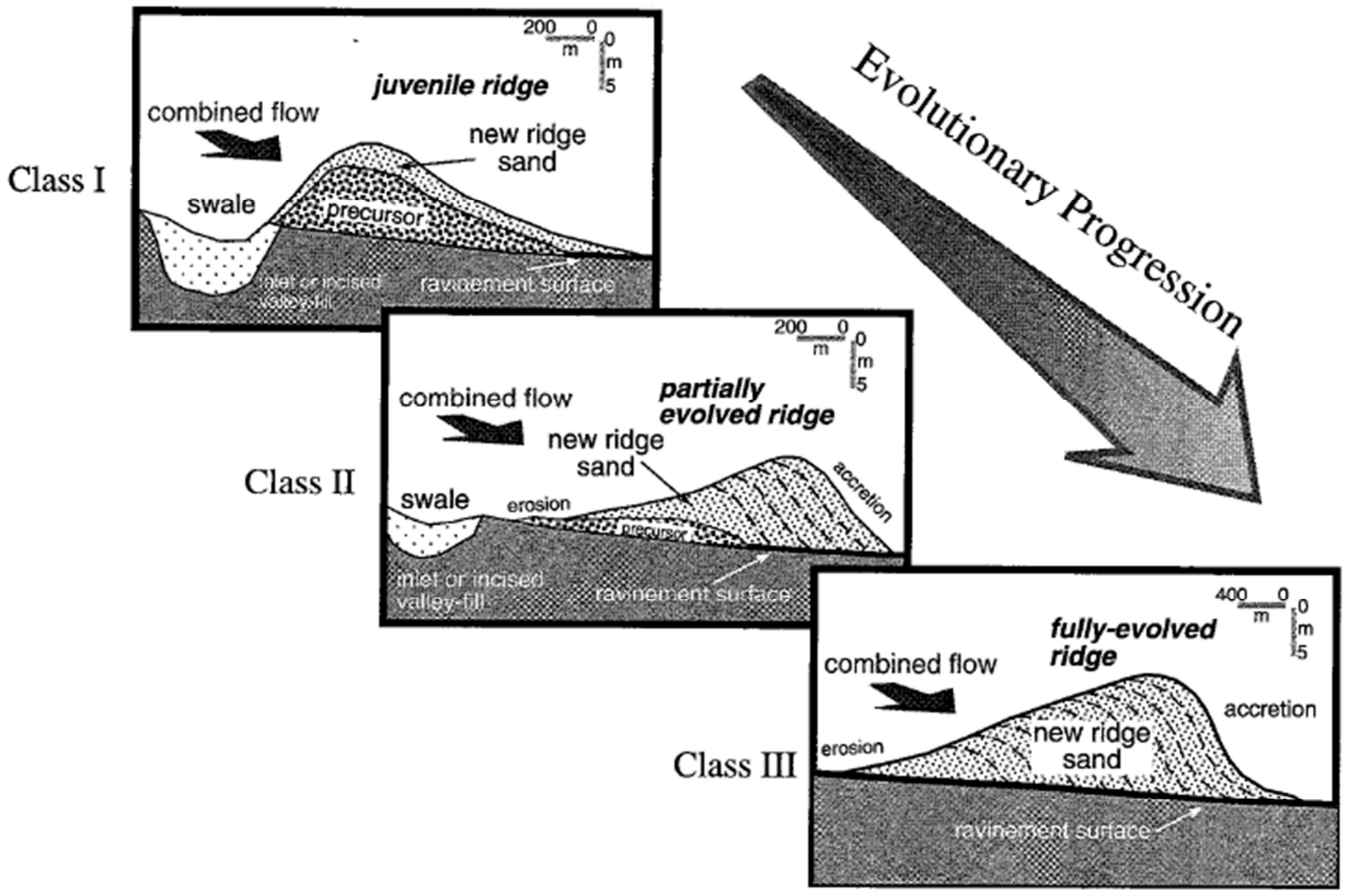

Figure 37: Schematic diagram of ridge classes evolving through time, demonstrating direction of erosion and accretion (from Snedden and Dalrymple, 1999).

6. Summary

1. Six vibracores were collected (2016) from Pamlico Sound, North Carolina and together with previously collected data were used to interpret the geologic history of the sand ridges behind Hatteras Island, Pamlico Sound, adjacent to the Hatteras Inlet.
2. Eleven lithofacies were recognized: mud, sandy mud, slightly gravelly sandy mud, bioturbated slightly muddy sand, rooted bioturbated slightly muddy sand, muddy sand, bioturbated muddy sand, mottled bioturbated muddy sand, mixed slightly gravelly muddy sand, mixed gravelly muddy sand, and bioclastic gravelly muddy sand.
3. Two biofacies, High Brackish biofacies A and B, were determined using foraminiferal assemblages from the six cores. High Brackish biofacies A consists of *Ammonia parkinsoniana, Ammonia tepida, Cibicides lobatulus, Elphidium excavatum, Elphidium gunteri, Elphidium mexicanum, Elphidium subarcticum,* and *Haynesina germanica* occurred in two samples. High Brackish biofacies B contain *Ammonia parkinsoniana, Elphidium excavatum,* and *Elphidium gunteri* occurred in ten samples. The two biofacies are differentiated by diversity of species A = >3.0 and B <3.0.
4. Four environmental facies were interpreted using lithofacies and biofacies; (EF I) Pleistocene, (EF II) low-energy estuary/channel, (EF III) high-energy estuary (>30 % shells), and (EF IV) high-energy estuary (<30 % shells). .
5. Twelve radiocarbon age estimates (nine mollusk, two foraminiferal and, one plant/wood) were acquired from four vibracores (EPamSh16-1, EPamSh16-4, EPamSh16-6, and EPamSh16-10). Age estimates from mollusk samples ranged from modern to 4735 cal yr. BP, foraminiferal samples aged from modern to 2873 cal yr. BP, plant/wood sample aged from 6664–6547 cal yr. BP.

6. Five seismic units (SU 1–5) and six seismic horizons were defined in approximately 48 km of subsurface seismic data collected in the field area. The H_{RS} and P (Holocene ravinement surface and Pleistocene subaerial unconformity) seismic horizons for the study area are amalgamated into P/H_{RS}, indicating ravinement of the Pleistocene surface during sea-level rise. The P/H_{RS} and H_{2500} horizon become amalgamated at the basinward end of the sand ridges. Estuarine conditions prevailed during deposition of SU 2 (4000–2500 cal yr. BP) but were replaced by higher energy conditions during deposition of SU 3 (2500–1000 cal yr. BP). Normal marine conditions were prevalent during deposition of SU 4 from 1000–500 cal yr. BP and estuarine conditions returned during deposition of SU 5 (500 cal yr. BP–modern).
7. EF IV sediments, present in all cores, are most likely the result of reworked Pleistocene interfluves. Sediments in EF IV are well to moderately sorted, coarsely skewed fine to medium sand consisting of >90 % quartz.
8. Sand ridge formation began after deposition of the H_{2500} horizon on the Pleistocene interfluve highs. However, data also suggest significant sand mobilization during the Medieval Climate Anomaly. The modern sand ridge is likely migrating to the west. However, currents reverse directions according to wind patterns, mitigating migration.
9. The sand ridges are approximately 6.5 km in length with a relief of 0.5–2.5 m. Grain-size ranges from fine to medium sand throughout the sand ridge (SU3, SU4, and SU5) and reside on top of a Pleistocene high. Therefore, the ridges are classified as Class I juvenile sand ridges.
10. Sand waves are superimposed on the western sand ridge of this study and can be observed farther to the east near the Hatteras Flats but are absent on the eastern ridge of

this study. The eastern ridge is most likely influenced by additional high current velocities associated with storm surge due to its proximity to Hatteras Inlet. Sand transport occurs across the ridges under normal elevated wind conditions (ca. 20 mph).

References

Abbene, I.J., Culver, S.J., Corbett, D.R., Buzas, M.A., and Tully, L.S., 2006, Distribution of Foraminifera in Pamlico Sound, North Carolina, over the past century: The Journal of Foraminiferal Research, v. 36, p. 135–151, doi: 10.2113/36.2.135.

Berné, S., Vagner, P., Guichard, F., Lericolais, G., Liu, Z., Trentesaux, A., Yin, P., and Yi, H.I., 2002, Pleistocene forced regressions and tidal sand ridges in the East China Sea: Marine Geology, v. 188, p. 293–315, doi: 10.1016/S0025-3227(02)00446-2.

Blott, S.J. and Pye, K., 2001, GRADISTAT: a grain-size distribution and statistics package for the analysis of unconsolidated sediments: Earth Surface Processes and Landforms, v. 26, p. 1237-1248, doi: 10.1002/esp.261.

Burdette, K.E. and Mallinson, D.J., 2008, Geologic Framework of the Currituck Sand Ridges, northeastern North Carolina: Southeastern Geology, v. 46, p. 1–16, doi: 10.1016/j.margeo.2013.11.011.

Burkholder, J., Eggleston, D., Glasgow, H., Brownie, C., Reed, R., Janowitz, G., Posey, M., Melia, G., Kinder, C., Corbett, R., Toms, D., Alphin, T., Deamer, N., Springer, J., and Field, C.B., 2004, Comparative impacts of two major hurricane seasons on the Neuse River and western Pamlico Sound Ecosystems: Proceedings of the National Academy of Sciences, v. 101, p. 9291–9296, doi: 10.1073/pnas.0306842101.

Clunies, G., 2014, Hydrodynamics of a large and shallow back-barrier estuarine system and responses to long-term changes in geomorphology [MS thesis]: Kingston, Ontario, Canada, Queen's University, p. 1–99.

Clunies, G.J., Mulligan, R.P., Mallinson, D.J., and Walsh, J.P., 2017, Modeling hydrodynamics of large lagoons: Insights from the Albemarle-Pamlico Estuarine System: Estuarine, Coastal and Shelf Science, v. 189, p. 90–103, doi: 10.1016/j.ecss.2017.03.012.

Cole, W.S., 1931, The Pliocene and Pleistocene foraminifera of Florida: Florida State Geological Survey bulletin, v. 6, p. 77.

Corbett, D.R., Vance, D., Letrick, E., Mallinson, D., and Culver, S., 2007, Decadal-scale sediment dynamics and environmental change in the Albemarle estuarine system, North Carolina: Estuarine, Coastal and Shelf Science, v. 71, p. 717–729, doi: 10.1016/j.ecss.2006.09.024.

Cronin, T., Willard, D., Karlsen, A., Ishman, S., Verardo, S., McGeehin, J., Kerhin, R., Holmes, C., Colman, S., and Zimmerman, A., 2000, Climatic variability in the eastern United States over the past millennium from Chesapeake Bay sediments: Geology, v. 28, p. 3–6, doi: CVITEU>2.3.CO;2.

Culver, S.J., Ames, D.V., Corbett, D.R., Mallinson, D.J., Riggs, S.R., Smith, C.G., and Vance, D.J., 2006, Foraminiferal and sedimentary record of late holocene barrier island evolution, Pea Island, North Carolina: The Role of Storm Overwash, Inlet Processes, and Anthropogenic Modification: Journal of Coastal Research, v. 22, p. 836–846, doi: 10.2112/03-0103.1.

Culver, S.J., Farrell, K.M., Mallinson, D.J., Horton, B.P., Willard, D.A., Thieler, E.R., Riggs, S.R., Snyder, S.W., Wehmiller, J.F., Bernhardt, C.E., and Hillier, C., 2008, Micropaleontologic record of late Pliocene and Quaternary paleoenvironments in the northern Albemarle Embayment, North Carolina, U.S.A: Palaeogeography, Palaeoclimatology, Palaeoecology, v. 264, p. 54–77, doi: 10.1016/j.palaeo.2008.03.012.

Culver, S.J., Grand Pre, C., Mallinson, D.J., Riggs, S.R., Corbett, D.R., Foley, J., Hale, M., Metger, L., Ricardo, J., and Rosenberger, J., 2007, Late Holocene barrier island collapse: Outer Banks, North Carolina, USA: The Sedimentary Record, v. 5, p. 4–8.

Cushman, J.A., 1926, Recent foraminifera from Puerto Rico: Publications of the Carnegie Institution of Washington, v. 342, p. 73–84.

Cushman, J.A., 1944. Foraminifera form the shallow water of the New England Coast: Cushman Laboratory for Foraminiferal Research, Special Publication No. 12, p. 1–37.

Dalrymple, R.W., Knight, R.J., Zaitlin, B.A., and Middleton, G.V., 1990, Dynamics and facies model of a macrotidal sand-bar complex, Cobequid Bay-Salmon River Estuary (Bay of Fundy): Sedimentology, v. 37, p. 577–612, doi: 10.1111/j.1365-3091.1990.tb00624.x.

Dalrymple, R.W., and Hoogendoorn, E.L., 1997, Erosion and deposition on migrating shoreface-attached ridges, Sable Island, Eastern Canada: Geoscience Canada, v. 24, p. 25–36.

d'Orgigny, A.D., 1839 Foraminiferes. In: dela Sagra, R., Histoire Physique, Politique et Naturelle de I'lle de Cuba, v 8. A. Bertrand: Paris, p. 224.

Donnelly, J.P., Hawkes, A.D., Lane, P., MacDonald, D., Shuman, B.N., Toomey, M.R., van Hengstum, P.J., and Woodruff, J.D., 2015, Climate forcing of unprecedented intense-hurricane activity in the last 2000 years: Earth's Future, v. 3, p. 49–65, doi: 10.1002/2014EF000274.

Duane, D.B., Field, M.E., Meisburger, E.P., Swift, D.J., and Williams, S.J., 1972, Linear shoals on the Atlantic inner continental shelf, Florida to Long Island: U.S.A., Army, Coastal Engineering Research Center, p. 1–52.

Ehrenberg, C.G., 1841, Uber noch jetzt zahlreich lebende Thierarten der Kreidebildung und den Organismus der Polythalamien: Koenigliche Preuss Akadaemie der Wissenschaften, Physik–Math, Il., Abhandl., Jahrg., p. 81–174.

Farrell, K.M., Harris, W.B., Mallinson, D.J., Culver, S.J., Riggs, S.R., Wehmiller, J.F., Moore, J.P., Self-Trail, J.M., and Lautier, J.C., 2013, Graphic logging for interpreting process-generated stratigraphic sequences and aquifer/reservoir potential: With analog shelf to shoreface examples from the Atlantic Coastal Plain Province, U.S.A: Journal of Sedimentary Research, v. 83, p. 723–745, doi: 10.2110/jsr.2013.52.

Fisher, J.J., 1962, Geomorphic Expression of Former Inlets Along the Outer Banks of North Carolina [Masters thesis]: Chapel Hill, N.C, University of North Carolina at Chapel Hill, p. 120.

Foley, J.A., 2007, Foraminiferal, Sedimentological, and Geochemical Indications of Holocene Environmental Change in Pamlico Sound, North Carolina [Masters thesis]: Greenville, North Carolina, East Carolina University, p. 167.

Folk, R.L., and Ward, W.C., 1957. Brazos River bar: a study in the significance of grain–size parameters: Journal of Sedimentary Research, v. 27.

Folk, 1974, *Petrology of Sedimentary Rocks*: Austin, Texas, Hemphill, p. 182.

Gibbons, R.M., 2017, Morphology, Geologic History and Dynamics of Wimble Shoals, Rodanthe, NC [MS thesis]: Greenville, N.C., East Carolina University.

Giese, G.L., Wilder, H.B., Parker, G.G., 1985, Hydrology of major estuaries and sounds of North Carolina: U.S. G.P.O, Report 2221; 2221, 108 p.

Goff, J.A., 2014, Seismic and core investigation off Panama city, Florida, reveals sand ridge influence on formation of the shoreface ravinement: Continental Shelf Research, v. 88, p. 34–46, doi: 10.1016/j.csr.2014.07.006.

Grand Pre, C., Culver, S.J., Mallinson, D.J., Farrell, K.M., Corbett, D.R., Horton, B.P., Hillier, C., Riggs, S.R., Snyder, S.W., and Buzas, M.A., 2011, Rapid Holocene coastal change revealed by high-resolution micropaleontological analysis, Pamlico Sound, North Carolina, USA: Quaternary Research, v. 76, p. 319–334.

Grossman, S. and Benson, R.H., 1967, Ecology of Rhizopodea and Ostracoda of southern Pamlico Sound region, North Carolina: Kansas University, Paleontology Contributions, 44, 1–90.

Hale, M., 2008, Late Holocene Geologic Evolution of Central Ocracoke Island, Outer Banks, North Carolina [MS thesis]: Greenville, North Carolina, East Carolina University, p. 213.

Harrison, S.E., Locker, S.D., Hine, A.C., Edwards, J.H., Naar, D.F., Twichell, D.C., and Mallinson, D.J., 2003, Sediment-starved sand ridges on a mixed carbonate/siliciclastic inner shelf off west-central Florida: Marine Geology, v. 200, p. 171–194, doi: 10.1016/S0025-3227(03)00182-8.

Hindes, H., 2016, Holocene Sedimentary record from the Sunda Shelf off Peninsular Malaysia: Insights from Elembental, Isotopic, and Bulk Sediment Magnetic Susceptibility Analyses, North Carolina [Masters thesis]: Greenville, North Carolina, East Carolina University, p. 60.

Hoogendoorn, E.L., and Dalrymple, R.W., 1986, Morphology, lateral migration, and internal structures of shoreface-connected ridges, Sable Island Bank, Nova Scotia, Canada: Geology, v. 14, p. 400–403, doi: MLMAIS>2.0.CO;2.

Hornbach, M.J., Lavier, L.L., and Ruppel, C.D., 2007, Triggering mechanism and tsunamogenic potential of the Cape Fear Slide complex, U.S. Atlantic margin: Geochemistry Geophysics, Geosystems, v. 8, doi: 10.1029/2007GC001722.

Horton, B.P., Peltier, W.R., Culver, S.J., Drummond, R., Engelhart, S.E., Kemp, A.C., Mallinson, D., Thieler, E.R., Riggs, S.R., and Ames, D.V., 2009, Holocene sea-level changes along the North Carolina Coastline and their implications for glacial isostatic adjustment models: Quaternary Science Reviews, v. 28, p. 1725–1736.

Kemp, A.C., Horton, B.P., Culver, S.J., Corbett, D.R., van de Plassche, O., Gehrels, W.R., Douglas, B.C., and Parnell, A.C., 2009, Timing and magnitude of recent accelerated sea-level rise (North Carolina, United States): Geology, v. 37, p. 1035–1038, doi: 10.1130/G30352A.1.Kemp, A.C., Horton, B.P., Donnelly, J.P., Mann, M.E., Vermeer, M., and Rahmstorf, S., 2011, Climate related sea-level variations over the past two millennia: Proceedings of the National Academy of Sciences, v. 108, p. 11017–11022, doi: 10.1073/pnas.1015619108.

Kopp, R.E., Horton, B.P., Kemp, A.C., and Tebaldi, C., 2015, Past and future sea-level rise along the coast of North Carolina, USA: Climatic Change, v. 132, p. 693–707.

Kornfeld, M.M., 1931, Recent littoral Foraminifera from Texas and Louisana: Contributions from the Department of Geology of Stanford University, v. 1, P. 77–101.

Luettich, R.A., Carr, S.D., Reynolds-Fleming, J.V., Fulcher, C.W., and McNinch, J.E., 2002, Semi-diurnal seiching in a shallow, micro-tidal lagoonal estuary: Continental Shelf Research, v. 22, p. 1669–1681, doi: 10.1016/S0278-4343(02)00031-6.

Mallinson, D.J., Culver, S.J., Riggs, S.R., Thieler, E.R., Foster, D., Wehmiller, J., Farrell, K.M., and Pierson, J., 2010, Regional seismic stratigraphy and controls on the Quaternary evolution of the Cape Hatteras region of the Atlantic passive margin, USA: Marine Geology, v. 268, p. 16–33, doi: 10.1016/j.margeo.2009.10.007.

Mallinson, D.J., Smith, C.W., Mahan, S., Culver, S.J., and McDowell, K., 2011, Barrier island response to late Holocene climate events, North Carolina, USA: Quaternary Research, v. 76, p. 46–57.

Mallinson, D., Culver, S., Leorri, E., Mitra, S., Mulligan, R., and Riggs, S., 2017, Barrier Island and estuary co-evolution in response to Holocene climate and sea-level change: Pamlico Sound and the Outer Banks Barrier Islands, North Carolina, USA, *in* Moore, L.J. and Murray, A.B., eds., Barrier Dynamics and Response to Changing Climate: Springer Publishing, New York, p. 91–120.

Mallinson, D., Riggs, S., Thieler, E.R., Culver, S., Farrell, K., Foster, D.S., Corbett, D.R., Horton, B., and Wehmiller, J.F., 2005, Late Neogene and Quaternary evolution of the northern Albemarle Embayment (mid-Atlantic continental margin, USA): Marine Geology, v. 217, p. 97–117, doi: 10.1016/j.margeo.2005.02.030.

Mann, M.E., Woodruff, J.D., Donnelly, J.P., and Zhang, Z., 2009, Atlantic hurricanes and climate over the past 1,500 years: Nature, v. 460, p. 880–883, doi: 10.1038/nature08219.

McBride, R.A. and Moslow, T.F., 1991, Origin, evolution, and distribution of shoreface sand ridges, Atlantic inner shelf, U.S.A: Marine Geology, v. 97, p. 57–85, doi: 10.1016/0025-3227(91)90019-Z.

McDowell, K.L., 2009, Holocene Geologic Development of Central Hatteras flats and Buxton Beach Ridges, Outer Banks, North Carolina [MS thesis]: Greenville, North Carolina, East Carolina University, p. 235.

McNinch, J.E., 2004, Geologic control in the nearshore: shore–oblique sandbars and shoreline erosional hotspots, Mid–Atlantic Bight, USA: Marine Geology, v. 211, p. 121–141, doi: 10.1016/j.margeo.2004.07.006.

Metger, M.L., 2009, Holocene Paleoenvironmental Change in southern Pamlico Sound, North Carolina [Masters thesis]: Greenville, North Carolina, East Carolina University, p. 178.

Minnehan, J.J., 2014, Using Sediment Organic Geochemistry to Interpret late Holocene Barrier Island and Estuarine Evolution, North Carolina, USA [MS thesis]: Greenville, North Carolina, East Carolina University, p. 138.

Mulligan, R.P., Walsh, J.P., and Wadman, H.M., 2015, Storm surge and surface waves in a shallow lagoonal estuary during the crossing of a hurricane: Journal of Waterway, Port, Coastal and Ocean Engineering, v. 141, p. 1–11, doi: 10.1061/(ASCE)WW.1943-5460.0000260.

Mulligan, R.P., Walsh, J.P., Miller, R.L., and Corbett, D.R., 2011, Sediment resuspensiona and transport in a large, shallow estuary: Pamlico Sound, NC. Proceedings of Physical Processes in Natural Waters, Burlington, Canada.

Munsterman, D. and Kerstholt, S., 1996, Sodium polytungstate, a new non-toxic alternative to bromoform in heavy liquid separation: Review of Palaeobotany and Palynology, v. 91, p. 417–422, doi: 10.1016/0034-6667(95)00093-3.

Park, S., Han, H., and Yoo, D., 2003, Transgressive sand ridges on the mid-shelf of the southern sea of Korea (Korea Strait): formation and development in high-energy environments: Marine Geology, v. 193, p. 1–18, doi: 10.1016/S0025-3227(02)00611-4.

Peek, K.M., Mallinson, D.J., Culver, S.J., and Mahan, S.A., 2014, Holocene geologic development of the Cape Hatteras region, Outer Banks, North Carolina, USA: Journal of Coastal Research, v. 30, p. 41–58, doi: 10.2112/JCOASTRES-D-12-00192.1.

Pruitt, R.J., Culver, S.J., Buzas, M.A., Corbett, D.R., Horton, B.P., and Mallinson, D.J., 2010, Modern foraminiferal distribution and recent environmental change in Core Sound, North Carolina, USA: Journal of Foraminiferal Research, v. 40, p. 344–365, doi: 10.2113/gsjfr.40.4.344.

Riggs, S.R., Bray, J.T., Wyrick, R.A., Klingman, C.R., Ames, D.V., Hamilton, J.C., Lueck, K.L., and Watson, J.S., 1993, Heavy metals in organic-rich muds of the Albemarle Sound estuarine system. Albemarle-Pamlico Estuarine Study US Environmental Protection Agency: US Environmental Protection Agency, Report 93–02, 173 p.

Riggs, S.R., 2011, The Battle for North Carolina's Coast: Evolutionary History, Present Crisis, & Vision for the Future: Chapel Hill, University of North Carolina Press at Chapel Hill, p. 142.

Riggs, S.R., 1996, Sediment Evolution and Habitat Function of Organic-Rich Muds within the Albemarle Estuarine System, North Carolina: Estuaries, v. 19, p. 169–185, doi: 10.2307/1352223.

Riggs, S.R., Ames, D.V., 2003, Drowning the North Carolina coast: sea-level rise and estuarine dynamics: Raleigh, N.C, North Carolina Sea Grant, p. 152.

Riggs, S.R., Ames, D.V., and Rudolph, G.L., 2000, Erosional scour and geologic evolution of Croatan Sound, northeastern North Carolina: Raleigh, N.C, Center for Transportation and the Environment, North Carolina State University, p. 115.

Riggs, S.R., Cleary, W.J., and Snyder, S.W., 1995, Influence of inherited geologic framework on barrier shoreface morphology and dynamics: Marine Geology, v. 126, p. 213–234, doi: 10.1016/0025-3227(95)00079-E.

Rosenberger, J.E., 2006, Late Holocene Back-Barrier Development of Portsmouth Island, Outer Banks, North Carolina [MS thesis]: Greenville, North Carolina, East Carolina University, p. 185.

Rudolph, G.L., 1999, Holocene Evolution of a Drowned Tributary Estuary, Croatan Sound, North Carolina [MS thesis]: Greenville, North Carolina, East Carolina University, p. 237.

Sager, E.D., 1996, A Complex Holocene Infill History of Albemarle Sound, North Carolina: an Integrated Seismic, Litho-, and Chronostratigraphic synthesis [MS thesis]: Greenville, North Carolina, East Carolina University, p. 192.

Sager, E.D. and Riggs, S.R., 1998, Models for the Holocene valley-fill history of Albemarle Sound, North Carolina, USA: In: Alexander, C., Henry, V.J., Davis, R. (Eds.), Tidalites:Processes and Products. Journal of Sedimentary Research, Special Publication, v. 61, p. 119–128.

Saha, S., Burley, S.D., Banerjee, S., Ghosh, A., and Saraswati, P.K., 2016, The morphology and evolution of tidal sand bodies in the macrotidal Gulf of Khambhat, western India: Marine and Petroleum Geology, v. 77, p. 714–730, doi: 10.1016/j.marpetgeo.2016.03.028.

Schnitker, D.F., 1971, Distribution of Foraminifera on the North Carolina continental Shelf, Tulane Studies in Geology and Paleontology, v 8, p. 169–215.

Smith, C.F., 2016, Holocene Evolution of the Ocracoke Inlet Flood-tide Delta Region, Outer Banks, North Carolina [MS thesis]: Greenville, North Carolina, East Carolina University, p. 110.

Smith, C.G., Culver, S.J., Mallinson, D.J., Riggs, S.R., and Corbett, D.R., 2009, Recognizing former flood-tide deltas in the Holocene stratigraphic record from the Outer Banks, North Carolina, USA: Stratigraphy, v. 6, p. 61–78.

Snedden, J.W. and Dalrymple, R.W., 1999, Modern shelf sand ridges: Historical review of modern examples and a unified model of ridge origin and evolution: In Snedden, J.W., Bergman, K., Isolated Shallow Marine Sand Bodies: Sequence Stratigraphic Analysis and Sedimentologic Interpretation: Society for Sedimentary Geology Special Publication, v. 64, p. 13–28.

Snedden, J.W., and Bergman, K.M., 1999, Isolated shallow marine sand bodies: deposits for all interpretations, In Snedden, J.W., Bergman, K., Isolated Shallow Marine Sand Bodies: Sequence Stratigraphic Analysis and Sedimentologic Interpretation: Society for Sedimentary Geology Special Publication, v. 64, p. 1–12.

Stuiver, M. and Reimer, P.J., 1993, Extended ^{14}C data base and revised CALIB 3.0 ^{14}C age calibration program: Radiocarbon, v. 35, p. 215–230.

Swift, D.J.P., 1985, Response of the shelf floor to flow: In Tillman, R.W., Swift, D.J.P., and Walker, R.G. (eds.), Shelf Sands and Sandstone Reservoirs: Society for Sedimentology Geology Special Publication, v. 13, p. 135–241.

Swift, D.J.P., and Field, M.E., 1981, Evolution of a classic sand ridge field: Maryland sector, North American inner shelf: Sedimentology, v. 28, p. 461–482, doi: 10.1111/j.1365-3091.1981.tb01695.x.

Swift, D.J., Kofoed, J.W., Saulsbury, F.P., and Sears, P., 1972, Holocene evolution of the shelf surface, central and southern Atlantic shelf of North America, In Swift, D.J.P., Duane, D.B., and Pilkey, O.J. (eds.), Shelf Sediment Transport: Process and Pattern, Stroudsburg, Pennsylvania, Dowden, Hutchinson and Ross, p. 499–574.

Tanner, W.F., 1960, Florida coastal classification: Gulf Coast Association of Geological Societies, v. 10, p. 259–266.

Terquem, O., 1875, Essai sur le classement des animaux qui vivent sur la plage et dans les environs de Dunquerque: Paris, Fasc. 1, p. 1–54.

Thieler, E., Foster, D.S., Himmelstoss, E.A., and Mallinson, D.J., 2014, Geologic framework of the northern North Carolina, USA inner continental shelf and its influence on coastal evolution: Marine Geology, v. 348, p. 113–130, doi: 10.1016/j.margeo.2013.11.011.

Thomas, D.H., 2008, Native American landscapes of St. Catherines Island, Georgia: I. The theoretical framework: New York, American Museum of Natural History.

Twamley, D.F., 2006, Holocene Geologic Development of the Hatteras Village area, Outer Banks, North Carolina [MS thesis]: Greenville, North Carolina, East Carolina University, p. 157.

Twichell, D., Brooks, G., Gelfenbaum, G., Paskevich, V., and Donahue, B., 2003, Sand ridges off Sarasota, Florida: a complex facies boundary on a low-energy inner shelf environment: Marine Geology, v. 200, p. 243–262, doi: 10.1016/S0025-3227(03)00185-3.

Vance, D.J., Culver, S.J., Corbett, D.R., and Buzas, M.A., 2006, Foraminifera in the Albemarle estuarine system, North Carolina: Distribution and recent Environmental Change: The Journal of Foraminiferal Research, v. 36, p. 15–33, doi: 10.2113/36.1.15.

Verosub, K.L. and Roberts, A.P., 1995, Environmental magnetism: past, present, and future: Journal of Geophysical Research: Solid Earth, v. 100, p. 2175–2192, doi: 10.1029/94JB02713.

Walker, G. and Jacob, E., 1798, In: Adams, G. (ed.), essays on the Microscope. Containing a practical description of the most improved microscopes; a general history of insects. A description of 383 animalicula etc. 2nd edition with considerable additions and improvements by K. Kanmacher: Dillion and Keating, London, p. 712.

Wells, J.T., and Kim, S., 1989, Sedimentation in the Albemarle-Pamlico lagoonal system: synthesis and hypotheses: Marine Geology, v. 88, p. 263–284, doi: 10.1016/0025-3227(89)90101-1.

Wright, J., Colling, A., and Park, D., 1999, *Waves, tides, and shallow–water processes*: Burlington, MA, Gulf Professional Publishing, p. 125–148.

Woo, H.J., Culver, S.J., and Oertel, G.F., 1997, Benthic foraminiferal communities of a barrier-lagoon system, Virginia, USA: Journal of Coastal Research, v. 13, p. 1192–1200.

Workman, R.R., 1981, Foraminiferal Assemblages of the Nearshore Inner Continental Shelf, Nags Head and Wilmington areas, North Carolina [MS thesis]: Greenville, North Carolina, East Carolina University, p. 161.

Yang, H., Weisberg, R.H., Niiler, P.P., Sturges, W., and Johnson, W., 1999, Lagrangian circulation and forbidden zone on the West Florida Shelf: Continental Shelf Research, v. 19, p. 1221–1245.

Zaremba, N., 2014, Holocene Stratigraphy and Paleoenvironmental Change of Pamlico Sound, North Carolina, USA [MS thesis]: Greenville, North Carolina, East Carolina University, p. 95.

Zaremba, N., Mallinson, D.J., Leorri, E., Culver, S., Riggs, S., Mulligan, R., Horsman, E., and Mitra, S., 2016, Controls on the stratigraphic framework and paleoenvironmental change within a Holocene estuarine system: Pamlico Sound, North Carolina, USA: Marine Geology, v. 379, p. 109-123, doi: 10.1016/j.margeo.2016.04.012.

Appendix A: Digital Images of Vibracores

EPamSh16-1

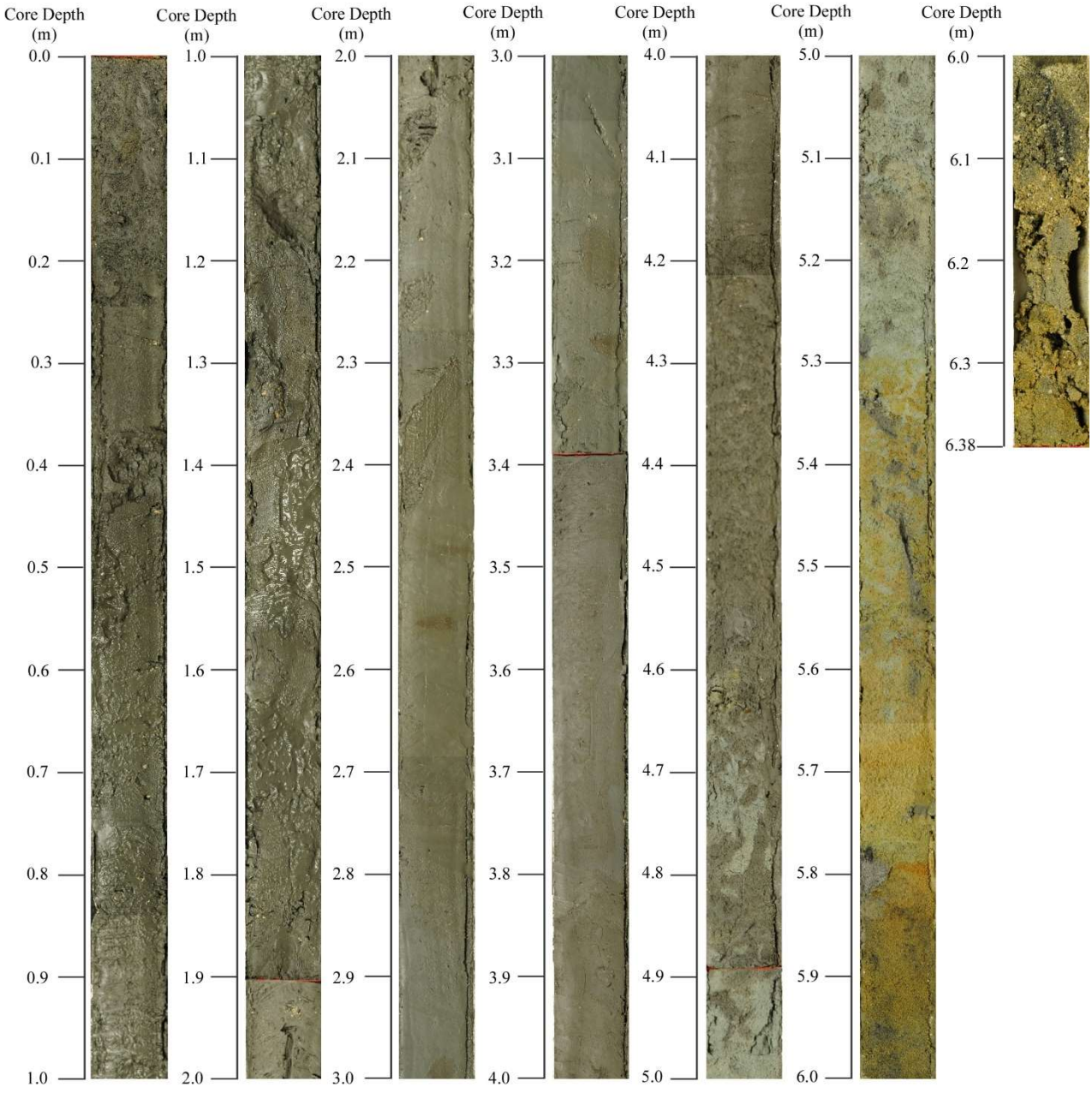
Core Depth (m)
0.0
0.1
0.2
0.3
0.4
0.5
0.6
0.7
0.8
0.9
1.0
Core Depth (m)
1.0
1.1
1.2
1.3
1.4
1.5
1.6
1.7
1.8
1.9
2.0
Core Depth (m)
2.0
2.1
2.2
2.3
2.4
2.5
2.6
2.7
2.8
2.9
3.0
Core Depth (m)
3.0
3.1
3.2
3.3
3.4
3.5
3.6
3.7
3.8
3.9
4.0
Core Depth (m)
4.0
4.1
4.2
4.3
4.4
4.5
4.6
4.7
4.8
4.9
5.0
Core Depth (m)
5.0
5.1
5.2
5.3
5.4
5.5
5.6
5.7
5.8
5.9
6.0
Core Depth (m)
6.0
6.1
6.2
6.3
6.38

EPamSh16-2

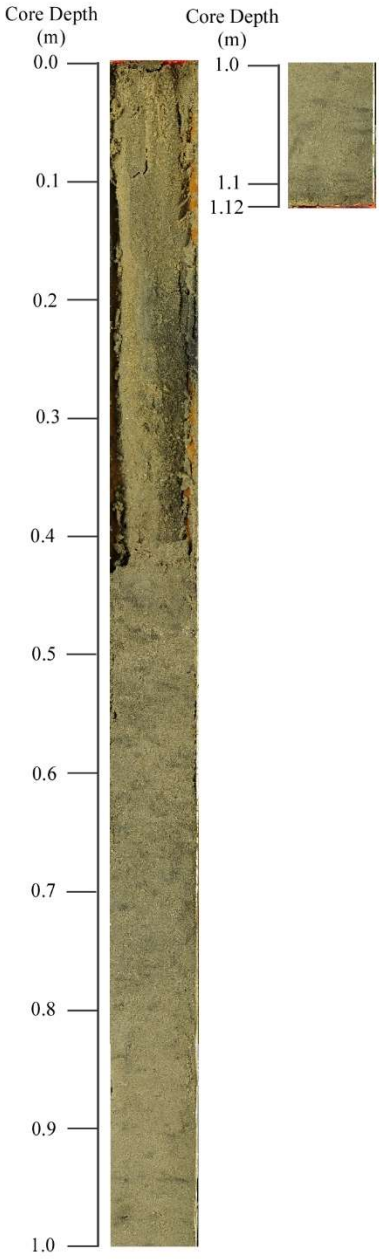

EPamSh16-4

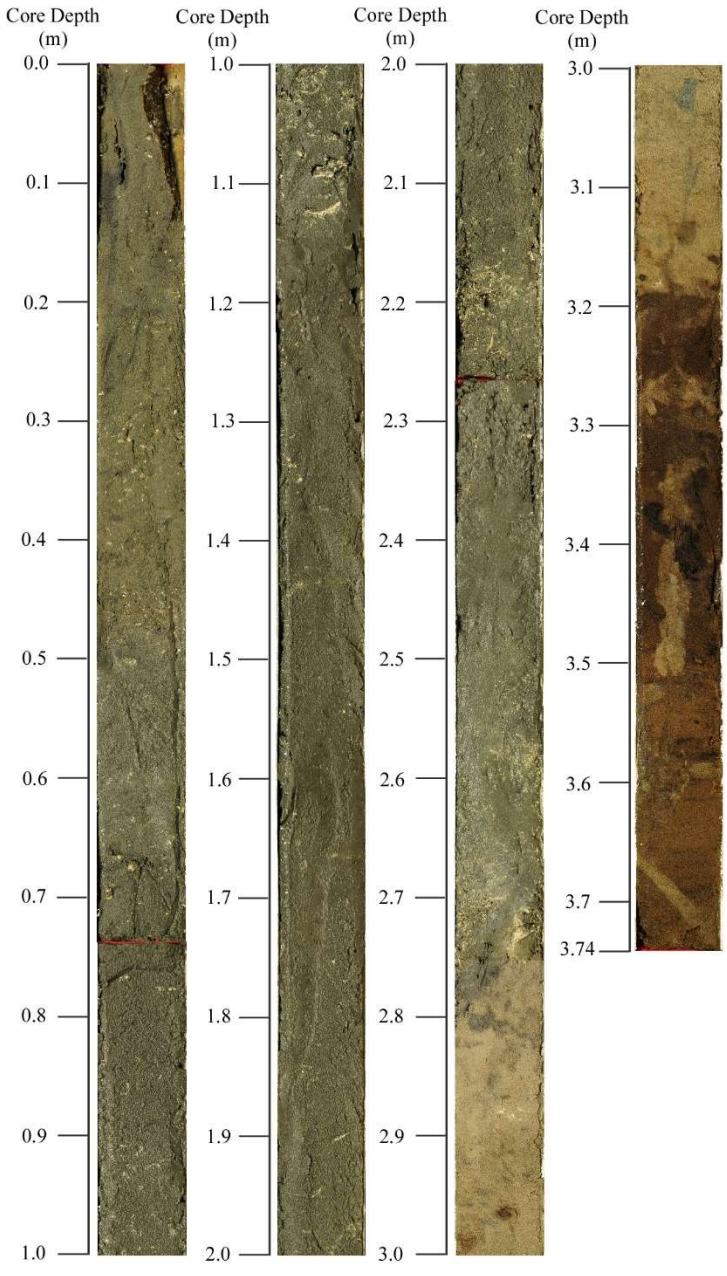
Core Depth (m)
0.0
0.1
0.2
0.3
0.4
0.5
0.6
0.7
0.8
0.9
1.0
Core Depth (m)
1.0
1.1
1.2
1.3
1.4
1.5
1.6
1.7
1.8
1.9
2.0
Core Depth (m)
2.0
2.1
2.2
2.3
2.4
2.5
2.6
2.7
2.8
2.9
3.0
Core Depth (m)
3.0
3.1
3.2
3.3
3.4
3.5
3.6
3.7
3.74

EPamSh16-6

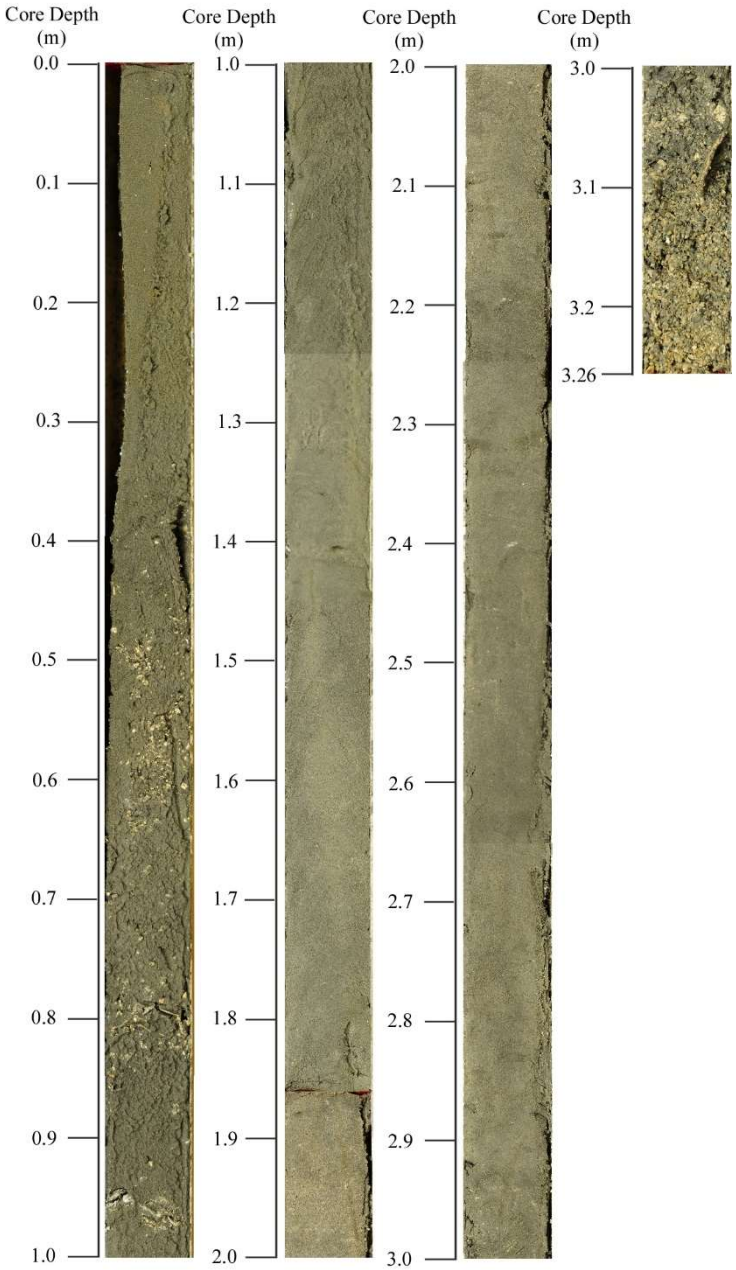
Core Depth (m)
0.0
0.1
0.2
0.3
0.4
0.5
0.6
0.7
0.8
0.9
1.0
Core Depth (m)
1.0
1.1
1.2
1.3
1.4
1.5
1.6
1.7
1.8
1.9
2.0
Core Depth (m)
2.0
2.1
2.2
2.3
2.4
2.5
2.6
2.7
2.8
2.9
3.0
Core Depth (m)
3.0
3.1
3.2
3.26

EPamSh16-8

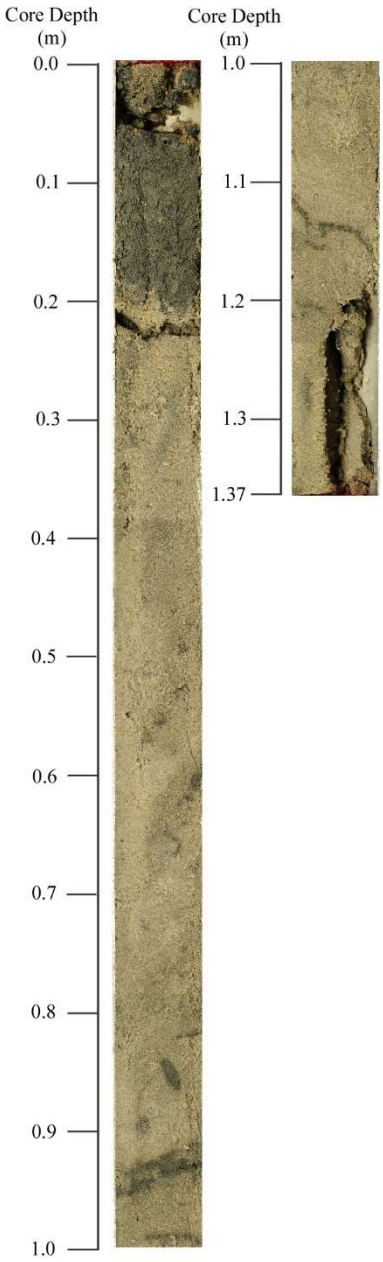
Core Depth
(m)
0.0
0.1
0.2
0.3
0.4
0.5
0.6
0.7
0.8
0.9
1.0
Core Depth
(m)
1.0
1.1
1.2
1.3
1.37

EPamSh16-10

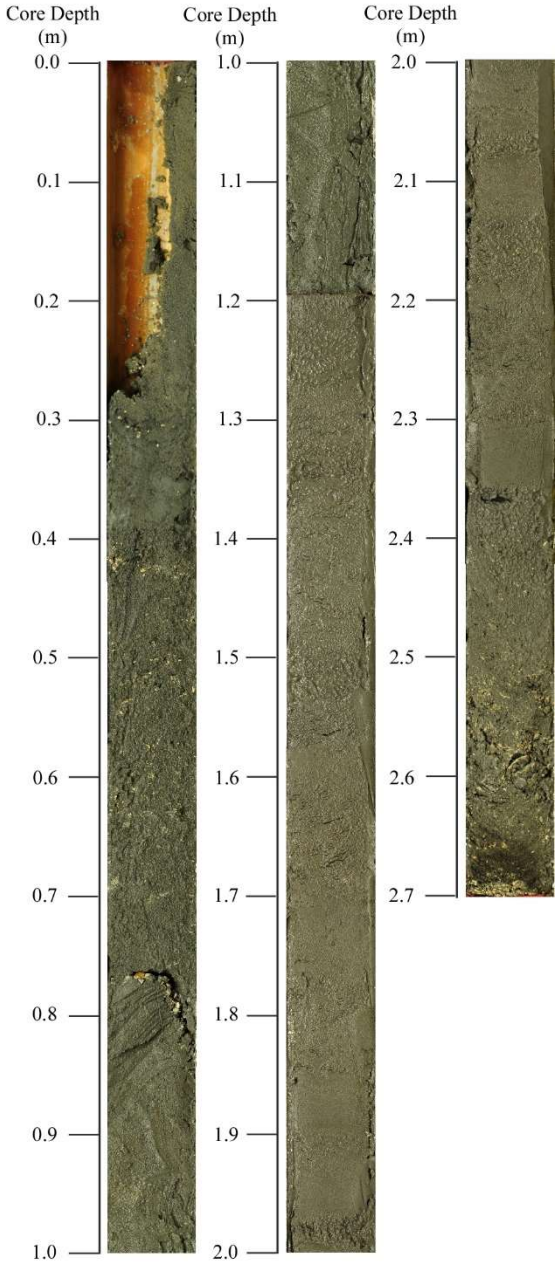
Core Depth (m)
0.0
0.1
0.2
0.3
0.4
0.5
0.6
0.7
0.8
0.9
1.0
Core Depth (m)
1.0
1.1
1.2
1.3
1.4
1.5
1.6
1.7
1.8
1.9
2.0
Core Depth (m)
2.0
2.1
2.2
2.3
2.4
2.5
2.6
2.7

Appendix B: Core Logs

CORE LOG KEY

Lithofacies

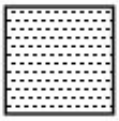

mud
M

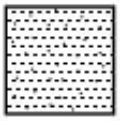

sandy mud
sM

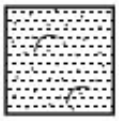

slightly gravelly
sandy mud
(g)sM

bioturbated
slightly muddy
sand biot (m)S

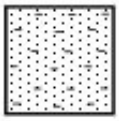

muddy sand
mS

bioturbated
muddy sand
biot-mS

mottled
bioturbated
muddy sand
mot-biot-mS

rooted bioturbated
slightly gravelly
muddy sand
rt-biot-(g)mS

mixed
slightly gravelly
muddy sand
mix-(g)mS

mixed
gravelly muddy
sand
mxd-gmS

bioclastic
gravelly muddy
sand
bio-gmS

Sedimentary Features

mottled

shell
fragments

rooted

bioturbation

○ indicates barren foraminiferal sample

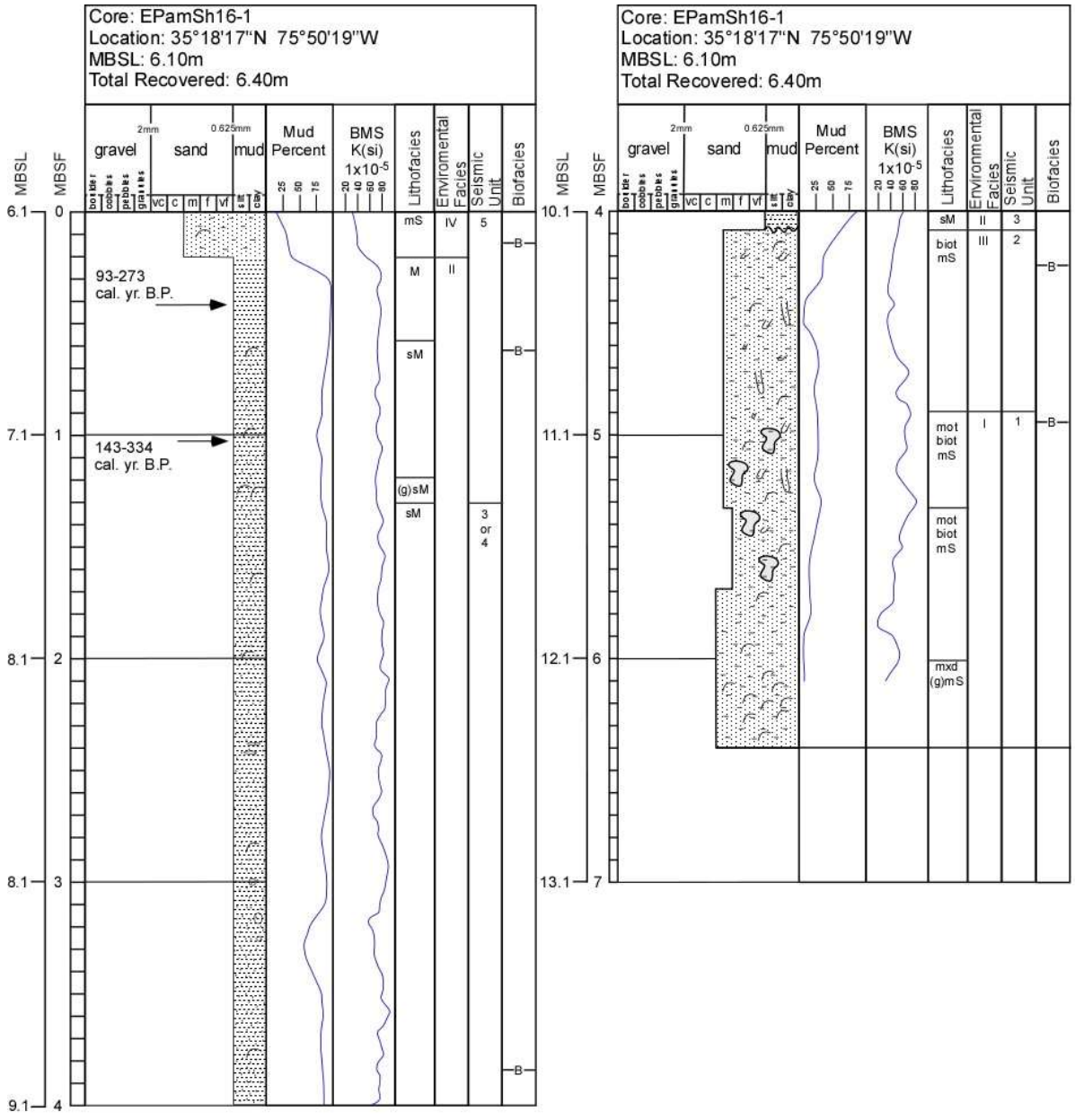
Core: EPamSh16-1
Location: 35°18'17"N 75°50'19"W
MBSL: 6.10m
Total Recovered: 6.40m
MBSL
MBSF
gravel
sand
mud
Mud Percent
BMS K(si) 1x10-5
Lithofacies
Enviromental Facies
Seismic Unit
Biofacies
93-273 cal. yr. B.P.
143-334 cal. yr. B.P.
mS
M
sM
(g)sM
sM
3 or 4
5
IV
II
B
Core: EPamSh16-1
Location: 35°18'17"N 75°50'19"W
MBSL: 6.10m
Total Recovered: 6.40m
Environmental Facies
sM
biot mS
mot biot mS
mot biot mS
mxd (g)mS
II
III
I
3
2
1

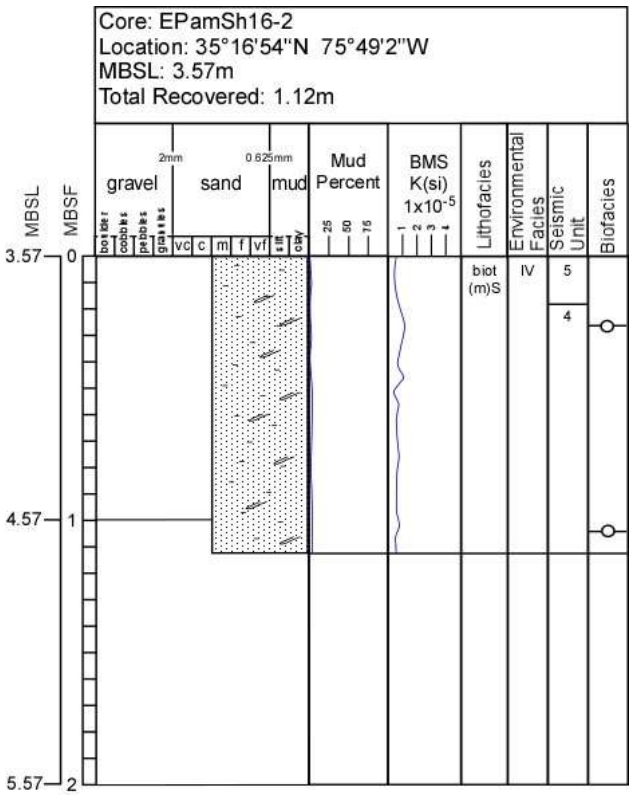
Core: EPamSh16-2
Location: 35°16'54"N 75°49'2"W
MBSL: 3.57m
Total Recovered: 1.12m
MBSL
MBSF
gravel
sand
mud
2mm
0.625mm
boulder
cobbles
pebbles
granules
vc
c
m
f
vf
silt
clay
Mud Percent
25
50
75
BMS K(si) 1x10-5
1
2
3
4
Lithofacies
Environmental Facies
Seismic Unit
Biofacies
3.57
4.57
5.57
0
1
2
biot (m)S
IV
5
4

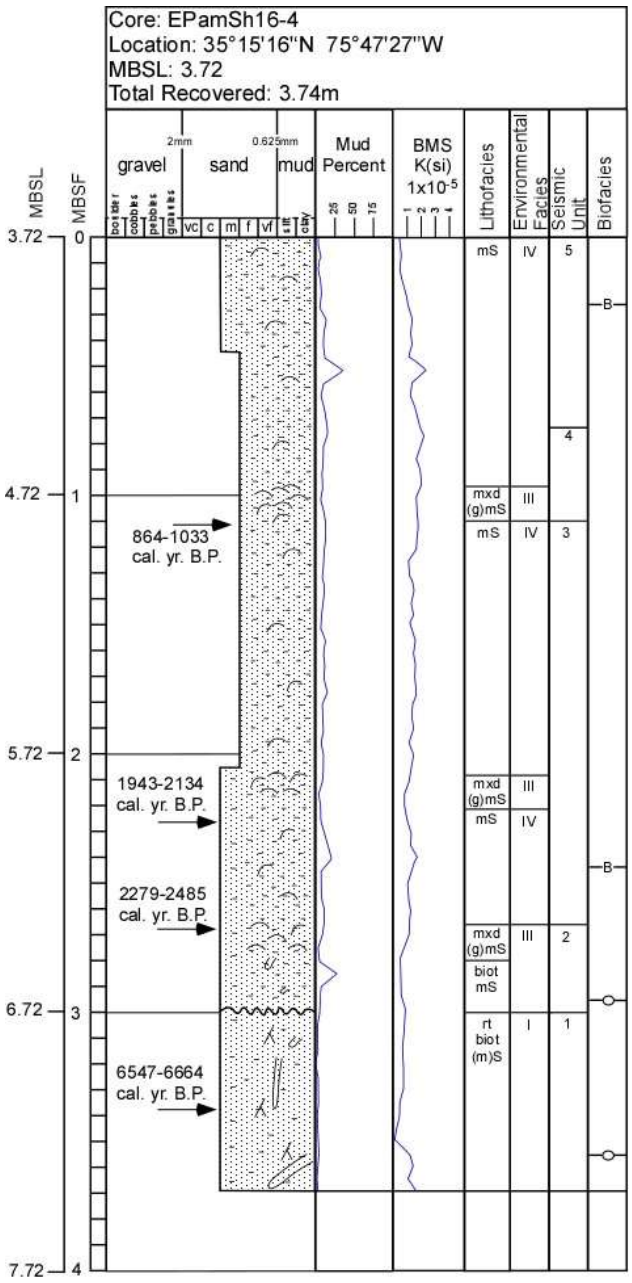
Core: EPamSh16-4
Location: 35°15'16"N 75°47'27"W
MBSL: 3.72
Total Recovered: 3.74m
MBSL
MBSF
gravel
sand
mud
2mm
0.625mm
vc
c
m
f
vf
Mud Percent
BMS K(si) 1x10-5
Lithofacies
Environmental Facies
Seismic Unit
Biofacies
3.72
0
4.72
1
5.72
2
6.72
3
7.72
4
864-1033 cal. yr. B.P.
1943-2134 cal. yr. B.P.
2279-2485 cal. yr. B.P.
6547-6664 cal. yr. B.P.
mS
IV
5
4
mxd (g)mS
III
mS
IV
3
mxd (g)mS
III
mS
IV
mxd (g)mS
III
2
biot mS
rt biot (m)S
I
1
B
B

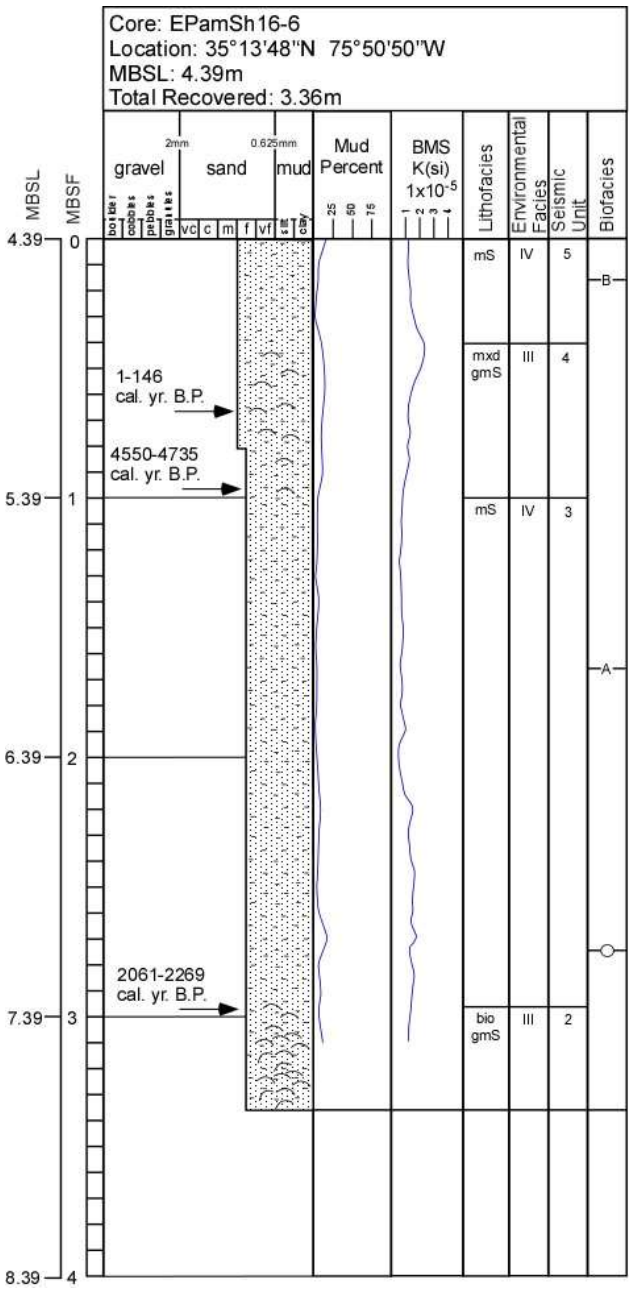
Core: EPamSh16-6
Location: 35°13'48"N 75°50'50"W
MBSL: 4.39m
Total Recovered: 3.36m
MBSL
MBSF
gravel
sand
mud
2mm
0.625mm
boulders
cobbles
pebbles
granules
vc
c
m
f
vf
silt
clay
Mud Percent
25
50
75
BMS K(si) 1x10-5
1
2
3
4
Lithofacies
Environmental Facies
Seismic Unit
Biofacies
4.39
0
5.39
1
6.39
2
7.39
3
8.39
4
1-146 cal. yr. B.P.
4550-4735 cal. yr. B.P.
2061-2269 cal. yr. B.P.
mS
IV
5
B
mxd gmS
III
4
mS
IV
3
A
bio gmS
III
2

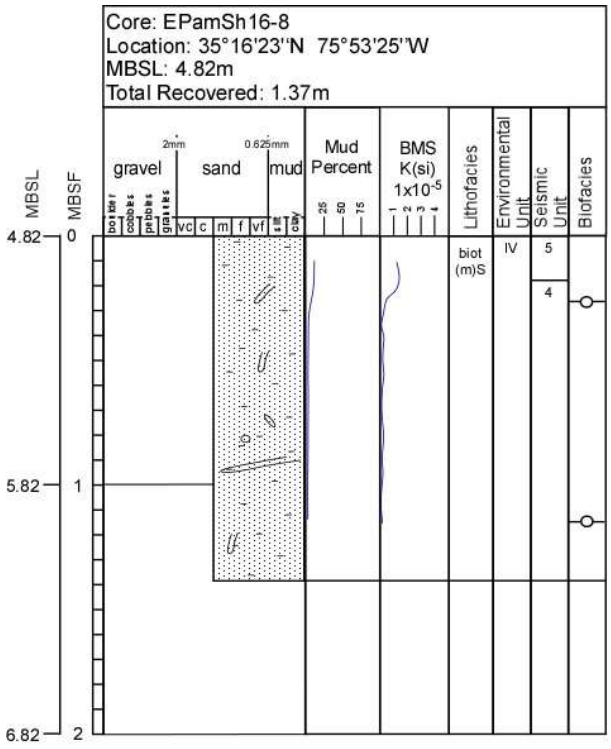
Core: EPamSh16-8
Location: 35°16'23''N 75°53'25''W
MBSL: 4.82m
Total Recovered: 1.37m
MBSL
MBSF
4.82
5.82
6.82
0
1
2
gravel
sand
mud
2mm
0.625mm
vc
c
m
f
vf
Mud Percent
25
50
75
BMS K(si) 1x10-5
1
2
3
4
Lithofacies
biot (m)S
Environmental Unit
IV
Seismic Unit
5
4
Biofacies

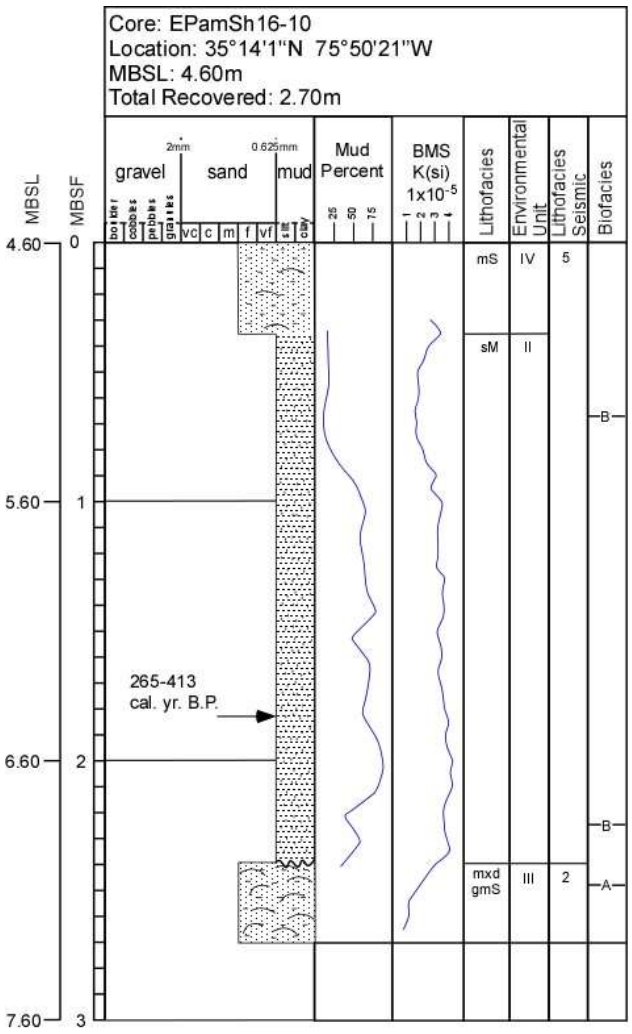
Core: EPamSh16-10
Location: 35°14'1"N 75°50'21"W
MBSL: 4.60m
Total Recovered: 2.70m
MBSL
MBSF
4.60
5.60
6.60
7.60
0
1
2
3
2mm
0.625mm
gravel
sand
mud
boulder
cobbles
pebbles
granules
vc
c
m
f
vf
silt
clay
Mud Percent
25
50
75
BMS K(si) 1x10-5
1
2
3
4
Lithofacies
Environmental Unit
Lithofacies Seismic
Biofacies
mS
IV
5
sM
II
B
B
mxd gmS
III
2
A
265-413
cal. yr. B.P.

Appendix C: Gradistat Results

Mass and percent of mud, sand, and gravel for all grain size samples and GRADISTAT results for mean, sorting, skewness and kurtosis (Folk and Ward, 1957; Folk, 1974) method reported in ϕ) for the sand fraction.

Core Name	Interval in Core (cm)	Bulk Mass (g)	mud (g)	sand (g)	gravel (g)	% mud	% sand	% gravel	Sand Fraction			
									mean (ϕ)	sorting (ϕ)	skewness (ϕ)	kurtosis (ϕ)
EPamSh16-1	0	18.54	2.63	15.89	0.02	14.20	85.69	0.11	0.99	0.42	0.05	1.02
EPamSh16-1	10	14.40	4.28	10.13	0.00	29.69	70.31	0.00	0.95	0.44	0.00	1.01
EPamSh16-1	20	14.43	5.19	9.24	0.00	35.95	64.05	0.00	0.67	0.60	-0.03	1.16
EPamSh16-1	30	6.41	6.27	0.14	0.00	97.82	2.18	0.00	0.98	0.92	0.27	0.80
EPamSh16-1	40	7.56	7.45	0.11	0.00	98.54	1.46	0.00	3.24	1.00	-0.68	1.58
EPamSh16-1	50	10.26	9.95	0.31	0.00	96.98	3.02	0.00	1.93	1.62	-0.21	0.60
EPamSh16-1	60	14.39	13.65	0.70	0.04	94.86	4.87	0.28	3.21	1.25	-0.79	2.41
EPamSh16-1	70	16.14	14.59	1.49	0.06	90.40	9.23	0.37	3.37	1.03	-0.76	5.64
EPamSh16-1	80	16.92	14.25	2.43	0.24	84.22	14.37	1.42	3.40	1.16	-0.73	4.75
EPamSh16-1	90	14.81	12.68	2.13	0.00	85.62	14.38	0.00	3.69	0.25	-0.24	1.40
EPamSh16-1	100	21.46	16.19	5.27	0.00	75.45	24.55	0.00	3.61	0.45	-0.49	2.51
EPamSh16-1	110	14.35	12.28	2.07	0.00	85.58	14.42	0.00	3.63	0.24	-0.21	1.28
EPamSh16-1	120	16.50	13.64	2.86	0.00	82.67	17.33	0.00	3.66	0.27	-0.28	1.36
EPamSh16-1	130	11.70	9.64	1.78	0.28	82.40	15.21	2.39	2.88	1.63	-0.85	4.32
EPamSh16-1	140	11.44	10.63	0.81	0.00	92.92	7.08	0.00	3.52	0.62	-0.59	2.44
EPamSh16-1	150	16.89	15.26	1.63	0.00	90.35	9.65	0.00	3.65	0.26	-0.25	1.19
EPamSh16-1	160	9.98	9.57	0.41	0.00	95.89	4.11	0.00	3.61	0.50	-0.54	3.02
EPamSh16-1	170	14.89	12.67	2.22	0.00	85.09	14.91	0.00	3.20	0.72	-0.58	1.20
EPamSh16-1	180	14.49	11.81	2.68	0.00	81.50	18.50	0.00	2.69	1.15	-0.31	0.76
EPamSh16-1	190	16.94	14.90	2.04	0.00	87.96	12.04	0.00	3.58	0.44	-0.50	2.21
EPamSh16-1	200	13.95	10.48	3.46	0.01	75.13	24.80	0.07	3.05	0.97	-0.68	0.89
EPamSh16-1	210	10.75	9.89	0.86	0.00	92.00	8.00	0.00	3.48	0.50	-0.51	1.33
EPamSh16-1	220	15.11	12.94	2.17	0.00	85.64	14.36	0.00	2.72	1.14	-0.41	0.87
EPamSh16-1	230	10.59	8.90	1.69	0.00	84.04	15.96	0.00	2.59	1.18	-0.37	0.74
EPamSh16-1	240	11.67	10.57	1.10	0.00	90.57	9.43	0.00	2.98	1.04	-0.71	0.87
EPamSh16-1	250	11.53	11.10	0.43	0.00	96.27	3.73	0.00	2.59	1.26	-0.42	0.73
EPamSh16-1	260	15.12	14.26	0.86	0.00	94.31	5.69	0.00	2.81	1.07	-0.48	0.71
EPamSh16-1	270	16.67	15.01	1.66	0.00	90.04	9.96	0.00	3.15	0.85	-0.66	1.01

Core Name	Interval in Core (cm)	Bulk Mass (g)	mud (g)	sand (g)	gravel (g)	% mud	% sand	% gravel	Sand Fraction			
									mean (ϕ)	sorting (ϕ)	skewness (ϕ)	kurtosis (ϕ)
EPamSh16-1	280	14.20	11.68	2.52	0.00	82.25	17.75	0.00	2.71	1.11	-0.39	0.73
EPamSh16-1	290	14.74	12.95	1.79	0.00	87.86	12.14	0.00	2.80	1.07	-0.50	0.76
EPamSh16-1	300	11.34	10.49	0.84	0.01	92.51	7.41	0.09	1.79	1.62	-0.08	0.65
EPamSh16-1	310	15.36	13.88	1.48	0.00	90.37	9.63	0.00	2.04	1.26	0.23	0.59
EPamSh16-1	320	17.07	11.02	6.05	0.00	64.56	35.44	0.00	2.80	0.99	-0.37	0.80
EPamSh16-1	330	17.21	9.57	7.64	0.00	55.59	44.41	0.00	2.74	1.06	-0.47	0.84
EPamSh16-1	340	13.61	9.33	4.28	0.00	68.55	31.45	0.00	2.91	0.98	-0.51	0.88
EPamSh16-1	350	11.98	10.07	1.91	0.00	84.05	15.95	0.00	3.09	0.85	-0.55	1.07
EPamSh16-1	360	10.69	9.30	1.39	0.00	87.00	13.00	0.00	2.56	1.22	-0.41	0.71
EPamSh16-1	370	13.42	11.02	2.40	0.00	82.11	17.89	0.00	2.38	1.11	-0.11	0.78
EPamSh16-1	380	10.49	8.77	1.72	0.00	83.60	16.40	0.00	2.74	1.08	-0.46	0.78
EPamSh16-1	390	12.40	10.89	1.51	0.00	87.82	12.18	0.00	1.77	1.04	-0.16	1.04
EPamSh16-1	400	12.94	11.32	1.62	0.00	87.48	12.52	0.00	1.49	0.87	-0.20	0.89
EPamSh16-1	410	15.12	8.95	6.17	0.00	59.20	40.80	0.00	1.69	1.02	-0.10	0.93
EPamSh16-1	420	19.22	6.77	12.45	0.00	35.24	64.76	0.00	1.85	0.95	-0.13	0.98
EPamSh16-1	430	20.43	7.12	13.31	0.00	34.85	65.15	0.00	1.68	0.99	-0.15	0.89
EPamSh16-1	440	16.42	1.37	15.05	0.00	8.33	91.67	0.00	1.98	0.89	-0.33	0.86
EPamSh16-1	450	21.49	0.99	20.49	0.01	4.59	95.36	0.05	1.70	0.89	-0.39	0.94
EPamSh16-1	460	21.98	5.59	16.39	0.00	25.42	74.58	0.00	1.80	0.91	-0.22	0.93
EPamSh16-1	470	20.02	5.95	14.02	0.05	29.72	70.03	0.25	1.82	0.92	-0.33	0.94
EPamSh16-1	480	23.09	4.99	18.05	0.05	21.62	78.16	0.22	1.90	0.89	-0.30	0.92
EPamSh16-1	490	15.18	3.93	11.22	0.03	25.89	73.91	0.20	1.91	0.95	-0.38	0.86
EPamSh16-1	500	21.14	5.91	15.23	0.00	27.95	72.05	0.00	2.08	0.83	-0.44	0.89
EPamSh16-1	510	18.44	5.18	13.19	0.07	28.09	71.53	0.38	1.54	1.00	0.04	0.81
EPamSh16-1	520	22.89	4.67	18.22	0.00	20.41	79.59	0.00	1.40	0.81	2.52	1.11
EPamSh16-1	530	18.30	6.03	12.27	0.00	32.94	67.06	0.00	2.56	0.50	-0.31	1.39
EPamSh16-1	540	19.84	5.40	14.44	0.00	27.23	72.77	0.00	2.35	0.65	-0.40	1.25
EPamSh16-1	550	21.19	3.86	17.33	0.00	18.21	81.79	0.00	2.05	0.76	-0.28	0.92

Core Name	Interval in Core (cm)	Bulk Mass (g)	mud (g)	sand (g)	gravel (g)	% mud	% sand	% gravel	Sand Fraction			
									mean (ϕ)	sorting (ϕ)	skewness (ϕ)	kurtosis (ϕ)
EPamSh16-1	560	23.13	3.09	20.04	0.00	13.36	86.64	0.00	2.00	0.77	-0.33	1.05
EPamSh16-1	570	22.89	3.12	19.77	0.00	13.63	86.37	0.00	2.03	0.78	-0.34	1.00
EPamSh16-1	580	18.96	3.32	15.63	0.01	17.49	82.45	0.05	1.59	0.54	-0.04	1.26
EPamSh16-1	590	25.63	1.27	24.17	0.19	4.96	94.30	0.74	1.41	0.61	-0.30	1.23
EPamSh16-1	600	26.51	1.54	24.73	0.24	5.80	93.29	0.91	1.39	0.67	-0.23	1.14
EPamSh16-1	610	15.49	1.12	13.99	0.38	7.24	90.30	2.45	1.00	0.92	-0.17	0.98
EPamSh16-2	0	13.64	0.20	13.43	0.01	1.44	98.48	0.07	1.14	0.65	0.08	1.04
EPamSh16-2	10	17.10	0.52	16.58	0.00	3.06	96.94	0.00	1.83	0.46	-0.12	0.92
EPamSh16-2	20	16.32	0.04	16.28	0.00	0.26	99.74	0.00	1.80	0.53	-0.23	1.04
EPamSh16-2	30	14.05	0.49	13.56	0.00	3.47	96.53	0.00	1.71	0.61	-0.24	0.88
EPamSh16-2	40	13.93	0.08	13.85	0.00	0.56	99.44	0.00	1.86	0.50	-0.23	1.00
EPamSh16-2	50	20.23	0.98	19.25	0.00	4.85	95.15	0.00	1.65	0.60	-0.17	0.88
EPamSh16-2	60	20.11	0.80	19.31	0.00	3.96	96.04	0.00	1.73	0.60	-0.26	0.89
EPamSh16-2	70	20.88	0.73	20.13	0.02	3.47	96.43	0.10	1.80	0.58	-0.30	1.03
EPamSh16-2	80	21.47	0.45	21.02	0.00	2.07	97.93	0.00	1.85	0.58	-0.33	1.09
EPamSh16-2	90	24.64	1.10	23.54	0.00	4.44	95.56	0.00	2.04	0.48	-0.26	1.24
EPamSh16-2	100	21.94	1.11	20.81	0.02	5.06	94.85	0.09	2.05	0.49	-0.25	1.27
EPamSh16-2	110	21.68	1.07	20.59	0.02	4.92	94.99	0.09	1.87	0.68	-0.39	1.25
EPamSh16-4	0	10.90	0.44	10.46	0.00	4.05	95.95	0.00	2.26	0.38	0.04	1.37
EPamSh16-4	5	11.80	0.82	10.97	0.00	6.99	93.01	0.00	2.29	0.38	0.06	1.32
EPamSh16-4	10	15.98	0.49	15.49	0.00	3.08	96.92	0.00	2.49	0.39	0.02	1.30
EPamSh16-4	15	20.95	1.50	19.45	0.00	7.17	92.83	0.00	2.24	0.39	0.01	1.34
EPamSh16-4	20	18.88	1.53	17.35	0.00	8.09	91.91	0.00	2.24	0.39	0.01	1.36
EPamSh16-4	25	11.99	0.66	11.30	0.03	5.52	94.23	0.25	2.23	0.39	-0.01	1.36
EPamSh16-4	30	20.81	2.86	17.79	0.16	13.75	85.48	0.77	2.25	0.41	0.00	1.40
EPamSh16-4	35	22.34	2.42	19.80	0.12	10.84	88.63	0.54	2.31	0.39	0.07	1.26
EPamSh16-4	40	20.25	2.05	18.20	0.00	10.13	89.87	0.00	2.35	0.40	0.08	1.08
EPamSh16-4	45	14.87	1.84	12.94	0.09	12.36	87.03	0.61	2.35	0.43	0.05	1.16

Core Name	Interval in Core (cm)	Bulk Mass (g)	mud (g)	sand (g)	gravel (g)	% mud	% sand	% gravel	Sand Fraction			
									mean (ϕ)	sorting (ϕ)	skewness (ϕ)	kurtosis (ϕ)
EPamSh16-4	50	22.85	8.39	14.46	0.00	36.70	63.30	0.00	2.53	0.55	0.20	1.19
EPamSh16-4	55	24.01	2.45	21.56	0.00	10.20	89.80	0.00	2.51	0.49	0.13	1.06
EPamSh16-4	60	19.16	1.39	17.68	0.09	7.25	92.28	0.47	2.58	0.52	0.05	1.05
EPamSh16-4	65	19.58	2.42	17.02	0.14	12.36	86.93	0.72	2.73	0.60	0.01	0.99
EPamSh16-4	70	21.46	3.18	18.17	0.11	14.81	84.67	0.51	2.80	0.64	-0.09	1.02
EPamSh16-4	75	19.01	3.11	15.90	0.00	16.37	83.63	0.00	2.84	0.64	-0.12	0.99
EPamSh16-4	80	20.71	2.05	18.66	0.00	9.90	90.10	0.00	2.81	0.62	-0.08	0.95
EPamSh16-4	85	17.35	1.76	15.52	0.07	10.13	89.46	0.40	2.80	0.64	-0.09	0.98
EPamSh16-4	90	19.55	1.67	17.86	0.02	8.55	91.35	0.10	2.77	0.62	-0.10	1.00
EPamSh16-4	95	20.33	2.00	18.31	0.02	9.84	90.06	0.10	2.73	0.64	-0.07	0.95
EPamSh16-4	100	20.08	1.45	18.14	0.49	7.22	90.34	2.44	2.64	0.83	-0.21	1.23
EPamSh16-4	105	19.52	2.06	17.38	0.08	10.54	89.05	0.41	2.68	0.65	-0.06	0.93
EPamSh16-4	110	23.04	3.11	19.66	0.27	13.51	85.32	1.17	2.68	0.66	-0.05	0.97
EPamSh16-4	115	22.71	3.08	19.62	0.01	13.56	86.40	0.04	2.65	0.54	0.00	1.13
EPamSh16-4	120	20.91	2.38	18.51	0.02	11.37	88.53	0.10	2.63	0.48	-0.06	1.12
EPamSh16-4	125	24.72	2.64	22.08	0.00	10.69	89.31	0.00	2.66	0.41	-0.05	1.22
EPamSh16-4	130	21.12	2.01	19.11	0.00	9.50	90.50	0.00	2.73	0.41	-0.01	1.27
EPamSh16-4	135	21.79	2.65	19.14	0.00	12.18	87.82	0.00	2.79	0.38	0.06	1.28
EPamSh16-4	140	19.99	2.00	17.99	0.00	10.01	89.99	0.00	2.80	0.37	0.07	1.29
EPamSh16-4	150	24.01	1.61	22.40	0.00	6.70	93.30	0.00	2.79	0.37	0.06	1.30
EPamSh16-4	155	21.35	2.86	18.49	0.00	13.40	86.60	0.00	2.83	0.39	0.07	1.19
EPamSh16-4	160	22.21	2.38	19.83	0.00	10.70	89.30	0.00	2.79	0.41	0.03	1.26
EPamSh16-4	165	21.65	2.72	18.93	0.00	12.58	87.42	0.00	2.80	0.42	0.03	1.22
EPamSh16-4	170	19.26	2.12	17.14	0.00	10.99	89.01	0.00	2.80	0.39	0.04	1.25
EPamSh16-4	175	19.50	3.06	16.43	0.01	15.71	84.24	0.05	2.75	0.43	-0.02	1.24
EPamSh16-4	180	22.67	1.92	20.75	0.00	8.47	91.53	0.00	2.70	0.43	-0.07	1.29
EPamSh16-4	185	22.27	2.11	20.14	0.02	9.48	90.43	0.09	2.71	0.48	-0.04	1.16
EPamSh16-4	190	24.40	2.58	21.82	0.00	10.57	89.43	0.00	2.65	0.46	-0.07	1.15

Core Name	Interval in Core (cm)	Bulk Mass (g)	mud (g)	sand (g)	gravel (g)	% mud	% sand	% gravel	Sand Fraction			
									mean (ϕ)	sorting (ϕ)	skewness (ϕ)	kurtosis (ϕ)
EPamSh16-4	195	23.57	1.73	21.81	0.03	7.36	92.52	0.13	2.60	0.49	-0.12	1.15
EPamSh16-4	200	22.48	2.41	20.06	0.01	10.70	89.25	0.04	2.55	0.48	-0.12	1.13
EPamSh16-4	205	20.84	2.25	18.59	0.00	10.80	89.20	0.00	2.50	0.51	-0.11	1.11
EPamSh16-4	210	20.22	2.00	18.20	0.02	9.87	90.03	0.10	2.48	0.47	-0.13	1.04
EPamSh16-4	215	18.75	0.84	17.66	0.25	4.49	94.18	1.33	2.58	0.69	-0.20	1.03
EPamSh16-4	220	18.58	1.23	17.12	0.23	6.61	92.15	1.24	2.16	0.83	-0.38	1.22
EPamSh16-4	225	21.92	1.53	20.35	0.04	6.98	92.83	0.18	2.35	0.56	-0.15	1.03
EPamSh16-4	230	21.04	2.55	18.49	0.00	12.11	87.89	0.00	2.37	0.51	-0.09	0.98
EPamSh16-4	240	22.13	4.67	17.46	0.00	21.11	78.89	0.00	2.47	0.44	-0.10	1.00
EPamSh16-4	245	18.39	1.25	17.14	0.00	6.77	93.23	0.00	2.40	0.51	-0.14	1.05
EPamSh16-4	250	22.68	1.58	21.09	0.01	6.97	92.99	0.04	2.31	0.62	-0.18	1.11
EPamSh16-4	255	23.97	1.83	22.06	0.08	7.64	92.03	0.33	2.22	0.75	-0.17	1.11
EPamSh16-4	260	23.68	2.73	20.79	0.16	11.53	87.79	0.68	2.19	0.78	-0.18	1.16
EPamSh16-4	265	18.43	2.10	16.17	0.16	11.39	87.74	0.87	2.01	0.87	-0.24	1.26
EPamSh16-4	270	25.06	2.34	22.39	0.33	9.34	89.34	1.32	2.08	0.67	-0.26	1.32
EPamSh16-4	275	24.93	0.92	24.01	0.00	3.68	96.32	0.00	2.29	0.44	-0.02	1.11
EPamSh16-4	280	22.63	1.20	21.43	0.00	5.30	94.70	0.00	2.23	0.50	-0.12	1.33
EPamSh16-4	285	17.79	5.18	12.59	0.02	29.11	70.78	0.11	2.20	0.52	-0.14	1.21
EPamSh16-4	290	23.25	1.61	21.64	0.00	6.92	93.08	0.00	2.41	0.41	-0.02	0.97
EPamSh16-4	300	23.81	1.27	22.52	0.02	5.35	94.57	0.08	2.15	0.47	-0.69	1.24
EPamSh16-4	305	19.79	0.55	19.24	0.00	2.78	97.22	0.00	2.16	0.49	-0.10	1.16
EPamSh16-4	310	23.49	0.87	22.62	0.00	3.69	96.31	0.00	2.19	0.48	-0.10	1.28
EPamSh16-4	315	22.27	0.80	21.46	0.01	3.61	96.35	0.04	2.03	0.54	-0.19	1.16
EPamSh16-4	320	18.73	0.02	18.71	0.00	0.12	99.88	0.00	2.18	0.49	-0.11	1.25
EPamSh16-4	325	20.92	0.86	20.06	0.00	4.10	95.90	0.00	2.18	0.46	-0.07	1.16
EPamSh16-4	330	19.64	0.90	18.74	0.00	4.57	95.43	0.00	2.17	0.49	-110.00	1.19
EPamSh16-4	335	22.70	1.01	21.68	0.01	4.45	95.51	0.04	2.17	0.46	-0.10	1.19
EPamSh16-4	340	18.35	0.48	17.69	0.18	2.60	96.42	0.98	2.20	0.51	-0.14	1.39

Core Name	Interval in Core (cm)	Bulk Mass (g)	mud (g)	sand (g)	gravel (g)	% mud	% sand	% gravel	Sand Fraction			
									mean (ϕ)	sorting (ϕ)	skewness (ϕ)	kurtosis (ϕ)
EPamSh16-4	345	18.27	0.67	17.60	0.00	3.69	96.31	0.00	1.98	0.52	-0.15	1.02
EPamSh16-4	350	25.62	0.91	24.71	0.00	3.54	96.46	0.00	1.80	0.63	-0.10	0.93
EPamSh16-4	355	17.19	0.79	16.40	0.00	4.57	95.43	0.00	2.15	0.54	-0.16	1.17
EPamSh16-4	360	22.43	0.69	21.74	0.00	3.06	96.94	0.00	2.35	0.28	0.29	1.13
EPamSh16-4	365	25.48	0.50	24.98	0.00	1.94	98.06	0.00	2.33	0.43	-0.02	1.01
EPamSh16-4	370	14.66	0.50	14.16	0.00	3.40	96.60	0.00	2.18	0.40	-0.07	1.35
EPamSh16-6	0	13.29	2.17	11.12	0.00	16.32	83.68	0.00	2.47	0.45	-0.10	1.01
EPamSh16-6	10	17.229	0.95	16.28	0.00	5.51	94.49	0.00	2.37	0.48	-0.06	0.96
EPamSh16-6	20	13.70	0.66	13.04	0.00	4.80	95.20	0.00	2.39	0.46	-0.10	0.94
EPamSh16-6	30	13.81	0.06	13.75	0.00	0.45	99.55	0.00	2.39	0.48	-0.09	0.93
EPamSh16-6	40	14.47	1.41	13.04	0.02	9.76	90.11	0.14	2.39	0.49	-0.07	0.97
EPamSh16-6	50	17.88	2.56	15.02	0.30	14.30	84.02	1.68	2.20	0.75	-0.30	1.43
EPamSh16-6	60	19.19	2.80	15.40	0.99	14.61	80.23	5.16	1.67	1.31	-0.57	1.41
EPamSh16-6	70	20.13	2.01	17.61	0.51	9.99	87.47	2.53	2.29	0.60	-0.17	1.23
EPamSh16-6	80	23.46	2.11	19.55	1.80	8.98	83.35	7.67	2.17	1.12	-0.46	2.47
EPamSh16-6	90	21.88	2.52	19.35	0.01	11.52	88.44	0.05	2.40	0.54	-0.15	1.15
EPamSh16-6	100	19.78	0.89	18.89	0.00	4.51	95.49	0.00	2.53	0.45	-0.16	1.08
EPamSh16-6	110	22.19	0.90	21.29	0.00	4.04	95.96	0.00	2.63	0.44	-0.19	1.36
EPamSh16-6	120	21.84	0.95	20.89	0.00	4.35	95.65	0.00	2.66	0.42	-0.09	1.18
EPamSh16-6	130	21.57	0.49	21.08	0.00	2.29	97.71	0.00	2.40	0.30	0.31	0.95
EPamSh16-6	140	21.23	1.41	19.82	0.00	6.63	93.37	0.00	2.71	0.40	-0.05	1.26
EPamSh16-6	150	20.07	0.84	19.23	0.00	4.19	95.81	0.00	2.22	0.48	0.06	0.78
EPamSh16-6	160	17.22	0.44	16.78	0.00	2.54	97.46	0.00	2.83	0.30	0.19	1.09
EPamSh16-6	170	20.17	0.82	19.35	0.00	4.08	95.92	0.00	2.83	0.35	0.06	1.30
EPamSh16-6	180	22.04	0.80	21.24	0.00	3.64	96.36	0.00	2.77	0.30	0.01	1.35
EPamSh16-6	190	22.44	0.33	22.11	0.00	1.46	98.54	0.00	2.36	0.49	-0.20	0.85
EPamSh16-6	200	25.68	1.04	24.64	0.00	4.04	95.96	0.00	2.53	0.47	-0.26	1.10
EPamSh16-6	210	23.30	1.23	22.07	0.00	5.27	94.73	0.00	2.70	0.38	-0.10	1.33

Core Name	Interval in Core (cm)	Bulk Mass (g)	mud (g)	sand (g)	gravel (g)	% mud	% sand	% gravel	Sand Fraction			
									mean (ϕ)	sorting (ϕ)	skewness (ϕ)	kurtosis (ϕ)
EPamSh16-6	220	24.37	2.21	22.16	0.00	9.05	90.95	0.00	2.81	0.36	0.07	1.29
EPamSh16-6	230	23.31	1.49	21.82	0.00	6.39	93.61	0.00	2.78	0.35	0.03	1.33
EPamSh16-6	240	26.15	1.40	24.75	0.00	5.35	94.65	0.00	2.84	0.34	0.11	1.22
EPamSh16-6	250	23.93	0.82	23.11	0.00	3.42	96.58	0.00	2.82	0.29	0.16	1.14
EPamSh16-6	260	26.62	1.52	25.10	0.00	5.70	94.30	0.00	2.84	0.36	0.04	1.31
EPamSh16-6	270	23.32	4.30	19.02	0.00	18.43	81.57	0.00	2.86	0.32	0.15	1.05
EPamSh16-6	280	26.94	1.26	25.68	0.00	4.68	95.32	0.00	2.83	0.31	0.15	1.17
EPamSh16-6	290	23.77	2.26	21.51	0.00	9.51	90.49	0.00	2.81	0.38	-0.01	1.51
EPamSh16-6	300	25.10	1.38	23.58	0.14	5.50	93.94	0.56	2.56	0.71	-0.45	2.14
EPamSh16-6	310	24.97	3.06	16.75	5.16	12.26	67.08	20.66	0.86	1.98	-0.41	0.64
EPamSh16-8	10	25.29	2.69	22.10	0.50	10.65	87.38	1.98	1.19	0.81	-0.33	0.98
EPamSh16-8	20	24.80	2.56	22.10	0.14	10.32	89.12	0.56	1.13	0.83	-0.25	0.89
EPamSh16-8	30	26.08	0.66	25.42	0.00	2.53	97.47	0.00	1.30	0.72	-0.20	0.89
EPamSh16-8	40	28.66	0.75	27.89	0.02	2.60	97.33	0.07	1.35	0.67	-0.22	0.96
EPamSh16-8	50	30.86	0.60	30.26	0.00	1.95	98.05	0.00	1.29	0.68	-0.15	0.91
EPamSh16-8	60	28.16	0.76	27.40	0.00	2.71	97.29	0.00	1.44	0.70	-0.24	0.96
EPamSh16-8	70	27.39	0.54	26.85	0.00	1.98	98.02	0.00	1.45	0.69	-0.23	0.97
EPamSh16-8	80	31.18	0.72	30.45	0.01	2.32	97.65	0.03	1.34	0.77	-0.19	0.83
EPamSh16-8	90	32.51	0.63	31.88	0.00	1.93	98.07	0.00	1.56	0.62	-0.20	0.98
EPamSh16-8	100	33.74	0.64	33.08	0.02	1.89	98.05	0.06	1.26	0.80	-0.18	0.87
EPamSh16-8	110	31.94	0.69	31.25	0.00	2.17	97.83	0.00	1.83	0.65	-0.21	1.00
EPamSh16-10	30	18.76	2.89	15.75	0.12	15.42	83.94	0.64	2.25	0.61	-0.12	1.05
EPamSh16-10	40	20.83	3.20	17.59	0.04	15.36	84.45	0.19	2.35	0.62	-0.25	9.47
EPamSh16-10	50	22.44	3.85	18.36	0.23	17.16	81.81	1.02	2.24	0.70	-0.20	1.17
EPamSh16-10	60	21.85	2.08	19.58	0.19	9.52	89.61	0.87	2.29	0.74	-0.24	1.19
EPamSh16-10	70	26.26	2.28	23.88	0.10	8.67	90.95	0.38	2.30	0.67	-0.19	1.08
EPamSh16-10	80	17.56	4.89	12.66	0.01	27.84	72.10	0.06	2.39	0.85	-0.12	1.12
EPamSh16-10	90	19.19	10.59	8.60	0.00	55.18	44.82	0.00	2.89	0.98	-0.41	0.99

Core Name	Interval in Core (cm)	Bulk Mass (g)	mud (g)	sand (g)	gravel (g)	% mud	% sand	% gravel	Sand Fraction			
									mean (ϕ)	sorting (ϕ)	skewness (ϕ)	kurtosis (ϕ)
EPamSh16-10	100	17.30	11.62	5.68	0.00	67.16	32.84	0.00	3.41	0.55	-0.53	1.21
EPamSh16-10	110	19.08	11.05	8.03	0.00	57.91	42.09	0.00	3.44	0.56	-0.55	1.34
EPamSh16-10	120	26.48	17.04	9.44	0.00	64.36	35.64	0.00	3.48	0.43	-0.40	1.03
EPamSh16-10	130	18.49	12.33	6.16	0.00	66.68	33.32	0.00	3.46	0.53	-0.53	1.33
EPamSh16-10	140	17.14	14.01	3.13	0.00	81.74	18.26	0.00	3.55	0.38	-0.43	1.34
EPamSh16-10	150	19.03	8.84	10.19	0.00	46.46	53.54	0.00	3.18	0.50	0.00	0.76
EPamSh16-10	160	18.00	13.33	4.67	0.00	74.05	25.95	0.00	3.39	0.63	-0.59	1.31
EPamSh16-10	170	18.11	12.73	5.36	0.02	70.29	29.60	0.11	3.07	0.71	-0.10	1.10
EPamSh16-10	180	16.28	9.85	6.43	0.00	60.50	39.50	0.00	3.22	0.72	-0.41	1.20
EPamSh16-10	190	14.32	12.04	2.28	0.00	84.08	15.92	0.00	3.06	0.99	-0.70	1.13
EPamSh16-10	200	12.38	11.42	0.96	0.00	92.25	7.75	0.00	2.94	1.09	-0.58	1.21
EPamSh16-10	210	16.05	13.26	2.79	0.00	82.61	17.39	0.00	3.26	0.87	-0.72	1.88
EPamSh16-10	220	21.27	7.80	13.47	0.00	36.66	63.34	0.00	3.04	0.73	-0.25	1.28
EPamSh16-10	230	13.74	8.51	5.23	0.00	61.93	38.07	0.00	3.26	0.52	-0.19	0.87
EPamSh16-10	240	18.72	5.83	12.87	0.02	31.13	68.76	0.11	2.47	0.99	-0.10	0.90

Appendix D: Surface Sample Grain–size Statistics

Mass and percent of mud, sand, and gravel for all grain size samples and GRADISTAT results for mean, sorting, skewness and kurtosis (Folk and Ward, 1957; Folk, 1974) method reported in ϕ).

Sample Number	Bulk Mass (g)	mud (g)	sand (g)	gravel (g)	% mud	% sand	% gravel	mean	sorting	skewness	kurtosis
17-1	30.07	28.15	1.91	0.01	93.61	6.35	0.03	5.857	1.345	-0.026	0.778
17-2	30.16	0.26	29.90	0.00	0.87	99.13	0.00	1.800	0.465	-0.113	0.994
17-3	30.27	0.40	29.87	0.00	1.31	98.69	0.00	1.792	0.576	-0.117	0.977
17-4	30.47	2.44	28.00	0.03	8.00	91.90	0.10	2.470	0.845	0.260	2.225
17-5	30.25	5.51	24.74	0.00	18.21	81.79	0.00	2.905	1.487	0.587	2.238
17-6	30.07	1.81	28.26	0.00	6.01	93.99	0.00	1.672	1.066	0.059	1.519
17-7	30.30	1.66	28.64	0.00	5.48	94.52	0.00	1.509	0.951	0.346	1.601
17-8	30.31	28.26	1.90	0.15	93.24	6.27	0.49	5.849	1.491	-0.114	0.955
17-10	30.34	24.66	5.45	0.23	81.28	17.96	0.76	5.447	1.837	-0.175	1.024
17-11	30.27	1.75	28.50	0.02	5.78	94.16	0.07	2.024	1.027	0.038	1.509
17-12	30.08	13.32	16.63	0.13	44.28	55.28	0.43	4.338	1.852	0.332	0.857
17-13	30.13	10.34	19.74	0.05	34.32	65.52	0.17	4.204	1.617	0.446	1.059
17-14	30.35	12.13	18.21	0.01	39.96	60.01	0.03	3.539	2.208	0.484	0.721
17-15	30.24	23.50	6.50	0.24	77.71	21.49	0.79	5.418	1.706	-0.075	0.868
17-17	30.24	27.15	2.28	0.82	89.76	7.53	2.71	5.762	1.857	-0.222	1.325
17-18	30.09	1.01	29.07	0.01	3.36	96.60	0.03	1.396	0.606	-0.063	1.052
17-19	30.18	0.43	29.75	0.00	1.42	98.58	0.00	1.850	0.564	-0.137	1.087
17-20	30.00	1.01	28.97	0.02	3.37	96.56	0.07	2.261	0.404	0.062	1.395
17-21	30.13	3.68	26.24	0.21	12.20	87.10	0.70	3.042	1.115	0.257	2.206
17-22	30.27	4.36	25.89	0.02	14.39	85.54	0.07	2.137	1.442	0.415	2.005
17-23	30.39	1.10	29.25	0.04	3.62	96.25	0.13	1.270	0.576	0.042	1.123
17-24	30.02	27.97	1.99	0.06	93.17	6.63	0.20	5.847	1.366	-0.037	0.796
17-26	30.29	24.97	5.19	0.13	82.43	17.14	0.43	5.549	1.584	-0.063	0.825
17-27	30.35	8.36	21.90	0.09	27.54	72.16	0.30	3.166	2.007	0.581	0.996
17-28	30.31	1.41	28.90	0.00	4.66	95.34	0.00	2.459	0.525	0.178	1.327

Appendix E: Down-Core Foraminiferal Census Data

Samples EPamSh16-2 @24–25 cm, EPamSh16-2 @104–105 cm, EPamSh16-4 @294–295 cm, EPamSh16-4 @354–355 cm, EPamSh16-6 @274–275 cm, EPamSh16-8 @14–15 cm, and EPamSh16-8 @114–115 cm were barren.

Core	EPamSh16 Vibracores											
	EPamSh16-1	EPamSh16-1	EPamSh16-1	EPamSh16-1	EPamSh16-1	EPamSh16-4	EPamSh16-4	EPamSh16-6	EPamSh16-6	EPamSh16-10	EPamSh16-10	EPamSh16-10
Taxon ↓ Sample ID (mbsf) →	0.14-0.15	0.64-0.65	3.84-3.85	4.24-4.25	4.94-4.95	0.24-0.25	2.44-2.45	0.14-0.15	1.64-1.65	0.64-0.65	2.24-2.25	2.44-2.45
Ammonia parkinsoniana	1	4	1	2			3	1	5	2	1	7
Ammonia tepida									1			1
Cibicides lobatulus												1
Elphidium excavatum	7	96	103	102	28	2	102	4	83	11	56	82
Elphidium gunteri									1	1		1
Elphidium mexicanum									2			
Elphidium sp.						2			1			
Elphidium subarcticum									2			1
Haynesina germanica									2			1
Indeterminate Rotaliid							1					
Planktonic												1
Total # of specimens picked	8	100	104	104	28	4	106	5	97	14	57	95

Appendix F: Down-Core Foraminiferal Percent Abundance Data

Samples EPamSh16-2 @24–25 cm, EPamSh16-2 @104–105 cm, EPamSh16-4 @294–295 cm, EPamSh16-4 @354–355 cm, EPamSh16-6 @274–275 cm, EPamSh16-8 @14–15 cm, and EPamSh16-8 @114–115 cmwere barren.

	EPamSh16 Vibracores											
Core	EPamSh16-1	EPamSh16-1	EPamSh16-1	EPamSh16-1	EPamSh16-1	EPamSh16-4	EPamSh16-4	EPamSh16-6	EPamSh16-6	EPamSh16-10	EPamSh16-10	EPamSh16-10
Taxon ↓ Sample ID (mbsf) →	0.14-0.15	0.64-0.65	3.84-3.85	4.24-4.25	4.94-4.95	0.24-0.25	2.44-2.45	0.14-0.15	1.64-1.65	0.64-0.65	2.24-2.25	2.44-2.45
Ammonia parkinsoniana	12.50	4.00	0.96	1.92			2.83	20.00	5.15	14.29	1.75	7.37
Ammonia tepida									1.03			1.05
Cibicides lobatulus												1.05
Elphidium excavatum	87.50	96.00	99.04	98.08	100.00	50.00	96.23	80.00	85.57	78.57	98.25	86.3
Elphidium gunteri									1.03	7.14		1.05
Elphidium mexicanum									2.06			
Elphidium sp.						50			1.03			
Elphidium subarcticum									2.06			1.05
Haynesina germanica									2.06			1.05
Indeterminate Rotaliid							0.94					
Planktonic												1.05
Total %	100.00	100.00	100.00	100.00	100.00	100.00	100.00	100.00	100.00	100.00	100.00	100.00

Appendix G: List of Foraminiferal Taxa with Original References

Alphabetical list of foraminiferal species with references to original publications.

Ammonia parkinsoniana (d'Orbigny): *Rosalina parkinsoniana* d'Orbigny, 1839b, p. 99, pl. 4, figs. 25-27.

Ammonia tepida (Cushman): *Rotalia beccarii* (Linneaus) var. *tepida* Cushman, 1926, p. 79, pl. 1. Figs 25-27.

Cibicides lobatulus (Walker and Jacob): *Nautilus lobatulus* Walker and Jacob, 1798, p. 642, pl. 14, fig. 36.

Elphidium excavatum (Terquem): *Polystomella excavata* Terquem, 1875, p. 25, pl. 2, figs. 2 a-f.

Elphidium gunteri Cole: *Elphidium gunteri* Cole 1931, p. 34, pl. 4, figs. 9, 10.

Elphidium mexicanum (Kornfeld): *Elphidium incertum* (Williamson) var. *mexicanum* Kornfeld, 1931, p. 89, pl. 16, figs. 1a, b, 2a, b.

Elphidium subarcticum Cushman: *Elphidium subarcticum* Cushman, 1944, p. 27, pl. 3, figs. 34, 35.

Haynesina germanica (Ehrenberg): *Nonionina germanica* (Ehrenberg), 1841, p. 23, pl. 2, figs. 1a-g.

Appendix H: Bulk Magnetic Susceptibility Data

Averaged values for KRe, Kim, KVol, and KMass after five repetitions obtained by using a Kappabridge MFK1-A by Advanced Geoscience Instruments Company (AGICO)

EPamSh16-1 Averages

MBSF	KRe [SI]	Kim [SI]	KVol [SI]	KMass [m3/kg]	Ph
0.00	1.544E-05	7.256E-07	2.807E-05	6.174E-09	2.682
0.05	1.807E-05	7.459E-07	3.286E-05	7.230E-09	2.362
0.10	1.973E-05	4.917E-07	3.588E-05	7.893E-09	1.420
0.15	1.842E-05	5.710E-07	3.349E-05	7.368E-09	1.768
0.20	2.641E-05	6.936E-07	4.803E-05	1.057E-08	1.502
0.25	3.804E-05	1.014E-06	6.916E-05	1.521E-08	1.522
0.30	3.879E-05	1.264E-06	7.053E-05	1.552E-08	1.862
0.35	3.477E-05	1.481E-06	6.321E-05	1.391E-08	2.438
0.40	3.644E-05	1.032E-06	6.626E-05	1.458E-08	1.620
0.45	3.817E-05	1.355E-06	6.939E-05	1.527E-08	2.028
0.50	3.726E-05	1.109E-06	6.775E-05	1.490E-08	1.700
0.55	3.615E-05	1.149E-06	6.572E-05	1.446E-08	1.814
0.60	3.624E-05	8.974E-07	6.588E-05	1.449E-08	1.414
0.65	3.535E-05	9.838E-07	6.428E-05	1.414E-08	1.586
0.70	3.612E-05	1.001E-06	6.567E-05	1.444E-08	1.580
0.75	3.811E-05	1.278E-06	6.929E-05	1.524E-08	1.916
0.80	3.190E-05	8.459E-07	5.800E-05	1.276E-08	1.510
0.85	3.541E-05	1.137E-06	6.439E-05	1.417E-08	1.832
0.90	3.971E-05	1.137E-06	7.219E-05	1.588E-08	1.636
0.95	3.381E-05	9.236E-07	6.147E-05	1.352E-08	1.562
1.00	3.458E-05	1.014E-06	6.286E-05	1.383E-08	1.676
1.05	3.900E-05	9.656E-07	7.091E-05	1.560E-08	1.412
1.10	3.755E-05	9.346E-07	6.826E-05	1.502E-08	1.422
1.15	3.528E-05	9.445E-07	6.414E-05	1.411E-08	1.528
1.20	3.367E-05	1.023E-06	6.121E-05	1.347E-08	1.738
1.25	3.498E-05	1.240E-06	6.360E-05	1.399E-08	2.030
1.30	3.503E-05	6.325E-07	6.369E-05	1.401E-08	1.004
1.35	3.704E-05	1.307E-06	6.734E-05	1.482E-08	2.020
1.40	4.078E-05	1.005E-06	7.415E-05	1.631E-08	1.410
1.45	3.600E-05	9.273E-07	6.545E-05	1.440E-08	1.470
1.50	3.636E-05	8.701E-07	6.611E-05	1.455E-08	1.364
1.55	4.320E-05	1.084E-06	7.854E-05	1.728E-08	1.434
1.60	3.846E-05	5.726E-08	6.992E-05	1.538E-08	0.078
1.65	3.921E-05	6.699E-07	7.130E-05	1.569E-08	0.978
1.70	3.638E-05	3.189E-07	6.614E-05	1.455E-08	0.482
1.75	3.536E-05	2.479E-07	6.429E-05	1.414E-08	0.386

MBSF	KRe [SI]	Kim [SI]	KVol [SI]	KMass [m3/kg]	Ph
1.80	3.594E-05	4.615E-07	6.534E-05	1.437E-08	0.730
1.85	4.144E-05	5.756E-07	7.535E-05	1.658E-08	0.792
1.90	3.879E-05	2.452E-06	7.052E-05	1.551E-08	3.614
1.95	3.899E-05	5.926E-07	7.090E-05	1.560E-08	0.868
2.00	4.100E-05	1.842E-07	7.455E-05	1.640E-08	0.246
2.05	3.675E-05	4.397E-07	6.682E-05	1.470E-08	0.680
2.10	4.471E-05	4.994E-07	8.129E-05	1.788E-08	0.630
2.15	4.193E-05	2.867E-07	7.623E-05	1.677E-08	0.386
2.20	4.263E-05	4.019E-07	7.751E-05	1.705E-08	0.532
2.25	4.044E-05	5.759E-07	7.353E-05	1.618E-08	0.812
2.30	3.401E-05	4.189E-07	6.184E-05	1.361E-08	0.704
2.35	3.530E-05	4.084E-07	6.417E-05	1.412E-08	0.664
2.40	3.300E-05	5.070E-07	6.000E-05	1.320E-08	0.880
2.45	3.984E-05	3.855E-07	7.244E-05	1.594E-08	0.552
2.50	3.579E-05	1.977E-05	6.508E-05	1.432E-08	14.306
2.55	3.574E-05	3.206E-07	6.498E-05	1.430E-08	0.516
2.60	4.009E-05	7.477E-07	7.290E-05	1.604E-08	1.066
2.65	3.450E-05	7.909E-07	6.272E-05	1.380E-08	1.312
2.70	3.000E-05	6.280E-07	5.455E-05	1.200E-08	1.196
2.75	3.658E-05	6.948E-07	6.650E-05	1.463E-08	1.088
2.80	3.525E-05	7.044E-07	6.410E-05	1.410E-08	1.142
2.85	3.988E-05	7.846E-07	7.251E-05	1.595E-08	1.126
2.90	4.220E-05	8.949E-07	7.673E-05	1.688E-08	1.214
2.95	4.483E-05	8.012E-07	8.150E-05	1.793E-08	1.022
3.00	4.253E-05	8.315E-07	7.732E-05	1.701E-08	1.118
3.05	4.212E-05	5.296E-07	7.658E-05	1.685E-08	0.722
3.10	3.808E-05	1.038E-06	6.923E-05	1.523E-08	1.562
3.15	3.730E-05	8.503E-07	6.782E-05	1.492E-08	1.304
3.20	2.630E-05	5.135E-07	4.783E-05	1.052E-08	1.110
3.25	3.301E-05	7.675E-07	6.002E-05	1.320E-08	1.330
3.30	3.357E-05	6.820E-07	6.104E-05	1.343E-08	1.160
3.35	3.280E-05	5.362E-07	5.964E-05	1.312E-08	0.936
3.40	3.530E-05	6.743E-07	6.418E-05	1.412E-08	1.092
3.45	4.056E-05	7.601E-07	7.374E-05	1.622E-08	1.072
3.50	4.040E-05	7.505E-07	7.345E-05	1.616E-08	1.064
3.55	3.687E-05	6.978E-07	6.704E-05	1.475E-08	1.084
3.60	4.553E-05	8.344E-07	8.279E-05	1.821E-08	1.050
3.65	4.202E-05	7.930E-07	7.641E-05	1.681E-08	1.080
3.70	3.493E-05	7.379E-07	6.351E-05	1.397E-08	1.212
3.75	3.899E-05	7.884E-07	7.089E-05	1.560E-08	1.156
3.80	4.123E-05	7.984E-07	7.496E-05	1.649E-08	1.112

MBSF	KRe [SI]	Kim [SI]	KVol [SI]	KMass [m3/kg]	Ph
3.85	3.374E-05	7.059E-07	6.135E-05	1.350E-08	1.198
3.90	3.783E-05	7.833E-07	6.879E-05	1.513E-08	1.186
3.95	3.627E-05	8.830E-07	6.594E-05	1.451E-08	1.392
4.00	3.867E-05	8.029E-07	7.031E-05	1.547E-08	1.190
4.05	2.625E-05	6.170E-07	4.772E-05	1.050E-08	1.346
4.10	2.607E-05	5.620E-07	4.740E-05	1.043E-08	1.232
4.15	2.507E-05	5.720E-07	4.558E-05	1.003E-08	1.306
4.20	2.161E-05	6.476E-07	3.930E-05	8.646E-09	1.714
4.25	2.053E-05	4.865E-07	3.733E-05	8.213E-09	1.356
4.30	2.070E-05	4.869E-07	3.764E-05	8.281E-09	1.346
4.35	1.721E-05	3.984E-07	3.129E-05	6.885E-09	1.324
4.40	1.756E-05	4.529E-07	3.193E-05	7.025E-09	1.478
4.45	2.265E-05	6.234E-07	4.117E-05	9.058E-09	1.576
4.50	1.692E-05	4.682E-07	3.075E-05	6.766E-09	1.584
4.55	1.680E-05	4.351E-07	3.054E-05	6.719E-09	1.478
4.60	1.979E-05	5.984E-07	3.599E-05	7.917E-09	1.724
4.65	2.177E-05	6.403E-07	3.958E-05	8.708E-09	1.682
4.70	2.557E-05	4.792E-07	4.650E-05	1.023E-08	1.054
4.75	3.505E-05	7.509E-07	6.373E-05	1.402E-08	1.224
4.80	3.063E-05	4.109E-07	5.570E-05	1.225E-08	0.750
4.85	2.086E-05	2.281E-07	3.792E-05	8.343E-09	0.558
4.90	3.349E-05	1.361E-06	6.089E-05	1.340E-08	2.316
4.95	3.691E-05	1.319E-06	6.711E-05	1.476E-08	2.044
5.00	3.009E-05	7.557E-07	5.470E-05	1.203E-08	1.432
5.05	3.109E-05	9.302E-07	5.653E-05	1.244E-08	1.708
5.10	3.353E-05	6.893E-07	6.097E-05	1.342E-08	1.176
5.15	2.611E-05	2.514E-07	4.748E-05	1.045E-08	0.540
5.20	2.287E-05	4.497E-07	4.159E-05	9.149E-09	1.120
5.25	2.912E-05	1.479E-07	5.294E-05	1.165E-08	0.276
5.30	3.581E-05	5.205E-08	6.512E-05	1.433E-08	0.062
5.35	4.287E-05	2.781E-06	7.795E-05	1.715E-08	3.696
5.40	3.258E-05	3.230E-07	5.925E-05	1.303E-08	0.562
5.45	2.986E-05	2.566E-07	5.430E-05	1.195E-08	0.484
5.50	2.527E-05	7.937E-08	4.595E-05	1.011E-08	0.162
5.55	3.022E-05	-5.190E-09	5.495E-05	1.209E-08	-0.018
5.60	1.952E-05	3.147E-07	3.550E-05	7.809E-09	0.922
5.65	2.240E-05	4.111E-07	4.074E-05	8.962E-09	1.040
5.70	2.261E-05	-1.152E-07	4.112E-05	9.046E-09	-0.328
5.75	2.074E-05	1.930E-07	3.770E-05	8.294E-09	0.518
5.80	2.238E-05	-3.945E-08	4.070E-05	8.954E-09	-0.130
5.85	9.613E-06	1.403E-07	1.748E-05	3.845E-09	0.830

MBSF	KRe [SI]	Kim [SI]	KVol [SI]	KMass [m3/kg]	Ph
5.90	8.335E-06	-5.084E-08	1.516E-05	3.334E-09	-0.464
5.95	2.274E-05	2.216E-07	4.134E-05	9.094E-09	0.548
6.00	2.496E-05	4.139E-07	4.539E-05	9.986E-09	0.946
6.05	2.812E-05	5.482E-07	5.113E-05	1.125E-08	1.112
6.10	2.020E-05	3.729E-07	3.673E-05	8.081E-09	1.046
6.15	1.570E-05	6.098E-06	2.854E-05	6.279E-09	21.242

EPamSh16-2 Averages

MBSF	KRe [SI]	Kim [SI]	KVol [SI]	KMass [m3/kg]	Ph
0.00	5.036E-06	-5.419E-08	9.157E-06	2.015E-09	-0.710
0.05	3.067E-06	4.833E-07	5.577E-06	1.227E-09	8.954
0.10	4.083E-06	6.199E-07	7.423E-06	1.633E-09	8.620
0.15	5.227E-06	5.970E-07	9.503E-06	2.091E-09	6.482
0.20	8.906E-06	6.830E-07	1.619E-05	3.562E-09	4.374
0.25	1.134E-05	8.326E-07	2.062E-05	4.536E-09	4.200
0.30	1.010E-05	7.575E-07	1.836E-05	4.040E-09	4.250
0.35	7.455E-06	7.454E-07	1.355E-05	2.982E-09	5.680
0.40	5.690E-06	6.006E-07	1.035E-05	2.276E-09	5.984
0.45	1.067E-05	8.267E-07	1.940E-05	4.268E-09	4.432
0.50	2.710E-06	2.770E-07	4.928E-06	1.084E-09	5.362
0.55	7.069E-06	4.525E-07	1.285E-05	2.828E-09	3.666
0.60	5.058E-06	5.691E-07	9.197E-06	2.023E-09	6.406
0.65	5.708E-06	6.433E-07	1.038E-05	2.283E-09	6.426
0.70	6.138E-06	7.140E-07	1.116E-05	2.455E-09	6.634
0.75	7.077E-06	6.732E-07	1.287E-05	2.831E-09	5.424
0.80	5.461E-06	4.492E-07	9.932E-06	2.184E-09	4.550
0.85	5.288E-06	4.170E-07	9.615E-06	2.115E-09	4.496
0.90	4.993E-06	7.010E-07	9.079E-06	1.997E-09	7.996
0.95	5.127E-06	5.401E-07	9.322E-06	2.051E-09	6.002
1.00	7.621E-06	6.740E-07	1.386E-05	3.049E-09	5.012
1.05	3.960E-06	5.591E-07	7.199E-06	1.584E-09	8.088
1.10	4.772E-06	2.517E-07	8.676E-06	1.909E-09	2.838

EPamSh16-4 Averages

MBSF	KRe [SI]	Kim [SI]	KVol [SI]	KMass [m3/kg]	Ph
0.00	4.507E-06	-2.345E-07	8.195E-06	1.803E-09	-3.034
0.05	5.265E-06	-4.909E-07	9.572E-06	2.106E-09	-5.356
0.10	5.193E-06	-1.537E-07	9.442E-06	2.077E-09	-1.832
0.15	6.342E-06	-2.050E-07	1.153E-05	2.537E-09	-2.020
0.20	9.234E-06	-2.053E-07	1.679E-05	3.693E-09	-1.312
0.25	9.920E-06	-2.586E-07	1.804E-05	3.969E-09	-1.542
0.30	1.337E-05	-1.258E-07	2.431E-05	5.348E-09	-0.542
0.35	1.181E-05	-2.302E-07	2.148E-05	4.725E-09	-1.126
0.40	1.289E-05	-3.884E-07	2.343E-05	5.155E-09	-1.758
0.45	1.029E-05	-1.708E-07	1.870E-05	4.114E-09	-0.958
0.50	2.297E-05	-2.590E-07	4.176E-05	9.187E-09	-0.648
0.55	1.330E-05	-7.657E-08	2.418E-05	5.320E-09	-0.344
0.60	1.178E-05	-2.993E-07	2.142E-05	4.711E-09	-1.490
0.65	1.517E-05	-2.045E-07	2.758E-05	6.067E-09	-0.778
0.70	1.741E-05	-1.135E-07	3.165E-05	6.964E-09	-0.372
0.75	2.121E-05	3.166E-08	3.856E-05	8.484E-09	0.080
0.80	1.829E-05	-2.475E-07	3.325E-05	7.316E-09	-0.792
0.85	1.671E-05	-3.625E-08	3.038E-05	6.684E-09	-0.126
0.90	1.927E-05	5.000E-07	3.504E-05	7.708E-09	1.452
0.95	1.992E-05	-1.028E-07	3.621E-05	7.967E-09	-0.302
1.00	1.604E-05	-4.890E-08	2.917E-05	6.418E-09	-0.180
1.05	1.608E-05	-3.003E-07	2.924E-05	6.433E-09	-1.102
1.10	1.721E-05	1.214E-07	3.129E-05	6.884E-09	0.402
1.15	1.654E-05	-2.097E-07	3.008E-05	6.618E-09	-0.730
1.20	1.638E-05	-2.151E-07	2.979E-05	6.555E-09	-0.752
1.25	1.138E-05	-1.398E-08	2.070E-05	4.553E-09	-0.084
1.30	1.140E-05	-1.610E-07	2.072E-05	4.559E-09	-0.828
1.35	1.486E-05	-2.755E-07	2.702E-05	5.945E-09	-1.080
1.40	1.219E-05	-1.062E-07	2.217E-05	4.877E-09	-0.520
1.45	1.416E-05	-1.604E-07	2.575E-05	5.664E-09	-0.656
1.50	1.162E-05	-1.464E-07	2.112E-05	4.647E-09	-0.736
1.55	1.571E-05	-4.777E-08	2.857E-05	6.285E-09	-0.178
1.60	1.458E-05	-2.171E-07	2.650E-05	5.830E-09	-0.860
1.65	1.554E-05	-1.574E-07	2.825E-05	6.215E-09	-0.582
1.70	1.496E-05	-1.286E-07	2.721E-05	5.985E-09	-0.502
1.75	1.625E-05	-1.434E-07	2.955E-05	6.500E-09	-0.508
1.80	1.386E-05	-8.239E-08	2.521E-05	5.546E-09	-0.360
1.85	1.322E-05	-1.062E-07	2.405E-05	5.290E-09	-0.490

MBSF	KRe [SI]	Kim [SI]	KVol [SI]	KMass [m3/kg]	Ph
1.90	1.437E-05	-9.474E-08	2.614E-05	5.751E-09	-0.382
1.95	1.139E-05	-2.095E-07	2.070E-05	4.554E-09	-1.072
2.00	1.401E-05	-1.500E-07	2.546E-05	5.602E-09	-0.616
2.05	1.309E-05	-2.023E-07	2.379E-05	5.234E-09	-0.902
2.10	1.182E-05	-2.324E-07	2.149E-05	4.727E-09	-1.142
2.15	7.844E-06	-2.867E-07	1.426E-05	3.137E-09	-2.134
2.20	7.711E-06	-1.561E-07	1.402E-05	3.084E-09	-1.212
2.25	9.227E-06	-2.061E-07	1.678E-05	3.691E-09	-1.320
2.30	1.189E-05	-2.555E-07	2.162E-05	4.756E-09	-1.240
2.35	1.285E-05	-2.200E-07	2.337E-05	5.141E-09	-0.988
2.40	1.649E-05	1.299E-07	2.999E-05	6.597E-09	0.460
2.45	1.232E-05	-9.142E-09	2.240E-05	4.928E-09	-0.054
2.50	1.007E-05	4.187E-07	1.831E-05	4.028E-09	2.362
2.55	1.083E-05	-9.954E-08	1.969E-05	4.332E-09	-0.556
2.60	1.224E-05	-2.114E-07	2.225E-05	4.895E-09	-0.994
2.65	1.111E-05	-2.387E-07	2.020E-05	4.444E-09	-1.258
2.70	1.111E-05	-3.157E-08	2.019E-05	4.442E-09	-0.172
2.75	8.075E-06	-1.978E-08	1.468E-05	3.230E-09	-0.162
2.80	5.418E-06	-1.182E-07	9.849E-06	2.167E-09	-1.546
2.85	5.667E-06	-1.998E-07	1.030E-05	2.267E-09	-2.090
2.90	6.090E-06	-1.478E-07	1.107E-05	2.436E-09	-1.524
2.95	6.011E-06	-1.946E-07	1.093E-05	2.404E-09	-2.090
3.00	8.864E-06	-2.199E-08	1.612E-05	3.545E-09	-0.148
3.05	8.237E-06	2.616E-08	1.498E-05	3.295E-09	0.124
3.10	6.808E-06	7.259E-08	1.238E-05	2.723E-09	0.586
3.15	7.012E-06	3.301E-07	1.275E-05	2.805E-09	2.498
3.20	6.890E-06	-2.648E-08	1.253E-05	2.756E-09	-0.286
3.25	6.247E-06	-1.453E-07	1.136E-05	2.499E-09	-1.490
3.30	7.183E-06	2.857E-08	1.306E-05	2.873E-09	0.212
3.35	4.198E-06	-2.826E-08	7.633E-06	1.679E-09	-0.570
3.40	4.813E-06	-1.269E-07	8.751E-06	1.925E-09	-1.654
3.45	2.019E-06	3.880E-10	3.671E-06	8.077E-10	-0.224
3.50	1.309E-06	-6.035E-08	2.381E-06	5.237E-10	-4.956
3.55	9.973E-06	1.780E-08	1.814E-05	3.989E-09	0.082
3.60	1.529E-05	1.385E-07	2.781E-05	6.118E-09	0.498
3.65	1.011E-05	1.233E-07	1.838E-05	4.044E-09	0.690
3.70	1.655E-05	3.730E-07	3.010E-05	6.622E-09	1.284

EPamSh16-6 Averages

MBSF	KRe [SI]	Kim [SI]	KVol [SI]	KMass [m3/kg]	Ph
0.00	1.284E-05	3.861E-07	2.333E-05	5.134E-09	1.724
0.05	1.306E-05	1.355E-07	2.375E-05	5.224E-09	0.580
0.10	1.226E-05	8.051E-08	2.230E-05	4.906E-09	0.368
0.20	1.440E-05	3.530E-08	2.618E-05	5.761E-09	0.132
0.25	1.405E-05	-3.980E-09	2.555E-05	5.621E-09	-0.048
0.30	1.608E-05	1.600E-07	2.923E-05	6.431E-09	0.558
0.35	1.893E-05	6.785E-09	3.443E-05	7.574E-09	0.012
0.40	2.380E-05	3.164E-08	4.327E-05	9.518E-09	0.058
0.45	2.383E-05	3.046E-08	4.332E-05	9.530E-09	0.068
0.50	2.136E-05	1.318E-07	3.884E-05	8.546E-09	0.350
0.55	1.727E-05	-2.091E-07	3.139E-05	6.907E-09	-0.724
0.60	1.451E-05	-1.236E-07	2.639E-05	5.805E-09	-0.548
0.65	1.294E-05	-3.725E-08	2.352E-05	5.175E-09	-0.164
0.70	1.251E-05	6.956E-07	2.275E-05	5.005E-09	3.130
0.75	1.454E-05	4.656E-08	2.643E-05	5.815E-09	0.164
0.80	1.205E-05	5.912E-08	2.190E-05	4.819E-09	0.272
0.85	1.389E-05	-2.394E-08	2.526E-05	5.557E-09	-0.154
0.90	1.234E-05	-4.185E-08	2.244E-05	4.937E-09	-0.200
0.95	9.704E-06	8.148E-08	1.764E-05	3.881E-09	0.462
1.00	8.981E-06	1.070E-07	1.633E-05	3.593E-09	0.670
1.05	8.766E-06	2.319E-07	1.594E-05	3.506E-09	1.522
1.10	8.126E-06	-9.003E-08	1.477E-05	3.251E-09	-0.798
1.15	8.836E-06	1.069E-07	1.606E-05	3.534E-09	0.690
1.20	7.900E-06	-2.150E-08	1.437E-05	3.160E-09	-0.186
1.25	6.684E-06	-1.904E-07	1.215E-05	2.674E-09	-1.860
1.30	7.847E-06	1.340E-07	1.427E-05	3.139E-09	0.934
1.35	8.065E-06	1.170E-07	1.466E-05	3.226E-09	0.816
1.40	8.458E-06	-3.794E-08	1.538E-05	3.383E-09	-0.372
1.45	8.181E-06	1.845E-07	1.487E-05	3.272E-09	1.282
1.50	9.647E-06	-6.478E-08	1.754E-05	3.859E-09	-0.432
1.55	9.012E-06	7.748E-08	1.639E-05	3.605E-09	0.440
1.60	8.672E-06	-3.578E-08	1.577E-05	3.469E-09	-0.262
1.65	7.092E-06	-7.270E-08	1.289E-05	2.837E-09	-0.614
1.70	8.692E-06	9.418E-08	1.580E-05	3.477E-09	0.594
1.75	9.116E-06	-1.476E-08	1.657E-05	3.647E-09	-0.180
1.80	7.109E-06	2.264E-07	1.293E-05	2.844E-09	1.804
1.85	9.412E-06	2.558E-07	1.711E-05	3.765E-09	1.536
1.90	1.137E-05	2.422E-07	2.068E-05	4.549E-09	1.174

MBSF	KRe [SI]	Kim [SI]	KVol [SI]	KMass [m3/kg]	Ph
1.95	6.621E-06	2.208E-07	1.204E-05	2.648E-09	1.874
2.00	6.047E-06	1.659E-07	1.099E-05	2.419E-09	1.516
2.05	6.834E-06	4.279E-08	1.243E-05	2.734E-09	0.114
2.10	8.684E-06	2.624E-07	1.579E-05	3.474E-09	1.722
2.15	1.020E-05	-2.719E-07	1.855E-05	4.081E-09	-1.644
2.20	1.658E-05	2.678E-07	3.014E-05	6.631E-09	0.922
2.25	1.380E-05	3.355E-07	2.510E-05	5.521E-09	1.388
2.30	1.241E-05	2.530E-07	2.256E-05	4.962E-09	1.148
2.35	1.388E-05	3.573E-07	2.523E-05	5.551E-09	1.470
2.40	1.439E-05	3.137E-07	2.616E-05	5.755E-09	1.240
2.45	1.757E-05	6.043E-07	3.194E-05	7.026E-09	1.970
2.50	1.670E-05	4.243E-07	3.036E-05	6.680E-09	1.454
2.55	1.547E-05	2.937E-07	2.812E-05	6.187E-09	1.082
2.60	1.637E-05	2.992E-07	2.975E-05	6.545E-09	1.026
2.65	1.337E-05	3.561E-07	2.430E-05	5.347E-09	1.522
2.70	1.940E-05	2.475E-07	3.527E-05	7.758E-09	0.722
2.75	1.302E-05	2.723E-07	2.367E-05	5.207E-09	1.190
2.80	1.476E-05	3.308E-07	2.685E-05	5.906E-09	1.274
2.85	1.736E-05	3.303E-07	3.156E-05	6.943E-09	1.086
2.90	1.552E-05	8.143E-07	2.822E-05	6.209E-09	3.012
2.95	1.470E-05	3.607E-07	2.672E-05	5.879E-09	1.402
3.00	1.416E-05	3.370E-07	2.574E-05	5.663E-09	1.358
3.05	1.292E-05	2.962E-07	2.349E-05	5.168E-09	1.306
3.10	1.318E-05	3.211E-07	2.396E-05	5.270E-09	1.392

EPamSh16-8 Averages

MBSF	KRe [SI]	Kim [SI]	KVol [SI]	KMass [m3/kg]	Ph
0.10	1.265E-05	4.714E-07	2.300E-05	5.061E-09	2.134
0.15	1.431E-05	3.680E-07	2.602E-05	5.724E-09	1.460
0.20	1.333E-05	4.691E-07	2.423E-05	5.331E-09	2.008
0.25	3.486E-06	-1.611E-07	6.339E-06	1.395E-09	-3.996
0.30	1.949E-06	-5.094E-08	3.543E-06	7.793E-10	-6.016
0.35	4.906E-07	-4.098E-08	8.920E-07	1.962E-10	-10.196
0.40	2.091E-06	2.622E-07	3.803E-06	8.366E-10	6.778
0.45	1.830E-06	3.565E-07	3.327E-06	7.318E-10	10.776
0.50	1.347E-06	2.664E-07	2.450E-06	5.390E-10	10.456
0.55	2.301E-06	5.361E-07	4.184E-06	9.206E-10	12.912
0.60	1.024E-06	9.956E-08	1.861E-06	4.094E-10	-7.750
0.65	5.073E-07	2.076E-07	9.221E-07	2.029E-10	4.610
0.70	7.271E-07	2.073E-07	1.322E-06	2.908E-10	8.594
0.75	1.256E-06	7.170E-07	2.283E-06	5.023E-10	29.542
0.80	1.992E-06	3.998E-07	3.623E-06	7.970E-10	11.240
0.85	1.369E-06	3.169E-07	2.489E-06	5.477E-10	12.518
0.90	7.988E-07	3.163E-07	1.452E-06	3.195E-10	21.552
0.95	1.582E-06	2.592E-07	2.876E-06	6.328E-10	7.256
1.00	4.294E-07	1.682E-07	7.808E-07	1.717E-10	-4.970
1.05	3.446E-08	2.096E-07	6.264E-08	1.378E-11	38.534
1.10	8.814E-08	1.696E-07	1.602E-07	3.524E-11	52.768
1.15	1.079E-06	1.934E-07	1.962E-06	4.317E-10	6.956

EPamSh16-10 Averages

MBSF	KRe [SI]	Kim [SI]	KVol [SI]	KMass [m3/kg]	Ph
0.30	2.704E-05	1.334E-06	4.916E-05	1.081E-08	2.824
0.35	3.586E-05	1.295E-06	6.519E-05	1.434E-08	2.068
0.40	2.566E-05	9.985E-07	4.666E-05	1.026E-08	2.226
0.45	2.292E-05	8.542E-07	4.167E-05	9.167E-09	2.134
0.50	1.781E-05	8.331E-07	3.238E-05	7.124E-09	2.676
0.55	1.906E-05	8.693E-07	3.466E-05	7.626E-09	2.608
0.60	1.902E-05	7.619E-07	3.457E-05	7.606E-09	2.290
0.65	1.613E-05	7.419E-07	2.932E-05	6.450E-09	2.624
0.70	1.765E-05	9.106E-07	3.209E-05	7.059E-09	2.948
0.75	1.643E-05	7.670E-07	2.988E-05	6.573E-09	2.668
0.80	2.186E-05	7.731E-07	3.975E-05	8.745E-09	2.018
0.85	2.420E-05	7.103E-07	4.401E-05	9.683E-09	1.670
0.90	3.205E-05	8.108E-07	5.828E-05	1.282E-08	1.450
0.95	2.697E-05	8.719E-07	4.903E-05	1.079E-08	1.850
1.00	3.622E-05	8.244E-07	6.585E-05	1.449E-08	1.300
1.05	3.464E-05	9.725E-07	6.299E-05	1.386E-08	1.608
1.10	3.220E-05	8.739E-07	5.854E-05	1.288E-08	1.550
1.15	3.287E-05	9.594E-07	5.976E-05	1.315E-08	1.672
1.20	3.278E-05	9.131E-07	5.960E-05	1.311E-08	1.596
1.25	3.136E-05	9.386E-07	5.703E-05	1.255E-08	1.712
1.30	3.784E-05	1.013E-06	6.881E-05	1.514E-08	1.534
1.35	3.515E-05	9.461E-07	6.391E-05	1.406E-08	1.542
1.40	3.714E-05	9.430E-07	6.753E-05	1.486E-08	1.454
1.45	3.708E-05	9.331E-07	6.741E-05	1.483E-08	1.444
1.50	3.144E-05	8.211E-07	5.716E-05	1.258E-08	1.494
1.55	3.454E-05	9.050E-07	6.280E-05	1.382E-08	1.500
1.60	3.584E-05	9.881E-07	6.517E-05	1.434E-08	1.578
1.65	3.186E-05	9.295E-07	5.793E-05	1.275E-08	1.672
1.70	3.467E-05	7.736E-07	6.303E-05	1.387E-08	1.276
1.75	3.653E-05	8.280E-07	6.643E-05	1.461E-08	1.294
1.80	3.681E-05	1.105E-06	6.692E-05	1.472E-08	1.718
1.85	4.084E-05	8.799E-07	7.425E-05	1.633E-08	1.232
1.90	3.779E-05	8.772E-07	6.871E-05	1.512E-08	1.338
1.95	3.906E-05	1.270E-06	7.102E-05	1.563E-08	1.864
2.00	4.346E-05	6.933E-07	7.901E-05	1.738E-08	0.906
2.05	4.144E-05	8.261E-07	7.535E-05	1.658E-08	1.134
2.10	4.309E-05	-9.549E-07	7.835E-05	1.724E-08	-1.250
2.15	3.857E-05	9.098E-07	7.012E-05	1.543E-08	1.352

MBSF	KRe [SI]	Kim [SI]	KVol [SI]	KMass [m3/kg]	Ph
2.20	3.588E-05	7.508E-07	6.523E-05	1.435E-08	1.194
2.25	3.687E-05	7.414E-07	6.704E-05	1.475E-08	1.150
2.30	3.864E-05	9.138E-07	7.026E-05	1.546E-08	1.354
2.35	4.195E-05	9.422E-07	7.626E-05	1.678E-08	1.286
2.40	3.120E-05	7.851E-07	5.673E-05	1.248E-08	1.442
2.45	2.372E-05	5.680E-07	4.313E-05	9.488E-09	1.364
2.50	1.788E-05	6.527E-07	3.252E-05	7.154E-09	2.086
2.55	1.123E-05	5.317E-07	2.041E-05	4.490E-09	2.684
2.60	1.283E-05	6.017E-07	2.333E-05	5.132E-09	2.674